

Washington University in St. Louis

## Washington University Open Scholarship

---

Arts & Sciences Electronic Theses and  
Dissertations

Arts & Sciences

---

Summer 8-15-2018

### Topics in PT-symmetric Quantum Mechanics and Classical systems

Nima Hassanpour

*Washington University in St. Louis*

Follow this and additional works at: [https://openscholarship.wustl.edu/art\\_sci\\_etds](https://openscholarship.wustl.edu/art_sci_etds)



Part of the [Mathematics Commons](#), and the [Quantum Physics Commons](#)

---

#### Recommended Citation

Hassanpour, Nima, "Topics in PT-symmetric Quantum Mechanics and Classical systems" (2018). *Arts & Sciences Electronic Theses and Dissertations*. 1625.

[https://openscholarship.wustl.edu/art\\_sci\\_etds/1625](https://openscholarship.wustl.edu/art_sci_etds/1625)

This Dissertation is brought to you for free and open access by the Arts & Sciences at Washington University Open Scholarship. It has been accepted for inclusion in Arts & Sciences Electronic Theses and Dissertations by an authorized administrator of Washington University Open Scholarship. For more information, please contact [digital@wumail.wustl.edu](mailto:digital@wumail.wustl.edu).

WASHINGTON UNIVERSITY IN ST. LOUIS

Department of Physics

Dissertation Examination Committee:

Carl M. Bender, Chair

Mark Alford

Erik Henriksen

Michael Ogilvie

Jung-Tsung Shen

Topics in PT-symmetric Quantum Mechanics and Classical systems

by

Nima Hassanpour

A dissertation presented to  
The Graduate School  
of Washington University in  
partial fulfillment of the  
requirements for the degree  
of Doctor of Philosophy

August 2018  
Saint Louis, Missouri

copyright by  
Nima Hassanpour  
2018

# Contents

List of Figures . . . . .	iv
List of Tables . . . . .	x
Acknowledgments . . . . .	xi
Abstract . . . . .	xiii
<b>1 Introduction . . . . .</b>	<b>1</b>
1.1 Overview of $\mathcal{PT}$ -Symmetric Systems . . . . .	2
1.2 Overview of $\mathcal{PT}$ -Symmetric Quantum Mechanics . . . . .	5
1.2.1 WKB Approximation . . . . .	6
1.2.2 Stokes Phenomenon . . . . .	9
1.2.3 Stokes Wedges of $\mathcal{PT}$ -Symmetric Quantum mechanics . . . . .	16
1.2.4 WKB solution approximation for energy eigenvalues of (1.32) . . . . .	19
1.2.5 Families of Solutions in $\mathcal{PT}$ -Symmetric Quantum mechanics . . . . .	21
1.2.6 Unitarity Problem of $\mathcal{PT}$ -Symmetric Hamiltonians . . . . .	23
1.3 Overview of Exceptional Points . . . . .	27
1.3.1 Exceptional points, Unbroken and Broken Regions of a $\mathcal{PT}$ -symmetric Hamiltonian . . . . .	30
<b>2 Time-independent Hamiltonian for any linear constant-coefficient evolution equation . . . . .</b>	<b>34</b>
2.1 Introduction . . . . .	35
2.2 Hamiltonian Description of the Damped Linear Harmonic Oscillator . . . . .	38
2.2.1 Prolle-Singer Procedure for Damped Harmonic Oscillator . . . . .	39
2.3 New Method of Derivation of Hamiltonian of Linear Constant-Coefficient Second-Order Differential Equation . . . . .	44
2.4 Hamiltonian for a Constant-Coefficient $n$ th-Order Equation . . . . .	54
2.4.1 Degenerate Frequencies . . . . .	55
2.5 Quantization . . . . .	56
2.6 Conclusion . . . . .	59
<b>3 Analytic Structure of Eigenvalue of Coupled quantum Systems . . . . .</b>	<b>60</b>
3.1 Introduction . . . . .	61

3.2	Analytic Continuation of Eigenvalue Problem for Harmonic Oscillator . . . .	65
3.3	Energy levels of the Coupled Harmonic Oscillator . . . . .	69
3.4	Partition Function for Zero-Dimensional Field Theories . . . . .	78
3.4.1	Interacting Quadratic Field Theory . . . . .	78
3.4.2	Interacting Sextic Field Theory . . . . .	80
3.5	Conclusions . . . . .	83
<b>4</b>	<b>Behavior of eigenvalues in a region of broken- <math>\mathcal{PT}</math> symmetry . . . . .</b>	<b>85</b>
4.1	Introduction . . . . .	86
4.2	Eigenvalue Behavior as $\epsilon \rightarrow -1$ . . . . .	90
4.2.1	Stokes wedges . . . . .	90
4.2.2	Numerical Behavior of the Eigenvalues as $\epsilon$ decreases below 0 . . . .	93
4.2.3	Asymptotic Study of the Eigenvalues near $\epsilon = -1$ . . . . .	94
4.3	Eigenvalue Behavior as $\epsilon \rightarrow -2$ . . . . .	101
4.4	Eigenvalue Behavior for $-4 < \epsilon < -2$ . . . . .	109
4.4.1	$\epsilon$ Slightly Below $-2$ . . . . .	111
4.4.2	Discrete and Continuous Eigenvalues . . . . .	113
4.4.3	Complex Coulomb Potential $\epsilon = -3$ . . . . .	115
4.4.4	Conformal Limit $\epsilon \rightarrow -4$ . . . . .	117
4.5	Conclusion . . . . .	119
<b>5</b>	<b>Series Solution of <math>\mathcal{PT}</math>-Symmetric Schrödinger Equation . . . . .</b>	<b>123</b>
5.1	Numerical Procedure . . . . .	124
5.2	Nodes and expectation values . . . . .	130
5.3	Numerical scheme applied to other potentials . . . . .	133
	<b>References . . . . .</b>	<b>138</b>

# List of Figures

1.1	The left box at $x = -a$ contains sink and the right one located at $x = a$ involves source. This system has $\mathcal{PT}$ -symmetry, since under the parity operator sink and source interchange their positions and sink transfers into source and vice versa with time operator and vice versa. . . . .	3
1.2	The solid lines show the Stokes lines of the Airy equation in complex plane. On the Stokes lines the solution of differential equation is oscillatory and is the linear combination of the dominant solutions on the Stokes wedges that are tangent at the Stokes lines. The curly line is the branch cut of WKB approximation to the Airy equation which can radiate from zero with arbitrary angle. . . . .	13
1.3	The solid lines shows the Stokes lines of the Airy equation and the dashed lines represent the anti-Stokes lines of this equation on which the imaginary part of the exponent of the WKB solution is zero. Therefore, the dominant and subdominant solution grow and decay with highest rate on these lines. . . . .	14
1.4	Stokes wedges for several values of $\epsilon$ are shown. As $\epsilon$ increases, the angle of Stokes wedges decreases and as soon as $\epsilon > 2$ whole the wedges rotate down the real axis. By allowing $\epsilon$ to approach infinity, the angle of wedge goes to zero. . . . .	18
1.5	Pattern of Stokes wedges for when $\epsilon = 1, 3,$ and $4$ . . . . .	22
1.6	A generic path on which the integral is define in complex plane. This path goes to infinity along the anti-Stokes line with helps the solution of Schrödinger goes to zero as fast as possible. But along every path in the shaded Stokes wedges, the integral and consequently $\mathcal{C}$ operator can be defined. . . . .	25
3.1	Regions (shaded) in the complex- $x$ pane where the boundary condition $\psi(x) \rightarrow 0$ is satisfied as $ x  \rightarrow \infty$ for the eigenvalue problem in (3.12). Note that the harmonic oscillator is actually <i>two</i> problems, one on the real axis and the other along the imaginary axis. . . . .	66
3.2	Sheet 1 of the complex Riemann surface of $E(g)$ in (3.27). On this sheet both the inner and outer square roots are positive when their argument are positive. Branch points are indicated by blue dots and branch cuts by red dashed lines. On this sheet $E(0) = \nu + \omega$ . . . . .	70

3.3	Sheet 2 of the complex Reimann surface of $E(g)$ in (3.27). On this sheet the inner square root in (3.27) is negative and the outer square root is positive when their argument are positive. On this sheet $E(0)$ is $\nu - \omega$ (assuming that $\nu - \omega$ is positive). . . . .	72
3.4	Sheet 3 of the complex Reimann surface of $E(g)$ in (3.27). On this sheet both the inner and outer square roots are negative when their arguments are positive and thus $E(0) = -\nu + \omega$ . . . . .	74
3.5	Sheet 4 of the complex Reimann surface of $E(g)$ in (3.27). On this sheet the inner square root is positive and while the outer square root is negative when their argument are positive. On this sheet $E(0) = \nu - \omega$ . . . . .	75
3.6	First four quartets of energy levels associated with the Hamiltonian (3.1). The quartets are labeled $(m, n)$ , and the quartets shown are for $m = 0, 1$ and have $n = 0, 1$ . We have chosen the values $\nu = 2$ and $\omega = 1$ and have plotted the values of $E(0)$ to scale. Note that each energy eigenvalue corresponds to the lowest such state on a different Reimann sheet. . . . .	77
4.1	Real eigenvalues of the Hamiltonian $H = p^2 + x^2(ix)^\epsilon$ plotted as function of the parameter $\epsilon$ . When $\epsilon \geq 0$ (the region of unbroken $\mathcal{PT}$ symmetry), the spectrum is real, positive, and discrete. However, as $\epsilon$ goes below 0 ( $\epsilon < 0$ is known as the region of <i>broken <math>\mathcal{PT}</math> symmetry</i> ) the real eigenvalues begin to merge pairwise and form complex-conjugate pair. When $-1 < \epsilon < 0$ , there are only a finite number of real positive eigenvalues and an infinite number of complex-conjugate pairs of eigenvalues. When $\epsilon \leq -0.57793$ , only one real eigenvalue survives and as $\epsilon$ approaches $-1^+$ , this real eigenvalue becomes infinite. The behavior of the complex eigenvalues in the region of broken $\mathcal{PT}$ symmetry is not shown in this graph and has not been explored until now. . . . .	88
4.2	Stokes wedges associated with the eigenvalue problem for the Hamiltonian $H = p^2 + x^2(ix)^\epsilon$ for eight values of $\epsilon$ . The location of center lines, the upper edges, and the lower edges of the Stokes wedges are given in (4.3)-(4.8). The left wedge is colored blue and the right wedge is colored red. As $\epsilon$ decreases, the wedges get wider and rotate upwards. At $\epsilon = -1$ the two wedges touch and fuse into one wedge. However, when $\epsilon$ goes below $-1$ , the sheets are again distinct; the left wedge rotate clockwise into sheet $-1$ and the right wedge rotates anticlockwise into sheet 1. . . . .	91

4.3	Eigenvalues of the Hamiltonian $H = p^2 + x^2(ix)^\epsilon$ plotted as functions of the parameter $\epsilon$ for $-1.1 < \epsilon < 0$ . This graph is a continuation of the graph in Fig. 4.3. As $\epsilon$ decreases below 0 and enters the region of broken $\mathcal{PT}$ symmetry, real eigenvalues (solid black lines) become degenerate and then form complex-conjugate pairs. The real parts of these pairs of eigenvalues (solid blue lines) initially decrease as $\epsilon$ decreases but blow up suddenly as $\epsilon$ approaches $-1$ . The real parts then decrease as $\epsilon$ decreases below $-1$ . The imaginary parts of the eigenvalue pairs (dashed red lines) remain finite and appear to suffer discontinuous jumps at $\epsilon = -1$ . However, a closer look shows that these dashed lines rapidly decay to 0 near $\epsilon = -1$ and then rapidly come back up to different values as $\epsilon$ passes through $-1$ . A blow-up of the region near $\epsilon = -1$ is given in Fig. 4.4. . . . . .	94
4.4	Detailed view of Fig. 4.3 showing the behavior of the eigenvalues of the Hamiltonian $H = p^2 + x^2(ix)^\epsilon$ plotted as functions of the parameter $\epsilon$ for $-1.05 \leq \epsilon \leq -0.95$ . There is one real eigenvalue for $\epsilon > -1$ (solid black line). The real parts of the complex eigenvalues (blue solid lines) and the real eigenvalue diverge at $\epsilon = -1$ . The complex eigenvalues occur in complex-conjugate pairs and the imaginary parts of the eigenvalues rapidly go to 0 at $\epsilon = -1$ . These behaviors are expressed quantitatively in (4.24). . . . .	95
4.5	Behavior of eigenvalues of the Hamiltonian $H = p^2 + x^2(ix)^\epsilon$ as the parameter $\epsilon$ winds around the exceptional point at $\epsilon = -1$ in a circle of radius 0.05 in the complex- $\epsilon$ plane. This singular point is an infinit-order exceptional point, and all of the complex eigenvalues analytically continue into one another as one encircles the exceptional point. The lines are shaded blue when $\text{Re}\epsilon > 0$ and red line $\text{Im}\epsilon < 0$ . The behavior of the imaginary parts of the eigenvalues (left panel) are easier to visualize because they exhibit a simple logarithmic spiral. The dot shows that the imaginary part of an eigenvalue (the eigenvalue shown in black in Figs. 4.3 and 4.4) vanishes (the eigenvalue is real) when $\text{Re}\epsilon > 0$ . However, as we wind in one direction the imaginary parts of the eigenvalues increases in a helical fashion and as we wind in the opposite direction the imaginary parts of the eigenvalues decrease in a helical fashion. As we pass the real- $\epsilon$ axis we pass through the values plotted on the red dashed line shown in Figs. 4.3 and 4.4. A shaded cylinder has been drawn to assist the eye in following this helix. The two helices intersect four times each time the singular point at $\epsilon = -1$ is encircled, and they intersect at $90^\circ$ intervals. If we begin at the dot, we see that the real parts of the eigenvalues increase as we rotate about $\epsilon = -1$ in either direction. Each time $\epsilon$ crosses the real axis in the complex- $\epsilon$ plane the curves pass through the values shown at the left and right edges of Fig. 4.4 . . . . .	100

4.6	First three complex-conjugate pairs of eigenvalues of the Hamiltonian $H = p^2 + x^2(ix)^\epsilon$ plotted as of Fig. 4.3. Note that the real parts of the eigenvalues coalesce to $-1$ and the imaginary parts coalesce to $0$ as $\epsilon$ approaches $-2$ . The results of a WKB calculation of these eigenvalues near $\epsilon = -2$ is given in (4.46). Note that the real parts of the eigenvalues near $\epsilon = -1.3$ , but they do not all cross at the same point as can be seen in Fig. 4.7 . . . . .	102
4.7	Detail of Fig. 4.6 showing the behavior of the real parts of the first six eigenvalues of the Hamiltonian $H = p^2 + x^2(ix)^\epsilon$ for $-1.4 \leq \epsilon \leq -1.2$ . The real parts of the eigenvalues cross almost at the same value of $\epsilon$ but the imaginary parts of the eigenvalues remain well separated. . . . .	104
4.8	Contour in the complex- $s$ plane for the complex Coulomb potential $\epsilon = -3$ . The contour comes in from $\infty$ parallel to the positive-real axis at an angle of $-2\pi$ in the center of the left Stokes wedge (right panel). Next, it loops around the origin in the positive direction (center panel). Finally, it goes back out to $\infty$ parallel to the positive-real axis at an angle of $2\pi$ in the center of the right Stokes wedge (left panel). The total rotation about the origin is $4\pi$ . . . . .	109
4.9	Eigenvalue contours in the complex- $s$ plane for the cases $\epsilon = -2.5$ and $\epsilon = -3.5$ . . . . .	110
4.10	Eigenvalues of the Hamiltonian $H = p^2 + x^2(ix)^\epsilon$ for $\epsilon = -2.0001$ and $-2.001$ . (The right panels are magnifications of the left panel.) The spectrum lies in the left-half complex plane and is partly continuous and partly discrete. The eigenvalues in the continuous part of the spectrum lie on a pair of complex-conjugate curves that radiate away from $-1$ and as we calculate more eigenvalues, the points on these curves become denser. The discrete part of the spectrum consists of eigenvalues lying on two complex-conjugate curves that are much closer to the negative-real axis. There is an elaborate structure near $\epsilon = -1$ , As $\epsilon$ goes below $-2$ , the eigenvalues move away from $-1$ ; specially, for $\epsilon = -2.0001$ the distance from $-1$ to the nearest eigenvalue is about $0.0005$ and for $\epsilon = -2.001$ the distance to the nearest eigenvalue is about $0.008$ . . . . .	112
4.11	Discrete and continuous parts of the spectrum of the $\mathcal{PT}$ -symmetric Hamiltonian $H = p^2 + x^2(ix)^\epsilon$ for the case $\epsilon = -2.6$ . The discrete eigenvalues (orange squares) occur in pairs the left-half complex plane. The continuous eigenvalues (blue dots) lie on two complex-conjugate pairs of curves in the right-half complex plane. As we decrease the cell size in the Arnoldi algorithm, the dots become dense on these curves. The continuous curves of eigenvalues originate slightly to the left of the origin. . . . .	114
4.12	Detail of Fig. 4.11 showing the elaborate near the origin in the complex-eigenvalue plane for $\epsilon = -2.6$ . . . . .	115

4.13	Absolute values of the the eigenfunction $\psi(t)$ for the discrete eigenvalue $-1.79 \pm 4.31i$ for $\epsilon = -2.6$ . The eigenfunctions satisfy homogeneous boundary conditions ar $\pm(1 - \eta)$ for $\eta = 0.01$ and look like bound-state eigenfunctions in the sense that the eigenfunctions decay to 0 exponentially fast at both boundary points. The left and right panels are interchanged under $t \rightarrow -t$ , which corresponds to a $\mathcal{PT}$ reflection. . . . .	116
4.14	Absolute values of the eigenfunctions for the continuum eigenvalues $-0.01 \pm 0.18i$ for $\epsilon = -2.6$ . These eigenvalues belong to the continuous spectrum. The indication that they are part of the continuous spectrum is that at one of the boundary points the eigenfunctions suddenly drop to 0 rather than decaying exponentially to 0. As in Fig. 4.13, the left and right panels are interchanged under $t \rightarrow -t$ , which corresponds to a $\mathcal{PT}$ reflection. . . . .	117
4.15	Eigenvalues for the Coulomb case $\epsilon = -3$ . These are no discrete eigenvalues and the continuum eigenvalues lie on four curves in the left-half complex plane. . . . .	118
4.16	Detail of the region around the origin in the complex eigenvalue plane of Fig. 4.15 for $\epsilon = -3$ . For this figure we have chosen $\eta = 0.999$ and have taken the very small cell size 0.00001. . . . .	120
4.17	Eigenspectrum for $\epsilon = -3.8$ . The continuous part of the spectrum (blue dots) lies on two complex-conjugate pairs of curves in the left-half plane and resembles that of the Coulomb case (see Fig. 4.15). The discrete part of the spectrum (orange squares) consists of complex-conjugate eigenvalues in the left-half plane and real eigenvalues on the positive-real axis. . . . .	121
4.18	Plot of the absolute value of the eigenfunction associated with the discrete real eigenvalue $E = 0.0804$ for $\epsilon = -3.8$ . . . . .	122
4.19	First three real eigenvalues of the Hamiltonian $p^2 + x^2(ix)^\epsilon$ plotted as functions of the parameter $\delta$ , where $\epsilon = -4 + \delta$ . The eigenvalues clearly approach 0 as $\delta \rightarrow 0$ and we see strong evidence that the eigenvalues vanish linearly with $\delta$ . . . . .	122
5.1	The value of $\text{Im } c$ plotted as a function of $E$ . The first few energy levels in the $N = 3$ theory appear as roots of $\text{Im } c$ . . . . .	125
5.2	$\text{Im } c$ in the $N = 7$ theory $\mathcal{PT}$ symmetric spectra. The upper left plot is for the wedges centered at $\theta = \pi/6$ and $\theta = 5\pi/6$ ; the upper right plot has wedges centered at $\theta = -\pi/18$ and $\theta = -17\pi/18$ ; the lower plot has wedges centered at $\theta = -5\pi/18$ and $\theta = -13\pi/18$ . . . . .	126
5.3	Eigenfunction for the third excited state for $N = 3$ plotted along the real axis. . . . .	129
5.4	Plot of $\text{Im } c$ for the $N = 1.1$ , $N = 1.5$ , and $N = 1.9$ theories. All three of these theories are in the $\mathcal{PT}$ broken region. In the first case there is only one eigenvalue, in the second case there are three real eigenvalues, and in the third case there are many real eigenvalues. In all cases the numerical method used here provides highly accurate results. . . . .	131

5.5	Plot of $\text{Im } c$ for the $N = 2.1$ and $N = 2.5$ theories. These theories are in the $\mathcal{PT}$ unbroken region. . . . .	132
5.6	Plot of $\text{Im } c$ for the $V = -x^4$ and $V = x^4$ . . . . .	134
5.7	Plot of $\text{Im } c$ for the anharmonic oscillator potential $V = x^4 \pm x^2$ . . . . .	136

# List of Tables

4.1	Comparison of the real parts of the eigenvalues of the different equation (4.26) at $\delta = 0.01$ with the asymptotic approximation in (4.46). The rate at which the accuracy increases with increasing $k$ is similar to the increase in accuracy of the standard WKB approximation to the eigenvalues of the quartic anharmonic oscillator [1]. . . . .	107
4.2	Comparison of the imaginary parts of the eigenvalues of the differential equation (4.26) at $\delta = 0.01$ with the asymptotic approximation in (4.46). . . . .	108
4.3	First three real discrete eigenvalues as a function of $\delta$ , where $\epsilon = -4 + \delta$ . All the eigenvalues approach 0 as $\delta \rightarrow 0$ . In fact, Fig. 4.19 indicates that they approach zero in a linear fashion. . . . .	119
5.1	Energy levels and $c$ values in the $N = 3$ theory. . . . .	128
5.2	Energy levels and $c$ values in the $N = 3$ theory. . . . .	130
5.3	Eigenvalue in the broken $\mathcal{PT}$ regime for noninteger value of $N$ . . . . .	133
5.4	Eigenvalue in the broken $\mathcal{PT}$ regime for noninteger value of $N$ . . . . .	134
5.5	Eigenvalues of the harmonic oscillator $V = x^2$ ( $N = 2$ ), the $\mathcal{PT}$ -symmetric quartic oscillator $V = -x^4$ ( $N = 4$ ), and the conventional anharmonic oscillator $V = x^4$ obtained by using the numerical methods described before. . . . .	135
5.6	Eigenvalues of the single-well ( $V = x^4 + x^2$ ) and double-well ( $V = x^4 - x^2$ ) quartic anharmonic oscillators obtained by using the numerical methods described. The numerical accuracy is excellent and is roughly the same for either oscillator. . . . .	136
5.7	This table shows that this numerical methods fail if the potential is not $\mathcal{PT}$ symmetric; that is, it is not a real function of the variable $iz$ . . . . .	137

# Acknowledgments

During my PhD study, I have had the great opportunity to work with my advisor Prof. Carl M. Bender who helped me to start exploring different areas of the exciting field of theoretical physics. I would like to express my sincere gratitude to Prof. Bender for his inspiration, guidance and continuous support. It was a great pleasure for me to have him as my advisor during my doctoral studies. I have benefited a lot from his knowledge, experience, priceless ideas and inspiring discussions.

I am grateful to all of the Department faculty members for their help and support. Particularly, I would like to thank Prof. Mark Alford and Prof. Michael Ogilvie for their helpful discussion. I also would like to thank Prof. Mehdi Golshani, and Prof. Mohammad Maleak who had great role in my scientific journey.

I am also grateful to my family. Their unconditional support is largely the reason that this PhD is completed in the United States. No words are sufficient to describe my parents' contribution to my life.

Nima Hassanpour

*Washington University in Saint Louis*

*August 2018*

to my parents

## ABSTRACT OF THE DISSERTATION

Topics in  $\mathcal{PT}$ -symmetric Quantum Mechanics and Classical systems

by

Nima Hassanpour

Doctor of Philosophy in Physics

Washington University in St. Louis, 2018

Professor Carl M. Bender, Chair

Space-time reflection symmetry, or  $\mathcal{PT}$  symmetry, first proposed in quantum mechanics by Bender and Boettcher in 1998 [2], has become an active research area in fundamental physics. This dissertation contains several research problems which are more or less related to this field of study. After an introduction on complementary topics for the main projects in Chap.1, we discuss about an idea which is originated from the remarkable paper by Chandrasekar *et al* in Chap.2. They showed that the (second-order constant-coefficient) classical equation of motion for a damped harmonic oscillator can be derived from a Hamiltonian having one degree of freedom. We gives a simple derivation of their result and generalizes it to the case of an  $n$ th-order constant-coefficient differential equation.

In Chap.3 we studied the analytical continuation of the coupling constant  $g$  of a coupled quantum theory. We get to this conclusion that one can, at least in principle, arrive at a state whose energy is lower than the ground state of the theory. The idea is to begin with the uncoupled  $g = 0$  theory in its ground state, to analytically continue around

an exceptional point (square-root singularity) in the complex-coupling-constant plane, and finally to return to the point  $g = 0$ . In the course of this analytic continuation, the uncoupled theory ends up in an unconventional state whose energy is lower than the original ground-state energy. However, it is unclear whether one can use this analytic continuation to extract energy from the conventional vacuum state; this process appears to be exothermic but one must do work to vary the coupling constant  $g$ .

$\mathcal{PT}$ -symmetric quantum mechanics began with a study of the Hamiltonian  $H = p^2 + x^2(ix)^\epsilon$ . When  $\epsilon \geq 0$ , this portion of parameter space is known as the region of unbroken  $\mathcal{PT}$  symmetry. The region of unbroken  $\mathcal{PT}$  symmetry has been studied but the region of broken  $\mathcal{PT}$  symmetry which is related to the negative  $\epsilon$  has thus far been unexplored. In Chap.4 we present a detailed numerical and analytical examination of the behavior of the eigenvalues for  $4 < \epsilon < 0$ . In particular, it reports the discovery of an infinite-order exceptional point at  $\epsilon = 1$ , a transition from a discrete spectrum to a partially continuous spectrum at  $\epsilon = 2$ , a transition at the Coulomb value  $\epsilon = 3$ , and the behavior of the eigenvalues as  $\epsilon$  approaches the conformal limit  $\epsilon = 4$ .

Finally in Chap.5 we devised a simple and accurate numerical technique for finding eigenvalues, node structure, and expectation values of  $\mathcal{PT}$ -symmetric potentials. The approach involves expanding the solution to the Schrödinger equation in series involving powers of both the coordinate and the energy. The technique is designed to allow one to impose boundary conditions in  $\mathcal{PT}$ -symmetric pairs of Stokes sectors. The method is illustrated by using many examples of  $\mathcal{PT}$ -symmetric potentials in both the unbroken- and broken- $\mathcal{PT}$ -symmetric regions.

# Chapter 1

## Introduction

Mathematics has been an inseparable part of physics since the appearance of modern physics. The entanglement of these two fields culminated by the advent of quantum mechanics at the beginning of twentieth century. It has been observed frequently that each of these fields causes a progress in the other one, which motivated us to dedicate this thesis to mathematical topics in the physical context. The research presented here concerns projects in both classical and quantum mechanics. They are more or less related to the significant role of Parity-Time ( $\mathcal{PT}$ ) symmetry, which although was observed before [3–11], it has been understood deeply recently [2, 12]. Most crucially, this theory claims that the Hermiticity condition usually imposed on quantum mechanical observables is a highly restrictive mathematical condition that can be replaced by the more physical condition of  $\mathcal{PT}$ -symmetry. This has been a driving factor for paradigm change over the last decade. In this thesis we aim to investigate the properties of some classical and quantum systems from a  $\mathcal{PT}$ -symmetric viewpoint and to study in depth features that are the direct result of this paradigm shift. In this chapter we introduce the basic ideas of  $\mathcal{PT}$ -symmetric systems and the concepts that play an important role to well understand of the theory

behind research projects of next chapters, like Stokes wedges, WKB approximation, and exceptional point.

## 1.1 Overview of $\mathcal{PT}$ -Symmetric Systems

The Hamiltonian of a physical system contains symmetries of the system and consequences evolution equation in both classical and quantum mechanics. In order to solve the evolution equation we must impose appropriate boundary conditions to describe the complete behavior of the system. We are interested in type of physical systems that have both parity ( $\mathcal{P}$ ) which is the left-right symmetry and time ( $\mathcal{T}$ ) reversal symmetry simultaneously. Under  $\mathcal{P}$ ,  $x \rightarrow -x$  and  $p \rightarrow -p$ , and under  $\mathcal{T}$ ,  $t \rightarrow -t$ ,  $x \rightarrow -x$ , and  $p \rightarrow -p$ . In addition to these properties time operators must have another feature which transforms  $i \rightarrow -i$  in complex plane and this is because of its nonlinearity.

Based on the choice of boundary condition, the physical systems are classified into closed or open system; that is, isolated or non-isolated. A closed system does not have interaction with its environment and in quantum mechanics it is described by *Hermitian* Hamiltonian, which is  $H^\dagger = H$ . The eigenvalues of a Hermitian Hamiltonian are always real and positive. As a consequence of these property, the Hermitian Hamiltonian is *unitary* which conserve the probability in time. But the isolated system is not physical and in real world a system always has interaction with its environment. Otherwise, it cannot be observed and measured, because measurement requires that the systems has contact with external world. Therefore, open systems are the ones that are physically realistic.



Figure 1.1: The left box at  $x = -a$  contains sink and the right one located at  $x = a$  involves source. This system has  $\mathcal{PT}$ -symmetry, since under the parity operator sink and source interchange their positions and sink transfers into source and vice versa with time operator and vice versa.

A closed system does not have exchange of energy with environment and therefore, the probability density  $\rho = \psi^* \psi$  is conserved. On the other hand, energy flows into or out of open system, like the sink (gain) and source (loss) box in Fig. 1.1 separately. Since there is flow of energy in each of these boxes the probability is not conserved any more. For the sink box the probability density increases by time and it decreases for the source box. A smart and simple way to make the probability conserved is to contact the sink and source boxes by a proper coupling constant. If the rate of gain and loss for both boxes are the same the coupled system can be in equilibrium and has zero net probability flux.

An interesting point about this coupled system is that it has  $\mathcal{PT}$  symmetry. Under time reversal operator  $\mathcal{T}$  loss and gain are replaced and under parity operator  $\mathcal{P}$  the coordinate of the boxes are swapped  $x \rightarrow -x$ . In spite of its simplicity, the classical system of coupled gain and loss has a significant role in a deeper understanding of  $\mathcal{PT}$  symmetry of physical systems without sophisticated mathematics [13,14].

Quantitatively, the Hamiltonian that describes the time evolution of the source box is  $H = [E_1] = [re^{-i\theta}]$  [15], where  $r > 0$  and  $0 < \theta < \pi$ . In this case  $ImE_1 < 0$  which means this box is not in equilibrium and its energy is decreasing. Similarly, for the box in the left side of Fig. 1.1 the Hamiltonian that describes the time evolution of the source is a  $1 \times 1$  matrix  $H = [E_2] = [re^{i\theta}]$ , that has a positive imaginary part  $ImE_2 > 0$ , and its energy increases. The whole system can be described by the  $2 \times 2$  matrix Hamiltonian

$$H = \begin{bmatrix} re^{-i\theta} & g \\ g & re^{i\theta} \end{bmatrix}, \quad (1.1)$$

which is not Hermitian. However it is  $\mathcal{PT}$ -symmetric, where the parity operator is given by the matrix

$$\mathcal{P} = \begin{bmatrix} 0 & 1 \\ 1 & 0 \end{bmatrix}, \quad (1.2)$$

which interchanges the two boxes, and the time operator reverses the time and  $i \rightarrow -i$  simultaneously. If the boxes are isolated, which means that  $g = 0$ , they cannot exchange energy with each other and the system is not in equilibrium. The energy in left box decays to zero and it grows to infinity in the right box. Therefore, the system does not have a real eigenvalue and it is in the  $\mathcal{PT}$ -broken region. However, if  $g$  has a magnitude in a certain domain, the two boxes can transfer energy continuously and system can equilibrate, and the system is in the unbroken region of  $\mathcal{PT}$ -symmetry. For the Hamiltonian in (1.1) the eigenvalues are real if  $g^2 > r^2 \sin^2 \theta$ . In this region the system is in equilibrium, the eigenstates oscillate and do not grow or decay exponentially.

As a conclusion of these simple examples, we understand that  $\mathcal{PT}$ -symmetric systems can be interpreted as nonisolated physical systems having balanced loss and gain, such systems can be considered as intermediate between open systems and closed systems. If the parameters of the system are adjusted to support a sufficiently rapid internal circulation, the system resembles a closed Hamiltonian system in equilibrium. We then say that the system has an unbroken  $\mathcal{PT}$ -symmetry, and thus it mimics a closed system. However, if the parameters of the system are varied to weaken the internal circulation, the system undergoes a transition to a broken  $\mathcal{PT}$ -symmetric phase, and it is no longer in equilibrium. The  $\mathcal{PT}$ -symmetric system thus behaves like an open quantum system, such as a scattering experiment. (The broken and unbroken regions and their transition to each other is discussed by detailed in section 1.3).

## 1.2 Overview of $\mathcal{PT}$ -Symmetric Quantum Mechanics

In this section we give a detailed explanation for mathematical bases of  $\mathcal{PT}$ -symmetric quantum mechanics. One important topic is the WKB approximation which leads to calculate the eigenvalues of a  $\mathcal{PT}$ -symmetric Hamiltonian. Since the purpose is to solve a differential equation with WKB approximation, we need to define the boundary conditions which the concept of Stokes wedge addresses this necessity and paves the way that the WKB method plays a crucial role in  $\mathcal{PT}$ -symmetric quantum mechanics. In addition, we introduce the  $\mathcal{C}$  operator and explain its important role in constructing the inner product and resolving the unitarity problem of  $\mathcal{PT}$ -symmetric Hamiltonians in Hilbert space.

### 1.2.1 WKB Approximation

WKB theory is a powerful tool to provide a global approximation for linear differential equation whose highest derivative is multiplied by a small parameter  $\epsilon$  [1]. This method is highly popular in physics, since the second-order derivative term in the Schrödinger equation has a small coefficient  $\hbar^2$ , and is quite suitable for applying the WKB method. Following the notation in [16, 17] we introduce a new parameter  $\eta = 1/\hbar$  instead of  $\hbar$ . Then the Schrödinger equation reads

$$\left(-\frac{d^2}{dx^2} + \eta^2 Q(x)\right) \psi(x, \eta) = 0, \quad Q(x) = V(x) - E \quad (1.3)$$

Without imposing any boundary condition at infinity, we assume that the solution of this equation has the form

$$\psi(x) = \exp \left[ \int_a^x \phi(x, \eta) dx \right] \quad (1.4)$$

where  $a$  is an arbitrary lower limit of integral, therefore

$$-\phi^2 - \phi' + \eta^2 Q = 0. \quad (1.5)$$

If we expand  $\phi$  in the powers of  $\eta$ ,

$$\phi = \phi_0(x, \eta)\eta + \phi_1(x, \eta) + \phi_2(x, \eta)\eta^{-1} + \dots, \quad (1.6)$$

where each  $\phi_j(x, \eta)$  approaches to a limit as  $\eta \rightarrow \infty$  for fixed  $x$ , then substituting it in the differential equation yields

$$-\left(\phi_0^2 \eta^2 + 2\phi_0 \phi_1 \eta + \phi_1^2 + 2\phi_0 \phi_2 + \dots + \phi_0' \eta + \phi_1' + \dots\right) + \eta^2 Q = 0 \quad (1.7)$$

as far as terms in  $\eta^2, \eta$ , and  $\eta^0$  are concerned. Since the equality holds for all  $x$ , the coefficient of each power of  $\eta$  must be zero, which gives

$$-\phi_0^2 + Q = 0, \quad 2\phi_0 \phi_1 + \phi_0' = 0 \quad \phi_1^2 + 2\phi_0 \phi_2 + \phi_1' = 0. \quad (1.8)$$

By solving these algebraic equations we obtain

$$\phi_0 = \pm \sqrt{Q}, \quad \phi_1 = -\frac{\phi_0'}{2\phi_0} = -\frac{1}{2} \log \phi_0. \quad (1.9)$$

Therefore the approximate solution for  $\psi$  up to order of  $\eta^0$  is given by

$$\psi(x)_\pm \sim \exp \left[ \int_a^x \left( \eta \phi_0 - \frac{1}{2} \log \phi_0 \right) dx \right] = Q^{-1/4} \exp \left[ \pm \eta \int_a^x \sqrt{Q} dx \right] \quad (1.10)$$

These two solutions are known as the WKB approximation. Linear independence of them allows us to write the general solution for Schrödinger equation as follows

$$\psi(x) \sim c_1 Q(x)^{-1/4} \exp \left( \eta \int_a^x \sqrt{Q(x)} dx \right) + c_2 Q(x)^{-1/4} \exp \left( -\eta \int_a^x \sqrt{Q(x)} dx \right) \quad (1.11)$$

for large  $\eta$ . As can be seen, this solution is not valid in the vicinity of turning points, where  $Q(x) = 0$ . In the Schrödinger equation, turning points occur when  $V(x) = E$ , which is the border between the classically allowed region ( $V(x) < E$ , *i.e.*,  $Q(x) < 0$ ) and classically forbidden region ( $V(x) > E$ , *i.e.*  $Q(x) > 0$ ). One can analyze this kind of

problem by replacing  $Q(x)$  with a polynomial function of  $x$ . For instance, in the case of first-order zeros,  $Q(x)$  can be replaced by  $(x - x_0)$ . Therefore, the Schrödinger equation reduces to the Airy function, and the global solution is obtained by matching the solutions in different regions.

WKB theory is a singular perturbation theory, because the highest derivative term is multiplied by a small parameter, and as this parameter goes to zero, the order of differential equation changes abruptly. Because of that the WKB series usually diverges, but on the other hand it can give extremely accurate results just by calculating the first several terms of the series. There are two conditions to ensure that the WKB solutions are valid on an interval. First, it is necessary that the expansion terms of  $\phi$  be an asymptotic series as  $\eta \rightarrow 0$  for all  $x$  in the interval, which requires the asymptotic relations

$$\phi_{n+1} \ll \eta \phi_n \quad (\eta \rightarrow \infty) \quad (1.12)$$

However, because the WKB approximation appears in the exponent, the previous condition is not sufficient to get a good approximation for  $\psi$ . To ensure the WKB series, where truncated at the term  $\eta^{-N+1}\phi_N$ , is a proper approximation of solution, the next term must be small relative to 1 for all  $x$  in the interval

$$\eta^{-N}\phi_{N+1} \ll 1 \quad (\eta \rightarrow \infty). \quad (1.13)$$

If this relation holds the relative error between  $\psi$  and WKB approximation is small.

Another important point about the WKB solutions concerns the domain of validity, which we need to analyze in the complex plane. The solutions of the Schrödinger equation are single-valued and well-defined all over the domain free from singularities of  $Q$ , yet the

approximation solutions clearly cannot be single-valued because the roots of  $Q$  appear in the denominator of the WKB solution. This demonstrates that the solution can only be valid in some restricted domain of the complex plane. This analysis is the topic of the next section, which relates to *Stokes wedges* and *Stokes phenomena*. These concepts have a crucial role in calculating the eigenvalues and eigenfunctions of the Schrödinger equation when the potential has  $\mathcal{PT}$  symmetry.

## 1.2.2 Stokes Phenomenon

To get a deeper understanding of WKB solutions and their domain of validity we need to expand our analysis into complex- $z$  plane. We use the symbols  $(a, z)$  and  $(z, a)$  to simplify the solution

$$(a, z) = Q^{-1/4} \exp \left[ \eta \int_a^z \sqrt{Q} dz \right], \quad (1.14)$$

$$(z, a) = Q^{-1/4} \exp \left[ -\eta \int_a^z \sqrt{Q} dz \right], \quad (1.15)$$

where  $a$  is a point in complex plane, and the path of integral does not cross the branch cuts. Hence the solution can be written as

$$\psi(z) = c_1(a, z) + c_2(z, a) \quad (1.16)$$

obviously,  $(a, z)$  and  $(z, a)$  are multivalued functions of the complex variable  $z$ . As we go around the branch point of  $Q$  the solutions  $(a, z)$  and  $(z, a)$  will not return to the original value. This means that, if a specific solution of  $\psi$  is approximated at  $z \neq 0$  by a WKB solution, it is not approximated by the same value at  $z \exp(2\pi i)$ . On the other hand,

the solution of the differential equation  $\psi(z)$  is entire and single valued on the whole region [18]. The Stokes Phenomenon is a powerful theory that reconciles this discrepancy. We explain the element of Stokes Phenomenon by using a simple example [17].

For the second-order differential equation  $\psi(z)'' = \eta\psi(z)$  the independent WKB solutions are

$$(0, z) = e^{\eta z}, \quad (z, 0) = e^{-\eta z}, \quad (1.17)$$

which in this case are also the exact solutions too. When  $|z|$  is large, there are three classes of approximations:

- If  $\text{Re}z = x > 0$ ,  $\psi(z) \sim e^{\eta z}$ ;
- If  $\text{Re}z = x < 0$ ,  $\psi(z) \sim e^{-\eta z}$ ;
- If  $\text{Re}z = x = 0$ , neither approximation is valid and  $\psi(z) = e^{\eta z} + e^{-\eta z}$ .

This means that for  $-\frac{1}{2}\pi < \arg z < \frac{1}{2}\pi$ ,  $(0, z)$  is the *dominant* solution and  $(z, 0)$  is the subdominant one. We label them by  $(0, z)_d$  and  $(z, 0)_s$ . Conversely, in the domain  $\frac{1}{2}\pi < \arg z < \frac{3}{2}\pi$ , the  $(0, z)$  is subdominant and  $(z, 0)$  is dominant. In this example the dominant and subdominant property are reversed by crossing the lines where  $\text{Re}z = 0$  which are positive and negative imaginary axis. In general these lines can be found by solving

$$\text{Re} \int_a^z \sqrt{Q(z)} dz = 0. \quad (1.18)$$

These lines are called *Stokes lines* and the dominant and subdominant property of the WKB solutions are reversed by crossing these lines. Along these lines the solution is

combination of the dominant WKB expressions on each side of the line. According to above definitions, we can rewrite the WKB solution as follows:

$$\begin{aligned}
\psi_{WKB} &= (0, z) + (z, 0) && \left( \arg z = -\frac{1}{2}\pi \right), \\
\psi_{WKB} &= (0, z)_d + (z, 0)_s && \left( -\frac{1}{2}\pi < \arg z < \frac{1}{2}\pi \right), \\
\psi_{WKB} &= (0, z) + (z, 0) && \left( \arg z = \frac{1}{2}\pi \right), \\
\psi_{WKB} &= (0, z)_s + (z, 0)_d && \left( \frac{1}{2}\pi < \arg z < \frac{3}{2}\pi \right),
\end{aligned}$$

which are without approximation. We can eliminate the subdominant term if it is smaller than the magnitude of error. Very near the Stokes line, both solutions must be considered;  $|e^{-\eta z}|$  is ignorable when it is subdominant, but as  $z$  approaches the Stokes line its value increases quickly to unity. This simple equation clearly explains the effect of Stokes lines.

In the next step we study the Airy equation in order to clarify how to resolve the apparently multivalued solutions due to the existence of a branch cut. The Airy equation reads

$$y''(z) = zy(z). \tag{1.19}$$

We eliminate the large parameter  $\eta$ , which in the WKB method is still applicable. The complete solution of the differential equation is written as

$$y(z) = c_1 \text{Ai}(z) + c_2 \text{Bi}(z), \tag{1.20}$$

which is entire and single valued. On the other hand, the WKB approximation made up of two expressions

$$(0, z) = z^{-\frac{1}{4}} e^{\frac{2}{3} z^{3/2}}, \quad (z, 0) = z^{-\frac{1}{4}} e^{\frac{2}{3} z^{-3/2}}. \quad (1.21)$$

Stokes lines appear when  $\text{Re}z^{3/2} = 0$ , which happens where  $\arg z = \pm\frac{1}{3}\pi, \pi$ . The solution  $(0, z)_d$  is dominant in domain  $-\frac{1}{3}\pi < \arg z < \frac{1}{3}\pi$ , and subdominant in the regions  $\frac{1}{3}\pi < \arg z < \pi$ , and  $-\pi < \arg z < -\frac{1}{3}\pi$ , which is written as  $(0, z)_s$ . The other solution has the opposite situation in those regions.

The branch cut can be insert at  $z = 0$  with arbitrary argument. If  $(0, z)$  is considered on the negative side of the branch cut with angle of  $\delta$ , by crossing the branch cut an angle of  $2\pi$  is added to the argument. Then if  $z = re^{i\delta}$  there would be a transfer between the two WKB solutions

$$(0, z)_d = \left( re^{i\delta+2\pi} \right)^{-1/4} e^{\frac{2}{3} (re^{i\delta+2\pi})^{3/2}} = -ir^{-1/4} e^{-i\delta/4} e^{-\frac{2}{3} (re^{i\delta})^{3/2}} = -i(z, 0)_d \quad (1.22)$$

Therefore, crossing the branch cut for the WKB solutions of the Airy leads to the following change

$$(0, z) \rightarrow -i(z, 0), \quad (1.23)$$

$$(z, 0) \rightarrow -i(0, z), \quad (1.24)$$

the dominancy or subdominancy being preserved in the process. If such a process are traced over the branch cut in a negative direction, the  $-i$  is replaced by  $+i$ . Based on the

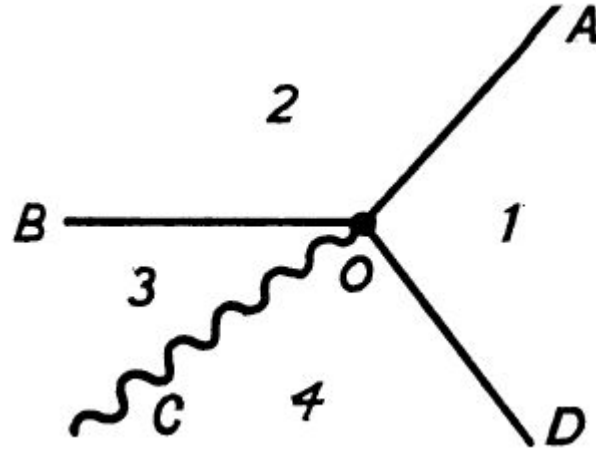


Figure 1.2: The solid lines show the Stokes lines of the Airy equation in complex plane. On the Stokes lines the solution of differential equation is oscillatory and is the linear combination of the dominant solutions on the Stokes wedges that are tangent at the Stokes lines. The curly line is the branch cut of WKB approximation to the Airy equation which can radiate from zero with arbitrary angle.

two rules that we have so far the  $(z, 0)_s$  solution in region 1 of Fig. 1.2 alters as follows

$$1 : (z, 0)_s, \quad 2 : (z, 0)_d, \quad 4 : (z, 0)_d, \quad 3 : i(0, z)_d \quad (1.25)$$

$$\text{if } \arg z = \pi : (z, 0) + i(0, z) \quad (1.26)$$

We need one more rule to determine the approximate solution for all  $\arg z$  that is introduced by the anti-Stokes line [17]. The anti-Stokes line is defined by

$$\text{Im} \int_a^z \sqrt{Q(z)} dz = 0. \quad (1.27)$$

Therefore the anti-Stokes lines of the Airy function are obtained by solving

$$\text{Im} z^{\frac{3}{2}} = 0. \quad (1.28)$$

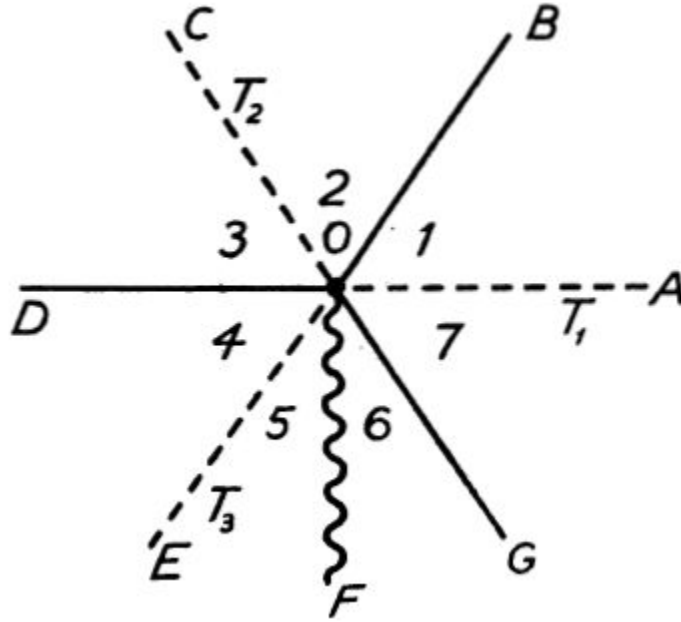


Figure 1.3: The solid lines shows the Stokes lines of the Airy equation and the dashed lines represent the anti-Stokes lines of this equation on which the imaginary part of the exponent of the WKB solution is zero. Therefore, the dominant and subdominant solution grow and decay with highest rate on these lines.

which leads to the lines with  $\arg z = 0, \pm \frac{2}{3}\pi$ , the lines that are bisector of the angles formed by two consecutive Stokes lines. Along anti-Stokes line the dominant solution has its maximum dominancy and subdominant solution attains its maximum subdominancy.

According to Fig. 1.3, if we have a subdominant solution in region 2, its coefficient must be changed discontinuously on angle  $\angle BOD$  in order to emerge on the next Stokes line  $OD$  with the appropriate coefficient, and appear as a dominant solution in the next domain 4. The discontinuous change does not violate the continuity of the WKB solution, because its magnitude is much smaller than the error allowed based on the dominant term. If dominant term does not appear in a domain, no change in the coefficient of subdominant term can take place. The alteration of coefficient of subdominant term is known

as *Stokes Phenomenon*, after its discoverer Sir George Stokes [19]. Quantitatively this theory asserts that as a subdominant function crosses an anti-stokes line, its new coefficient is expressed in terms of the original coefficient and the coefficient of the dominant term:

$$\text{New Subdominant Coefficient} = \text{Old Subdominant Coefficient} + C \times \text{Dominant Coefficient}, \quad (1.29)$$

where  $C$  is the *Stokes constant* according to the particular anti-Stokes line. If we track the subdominant solution in the negative direction  $+C$  will be replaced by  $-C$ . In other words the Stokes constant measures the lack of commutativity between the analytic continuations of the solutions and their asymptotic near infinity, when crossing the anti-Stokes line [20,21].

For the Airy equation there are three Stokes constants. We may prove that  $C_1 = C_2 = C_3 = i$  for all anti-Stokes lines following [17]. In order to do that let a general solution on the Stokes line  $OB$  be given by

$$\psi_{WKB} = A(0, z) + B(z, 0) \quad (1.30)$$

As can be seen in Fig. 1.3, based on the rules that have been explained we obtain the solution for regions 2 and 3 by tracking positively

$$\begin{aligned} 2 : A(0, z)_s + B(z, 0)_d , \\ 3 : (A + C_2 B)(0, z)_s + B(z, 0)_d . \end{aligned}$$

By crossing the anti-Stokes and Stokes lines negatively we get

$$1 : A(0, z)_d + B(z, 0)_s$$

$$7 : A(0, z)_d + (B - C_1 A)(z, 0)_s$$

$$6 : A(0, z)_s + (B - C_1 A)(z, 0)_d$$

$$5 : iA(z, 0)_s + i(B - C_1 A)(0, z)_d$$

$$4 : [iA - iC_3(B - C_1 A)](z, 0)_s + i(B - C_1 A)(0, z)_d$$

Where 1, 7, 6, 5, and 4 refer to regions in Fig. 1.3. By comparing the equation of  $(z, 0)$  and  $(0, z)$  in region 3 and 4, we obtain

$$B = iA - C_3 i(B - C_1 A) ,$$

$$A + C_2 B = i(B - C_1 A) .$$

The validity of these equations for all A, and B imply the following four equations

$$1 = -iC_3, \quad 0 = i + iC_3 C_1, \quad 1 = -iC_1, \quad C_2 = i, \quad (1.31)$$

yielding  $C_1 = C_2 = C_3 = i$ .

### 1.2.3 Stokes Wedges of $\mathcal{PT}$ -Symmetric Quantum mechanics

After comprehensive discussion on the Stokes phenomenon and Stokes wedges, we explain how these techniques can be applied in order to find the boundary conditions for a

$\mathcal{PT}$ -symmetric Hamiltonian, which finally leads to energy of the bound states. In this chapter and rest of this dissertation we consider a well-known class of Hamiltonians  $H = p^2 + x^2(ix)^\epsilon$  and attempt to find out the energy eigenvalues of this type of Hamiltonian for a different range of  $\epsilon$  [6]. Hence, the Schrödinger equation reads

$$-\psi''(z) + z^2(iz)^\epsilon \psi(z) = E\psi(z), \quad (1.32)$$

which is written in coordinate space, and we treat the variable  $z$  as a complex independent parameter.

Although we cannot solve this problem exactly we can find the asymptotic behavior of its solution by using the WKB approximation. As explained in the aforementioned section, we know that the exponential component of the asymptotic behavior of  $\psi(z)$  for large  $|z|$  has the form

$$\psi(z) \sim \exp \left[ \int^z ds \sqrt{Q(s)} \right], \quad (1.33)$$

where  $Q(z) = x^2(ix)^\epsilon - E$ . First we consider  $\epsilon = 0$  in order to identify the appropriate boundary condition to impose on  $\psi(z)$ . In this case we can see immediately that the WKB solutions behave roughly as  $\psi(z) \sim \exp \left( \pm \frac{1}{2} z^2 \right)$ . The requirement that the eigenfunctions must be square integrable implies that the negative sign must be chosen for a physical solution. In the complex plane we choose a solution that has negative real part so that it vanishes for large  $|z|$ . This solution is valid in the Stokes wedges with opening angle of  $\frac{\pi}{2}$  which their bisectors are positive and negative real axis. These two Stokes wedges create a  $\mathcal{PT}$ -symmetric region, as can be seen in Fig.1.4. The differential equation may be integrated along any path in the complex- $z$  plane as long as the ends of the path approach complex infinity inside the left wedge and the right wedge. But as

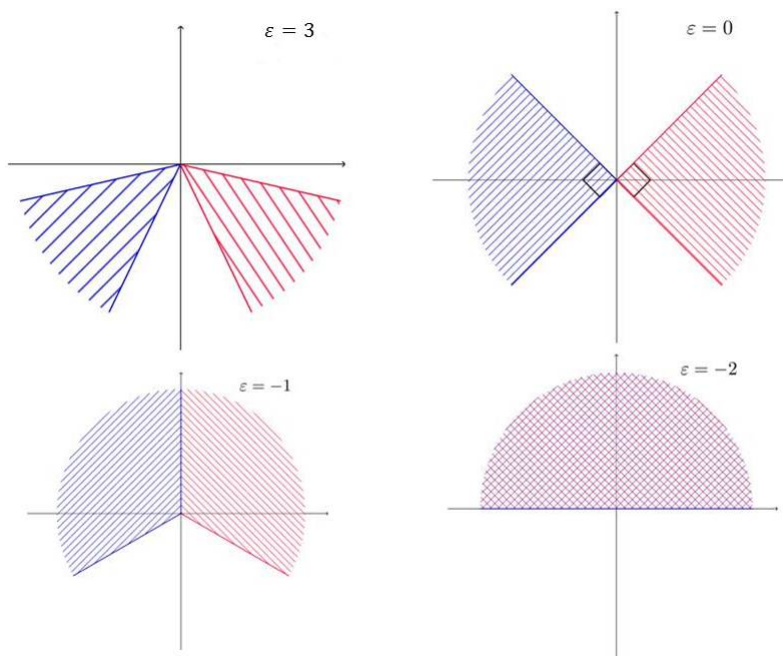


Figure 1.4: Stokes wedges for several values of  $\epsilon$  are shown. As  $\epsilon$  increases, the angle of Stokes wedges decreases and as soon as  $\epsilon > 2$  whole the wedges rotate down the real axis. By allowing  $\epsilon$  to approach infinity, the angle of wedge goes to zero.

mentioned before, the anti-Stokes line is the quickest path for decreasing of the subdominant solution. Therefore, it is reasonable to choose this as the default path for solving the Schrödinger equation, and run the numerical code along anti-Stokes line for finding eigenvalues.

As epsilon increases from zero, the logarithmic branch point appears at the origin  $z = 0$ . Without loss of generality, we may choose the branch cut to run up the imaginary axis from  $z = 0$  to  $i\infty$ . In this cut plane the solutions to the Schrödinger equation are single-valued. By reasoning that the real part of the exponent of WKB solution equals zero we can calculate the angles of Stokes wedges as functions of  $\epsilon$ . WKB analysis provides precise

formulas for the location of the center line of the Stokes wedges:

$$\begin{aligned}\theta_{right\ wedge, center} &= -\frac{\epsilon}{8+2\epsilon}\pi, \\ \theta_{left\ wedge, center} &= -\pi + \frac{\epsilon}{8+2\epsilon}\pi,\end{aligned}\tag{1.34}$$

the upper edges of Stokes wedges,

$$\begin{aligned}\theta_{right\ wedge, upper\ edges} &= \frac{2-\epsilon}{8+2\epsilon}\pi, \\ \theta_{left\ wedge, upper\ edges} &= -\pi - \frac{2-\epsilon}{8+2\epsilon}\pi,\end{aligned}\tag{1.35}$$

and the lower edges of Stokes wedges

$$\begin{aligned}\theta_{right\ wedge, lower\ edges} &= -\frac{2+\epsilon}{8+2\epsilon}\pi, \\ \theta_{left\ wedge, lower\ edges} &= -\pi + \frac{2+\epsilon}{8+2\epsilon}\pi.\end{aligned}\tag{1.36}$$

The opening angle of each of these wedges is  $\Delta = \frac{2\pi}{\epsilon+4}$ . As  $\epsilon$  is smaller than 2 the Stokes wedges contain real axis. As soon as it is larger than 2, the entire wedges rotate down below the real axis, which Fig. 1.4 shows this pattern clearly. When  $\epsilon \rightarrow \infty$ , opening angle  $\Delta$  goes to zero, and Stokes lines approach the negative imaginary axis.

#### 1.2.4 WKB solution approximation for energy eigenvalues of (1.32)

We have indicated the regions in which the wave function converge to in the complex plane. In order to do that we did not need the detailed solution of the associated Schrödinger

equation. It is sufficient to investigate the asymptotic behavior of the wave function as  $|z| \rightarrow \infty$  [6].

From the WKB approximation, one can determine the real eigenvalues associated with each potential by WKB quantization condition [22],

$$\int_{z_-}^{z_+} dz \sqrt{E_n - V(z)} = \left(n + \frac{1}{2}\right) \pi, \quad (1.37)$$

where  $z_-$  and  $z_+$  are the classical turning points which are found by  $E_n = V(z)$ . In the complex plane there can be more than two turning points. At this moment we consider the two turning points inside the  $\mathcal{PT}$ -Stokes wedges that are shown in Fig. 1.4. In those wedges the turning points are located at

$$z_- = E^{\frac{1}{\epsilon+2}} e^{i\pi\left(\frac{3}{2} - \frac{1}{\epsilon+2}\right)}, \quad z_+ = E^{\frac{1}{\epsilon+2}} e^{-i\pi\left(\frac{1}{2} - \frac{1}{\epsilon+2}\right)} \quad (1.38)$$

and they lie in the lower-half (upper-half) plane  $z$  plane when  $\epsilon > 0$  ( $\epsilon < 0$ ).

The path of integral for the leading-order WKB approximation (1.37) lies entirely in the lower-half plane when  $\epsilon > 0$ , and when  $\epsilon = 0$  (the case of harmonic oscillator) it coincides the real axis. However when  $\epsilon < 0$  the path is on the upper-half plane and crosses the branch cut on the positive imaginary axis. In this case there is no continuous path joining the turning points. Therefore, WKB fails as soon as  $\epsilon < 0$  [6]. When  $\epsilon \geq 0$ , we approximate the contour by one straight line from  $z_-$  to 0 and another one from 0 to  $z_+$ . After proper change of variable it gives

$$\left(\frac{1}{2} + n\right) \pi = 2 \cos\left(-\frac{\pi}{2} + \frac{\pi}{2 + \epsilon}\right) E^{\frac{\epsilon+4}{2\epsilon+4}} \int_0^1 dy \sqrt{1 - y^{\epsilon+2}} \quad (1.39)$$

We then evaluate the integral and solve the equation for  $E_n$

$$E_n \sim \left[ \frac{\Gamma\left(\frac{3}{2} + \frac{1}{\epsilon+2}\right) \sqrt{\pi} \left(n + \frac{1}{2}\right)}{\cos\left(-\frac{\pi}{2} + \frac{\pi}{2+\epsilon}\right) \Gamma\left(1 + \frac{1}{\epsilon+2}\right)} \right]^{\frac{2\epsilon+4}{\epsilon+4}} \quad (n \rightarrow \infty). \quad (1.40)$$

This approximation gives an accurate approximation for energy eigenvalues and shows that they are indeed real as  $\epsilon > 0$ . In Chap. 4 of this thesis we will investigate how eigenvalues behave as  $\epsilon$  varies in the range  $(-4, 0)$ .

### 1.2.5 Families of Solutions in $\mathcal{PT}$ -Symmetric Quantum mechanics

In general, for integer and noninteger  $\epsilon$ , the Schrödinger equation has more than two turning points. Hence, there can be many pairs of turning point, that can be chosen as the integral domain of WKB quantization. Those points can be written in the form

$$z_- = E_n^{\frac{1}{2+\epsilon}} e^{i\zeta}, \quad z_+ = E_n^{\frac{1}{2+\epsilon}} e^{i\gamma}, \quad (1.41)$$

where  $\zeta$  and  $\gamma$  are a specific angle of each turning point. With this definition (1.37) gives

$$\left(\frac{1}{2} + n\right) \pi = \left(e^{i\gamma} - e^{i\zeta}\right) E_n^{\frac{\epsilon+4}{2\epsilon+4}} \int_0^1 dy \sqrt{1 - y^{\epsilon+2}}, \quad (1.42)$$

Accordingly, the energy spectrum can be real only if  $\zeta = \pi - \gamma$ , which means that the turning points  $z_-$  and  $z_+$  must lie  $\mathcal{PT}$ -symmetrically to one another in order for the eigenvalues to be real.

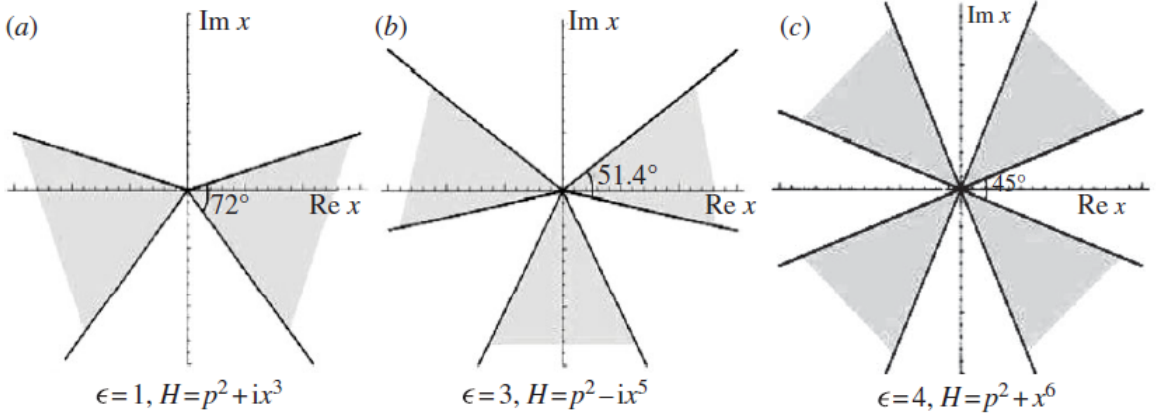


Figure 1.5: Pattern of Stokes wedges for when  $\epsilon = 1, 3,$  and  $4.$

Evaluating the integral in the above expression leads to

$$E_n(\gamma) \sim \left[ \frac{\Gamma\left(\frac{3}{2} + \frac{1}{\epsilon+2}\right) \sqrt{\pi} \left(n + \frac{1}{2}\right)^{\frac{2\epsilon+4}{\epsilon+4}}}{\cos(\gamma) \Gamma\left(1 + \frac{1}{\epsilon+2}\right)} \right] (n \rightarrow \infty), \quad (1.43)$$

with the consequence that the relationship between two families of spectra arising from different wedges with convergence angle  $\gamma$  and  $\gamma'$  is given by [23]

$$\frac{E_n(\gamma')}{E_n(\gamma)} = \left[ \frac{\cos(\gamma)}{\cos(\gamma')} \right]^{\frac{2\epsilon+4}{\epsilon+4}} \quad (1.44)$$

To clarify this point, the Stokes wedges of the Hamiltonian  $p^2 + x^2(ix)^\epsilon$  are shown in Fig. 1.5 for  $\epsilon = 1, 3, 4.$  When  $\epsilon = 1$  the turning points occur at  $E_n^{1/3} \exp(-i\pi/6), E_n^{1/3} \exp(-i5\pi/6),$  and  $E_n^{1/3} \exp(i\pi/2).$  Only the first two roots can be transferred to each other under  $\mathcal{PT}$  transformation. Also there is just one real spectrum for this potential via WKB calculation. For  $\epsilon = 3,$  the potential  $V(x) = -ix^5$  has five turning points at  $E_n^{1/5} \exp(i\pi/10), E_n^{1/5} \exp(i\pi/2), E_n^{1/5} \exp(-3i\pi/10), E_n^{1/5} \exp(-7i\pi/10),$  and  $E_n^{1/5} \exp(-11i\pi/10).$  In this case, there are two  $\mathcal{PT}$ -symmetric pairs of turning points,

the pair  $E_n^{1/5} \exp(i\pi/10)$ , and  $E_n^{1/5} \exp(-11i\pi/10)$  and the pair  $E_n^{1/5} \exp(-3i\pi/10)$  and  $E_n^{1/5} \exp(-7i\pi/10)$ . Each pair of turning points gives a distinct real spectrum, which are related by (1.44). Continuing this fashion, when  $\epsilon = 4$ , six possible turning points can be identified at angles  $0, i\pi/3, 2i\pi/3, 2i\pi, 4i\pi/3$ , and  $5i\pi/3$ , which leads to three pairs of  $\mathcal{PT}$ -symmetric turning points. The pair of shaded Stokes wedges on the lower-half plane and upper-half plane are symmetric respect to the real axis as is shown in Fig. 1.5. Therefore, their energy spectra are the same and these two pairs do not have different solutions, which means the potential  $V(x) = x^6$  has two distinct energy spectrum. Based on these observations, we conjecture the number of paths that can possibly lead to distinct real solutions is given by the number of pairs of noncontiguous  $\mathcal{PT}$ -symmetric Stokes wedges that is, Stokes wedges that are symmetric to the imaginary axis, while two pairs of Stokes wedges which are symmetric to the real axis may only be counted once [23]. In Chap. 5 we develop a numerical method that is capable of calculating the energy spectrum for different pairs of Stokes wedges of a potential. Our result also verifies this conjecture and makes it more reliable. The real spectrum of  $\mathcal{PT}$ -symmetric Hamiltonian has been proved [24,25] just for the pair of Stokes wedges that we considered in section 1.2.3 and the existence of a real spectrum for the other pairs of wedges needs similar rigorous proof.

## 1.2.6 Unitarity Problem of $\mathcal{PT}$ -Symmetric Hamiltonians

In conventional quantum mechanics, the Hermiticity of the Hamiltonian ensures the orthogonality and orthonormality of the eigenfunctions. This is based on the standard Hermitian inner product

$$(\psi, \phi) \equiv \int dx [\psi(x)]^* \phi(x) . \quad (1.45)$$

Also, according to the theory of linear operators on Hilbert spaces, the eigenfunctions of a Hermitian Hamiltonian are complete. Which means that any finite-norm vector  $\chi$  in the Hilbert space can be expressed as a linear combination of the eigenfunctions of  $H$ :

$$\chi = \sum_{n=0}^{\infty} a_n \psi_n. \quad (1.46)$$

This expression of this statement in coordinate space is the construction of the unit operator as a sum over the eigenfunctions

$$\sum_{n=0}^{\infty} [\psi_n(x)]^* \psi_n(y) = \delta(x - y) . \quad (1.47)$$

In addition to these properties, the time-evolution operator of the Hermitian Hamiltonian is unitary and it automatically preserves the inner product.

Based on analogy, if we naively extend the above features of  $\mathcal{PT}$ -symmetric Hamiltonians, then the associated inner product is

$$(\psi, \phi) \equiv \int_C dx [\psi(x)]^{\mathcal{PT}} \phi(x) = \int_C dx [\psi(-x)]^* \phi(x) , \quad (1.48)$$

where  $x$  is a variable in complex plane and  $C$  is a contour in the Stokes wedges shown in Fig. 1.6. It can be shown that pairs of eigenfunctions of  $H$  associated with different eigenvalues are orthogonal according to this definition for inner product [6]. However, this is not acceptable for formulating a valid quantum theory because the norm of a state is not necessary positive [26–28]. In order to resolve this problem we introduce a new operator  $\mathcal{C}$  which is a hidden inherent symmetry of  $\mathcal{PT}$ -symmetric Hamiltonian. To construct this operator in an unbroken  $\mathcal{PT}$ -symmetry region, first we mention the completeness

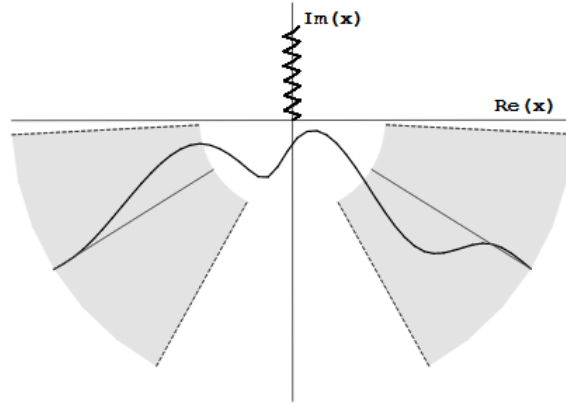


Figure 1.6: A generic path on which the integral is define in complex plane. This path goes to infinity along the anti-Stokes line with helps the solution of Schrödinger goes to zero as fast as possible. But along every path in the shaded Stokes wedges, the integral and consequently  $\mathcal{C}$  operator can be defined.

statement of  $\mathcal{PT}$ -symmetric quantum mechanics

$$\sum_n (-1)^n \phi_n(x) \phi_n(y) = \delta(x - y) , \quad (1.49)$$

which is a nontrivial result that has been confirmed numerically with high accuracy [29,30] and later its mathematical proof has been given in [31]. Also one can show that the algebraic sign of the  $\mathcal{PT}$  norm in (1.48) is  $(-1)^n$  for all  $n$  when  $\epsilon > 0$  [12]. This observation means that the Hilbert space is spanned by energy eigenstates, of which half have  $\mathcal{PT}$ -norm  $+1$  and half have  $\mathcal{PT}$ -norm  $-1$ . Because the norm has a probabilistic interpretation in conventional quantum mechanics, certainly negative probability raises an obstacle. This situation is similar to the problem which Dirac encountered in formulating the wave equation in relativistic quantum mechanics [32].

The problem of an indefinite norm can be solved by physical interpretation of the negative norm states. We observe that for any  $\mathcal{PT}$ -symmetric Hamiltonian there is a hidden symmetry, which the number of positive norm and negative norm eigenfunctions are equal. We introduce operator  $\mathcal{C}$  to describe this symmetry. This operator is constructed in terms of the energy eigenstates of the Hamiltonian. In position space the operator  $\mathcal{C}$  is

$$\mathcal{C}(x, y) = \sum_n \phi_n(x) \phi_n(y) \quad (1.50)$$

and it is easy to verify that

$$\int dy \mathcal{C}(x, y) \mathcal{C}(y, z) = \delta(x - z) , \quad (1.51)$$

which means that  $\mathcal{C}^2 = 1$ . Although  $\mathcal{P}^2 = 1$  too,  $\mathcal{P}$  and  $\mathcal{C}$  are not identical. The parity operator is real, and  $\mathcal{C}$  is complex. Also these two operators do not commute.

With this operator we define a new inner product which has positive definite norm

$$(\psi, \phi) \equiv \int_{\mathcal{C}} dx [\mathcal{CPT}\psi(x)] \phi(x) . \quad (1.52)$$

This inner product is phase independent and conserved in time space. The inner  $\mathcal{CPT}$  product generates positive norms because the  $\mathcal{C}$  operator multiplies the negative-norm eigenstates by a factor of  $-1$ . Therefore, in terms of the new inner product, the completeness condition reads

$$\sum_n \phi_n(x) [\mathcal{CPT}\phi_n(y)] = \delta(x - y) , \quad (1.53)$$

The operator  $\mathcal{C}$  does not appear in Hermitian quantum mechanics. For example if we set the parameter  $\epsilon$  to zero in the potential  $V(x) = x^2(ix)^\epsilon$ , the  $\mathcal{C}$  operator becomes identical

to  $\mathcal{P}$  in this limit. Hence,  $\mathcal{CPT}$  is reduced to  $\mathcal{T}$ , which means that the  $\mathcal{CPT}$  symmetry of a Hamiltonian collapses to the well-known Hermiticity condition because  $\mathcal{T}$  takes the complex conjugacy. There are several important remarks about  $\mathcal{C}$  operator

- The inner product which was defined above is path independent and different choices of contour do not affect the result of integral.
- As long as the  $\mathcal{CPT}$  symmetry is not spontaneously broken, the eigenvalues of the observable are real.
- According to the Dirac Hermiticity ansatz, the eigenvector and eigenvalues of the Hamiltonian are determined and the inner product is defined beforehand. In contrast, the inner product in  $\mathcal{PT}$ -symmetric quantum mechanics depends on the Hamiltonian itself. One must find the eigenstates of  $H$ , in order to find the associate inner product and Hilbert space.
- Calculating the  $\mathcal{C}$  operator is a complicated procedure that in most of the cases finding the exact solution is impossible [33–42], and it needs to be calculated by perturbation analysis. To do so, the process starts from the algebraic equations which are inherent into the symmetry of the Hamiltonian

$$[\mathcal{C}, \mathcal{PT}] = 0, \quad \mathcal{C}^2 = 1, \quad [\mathcal{C}, H] = 0 \quad (1.54)$$

### 1.3 Overview of Exceptional Points

Singularities of functions describing analytically observable quantities have always been in the scrutiny of theoretical investigation. For instance, the measured cross sections are

usually associated with pole terms in the complex-energy plane of the scattering amplitude [43]. Another example is the pattern of spectra when plotted versus an complex coupling. It usually shows the phenomenon of level repulsion, often associated with quantum chaos [44]. When such spectra are continued into the complex plane of the coupling constant, one encounters a different type of singularity where two separated levels are connected by a square-root branch point. If for a real strength parameter the Hamiltonian is Hermitian, the branch points always occur at complex parameter values, and continuously deform a Hermitian Hamiltonian into non-Hermitian one. As a consequence, the well-known properties associated with degeneracy of Hermitian operators are no longer valid. These singularities have been called *exceptional points* (EPs) by Kato [45] for the first time.

The physical significance of EPs was recognized in an early paper by Berry [46] based on the observation by Pancheratnam [47], in which the specific algebraic property of the dielectric tensor (it cannot be diagonalized) brings about particular physical effect that has been explained in great detail in [48] for a particular optical system. Optical systems constitute one major realm where the effects of EPs have been observed frequently. Yet, originating from a coupling-dependent eigenvalue problem EPs naturally occur and can give rise to dramatic effects in many physical problems, such as mechanics, electromagnetism, atomic and molecular physics, quantum phase transition, quantum chaos, and so on.

As a simple example that illustrate the importance of EPs, consider the following two by two matrix

$$M_0 = \begin{bmatrix} a & 0 \\ 0 & b \end{bmatrix}, \quad (1.55)$$

where its discrete eigenvalues are  $a$ , and  $b$ . Now we replace zeros by  $\epsilon$ , which is a complex variable:

$$M = \begin{bmatrix} a & \epsilon \\ \epsilon & b \end{bmatrix}. \quad (1.56)$$

In this case the eigenvalues  $\lambda_{\pm}$  are a functions of  $\epsilon$ ,

$$\lambda_{\pm}(\epsilon) = \frac{1}{2} \left( a + b \pm \sqrt{(a - b)^2 + 4\epsilon^2} \right), \quad (1.57)$$

and branch points (or EPs) of  $\lambda_{\pm}$  are located at  $\epsilon = \pm i/2(a - b)$  on the imaginary axis. Suppose that  $\lambda_{+}$  stays on the principal Riemann sheet. In this case  $\lambda_{+} = a$  at  $\epsilon = 0$ . By encircling the branch point at  $\epsilon = i/(a - b)/2$  we go into the next Riemann sheet on which the eigenvalue is  $\lambda_{-}$ . Now if we set  $\epsilon = 0$  the eigenvalue has a magnitude of  $b$ . As we encircle the other branch point on the negative part of imaginary axis, we come back to the principal sheet and the eigenvalue is  $\lambda_{+}$  again. This example shows how the discrete eigenvalues of the matrix  $M_0$  can be connected by analytic continuation of  $M$ 's eigenvalues into the complex plane which are evaluated on different Riemann sheets.

Although this procedure is just an abstract example, EPs have an undeniable role in physical phenomena, and more remarkably; theirs effect have been observed in laboratory recently [49,50].

### 1.3.1 Exceptional points, Unbroken and Broken Regions of a $\mathcal{PT}$ -symmetric Hamiltonian

Exceptional points and  $\mathcal{PT}$  symmetry quantum mechanics have a strong tie together. Here we discuss how the nature of a  $\mathcal{PT}$ -symmetric Hamiltonian comprises the concept of exceptional points. A  $\mathcal{PT}$ -symmetric Hamiltonian is conserved under parity and time operators simultaneously [6]

$$H = H^{\mathcal{PT}} . \quad (1.58)$$

The  $\mathcal{P}$  and  $\mathcal{T}$  are reflection operators, so their square is identity  $\mathcal{P}^2 = \mathcal{T}^2 = \mathbb{1}$ . Also the parity and time operators commute:

$$\mathcal{PT} - \mathcal{TP} = 0 , \quad (1.59)$$

which gives  $(\mathcal{PT})^2 = \mathbb{1}$ . Based on this equation and the definition of  $\mathcal{PT}$ -symmetry transformation of the Hamiltonian  $H^{\mathcal{PT}} = (\mathcal{PT})H(\mathcal{PT})$ , we can conclude that a  $\mathcal{PT}$ -symmetric Hamiltonian commutes with parity and time operators simultaneously

$$H(\mathcal{PT}) - (\mathcal{PT})H = 0. \quad (1.60)$$

The subtle point of this equation is related to time-reversal operator. Since it is nonlinear, the eigenfunction of the Hamiltonian  $H$  may or may not be the eigenfunction of  $\mathcal{PT}$  operator. To see this we assume that  $\psi$  is an eigenfunction of  $H$ . Therefore,

$$H(\mathcal{PT})\psi = (\mathcal{PT})H\psi \rightarrow H(\mathcal{PT})\psi = E^*(\mathcal{PT})\psi , \quad (1.61)$$

which means that  $\mathcal{PT}\psi$  is also an eigenfunction of  $H$ . In case of real eigenenergy we get  $\mathcal{PT}\psi = \alpha\psi$ , and multiplying both sides by  $\mathcal{PT}$ , we find that  $\alpha$  is just a phase  $\alpha = e^{i\theta}$ . But for the complex eigenenergy  $\mathcal{PT}\psi \neq \alpha\psi$  and the Hamiltonian and  $\mathcal{PT}$  operators cannot have the same eigenfunction. This means that although the Hamiltonian has  $\mathcal{PT}$ -symmetry the solutions of the Schrödinger equation may not contain this symmetry. In our case, this happens when the eigenvalues becomes complex and as a result the eigenfunctions do not have  $\mathcal{PT}$  symmetry any more. If both the Hamiltonian and  $\mathcal{PT}$  operator have a common eigenfunction, it is said that we are in the region of *unbroken*  $\mathcal{PT}$ -symmetry. As the eigenvalues become complex we enter into the *broken*  $\mathcal{PT}$ -symmetry region. The exceptional point signifies the moment that this phase transition occurs.

As a simple example, we consider the following  $2 \times 2$   $\mathcal{PT}$ -symmetric Hamiltonian [51],

$$H_{\mathcal{PT}} = \begin{bmatrix} e - i\frac{\gamma}{2} & \omega \\ \omega^* & e + i\frac{\gamma}{2} \end{bmatrix}, \quad (1.62)$$

which is invariant under time reversal that appears as the complex-conjugate operator and parity, which is represented by the  $\sigma_x$  matrix. Next we calculate eigenvalues of this matrix

$$\lambda_{\pm} = e \pm \frac{1}{2}\sqrt{4|\omega|^2 - \gamma^2}, \quad (1.63)$$

as  $\gamma < \pm\sqrt{4|\omega|^2}$  the two eigenvalues are real. At  $\gamma = \pm\sqrt{4|\omega|^2}$  they collapse to  $\lambda = e$ , and with further increase of  $\gamma$ ,  $\mathcal{PT}$ -symmetry breaking occurs and  $\lambda_{\pm} = e \pm \frac{i}{2}\sqrt{\gamma^2 - 4|\omega|^2}$ .

This simple idea was applied to observe the  $\mathcal{PT}$ -phase transition in optical physics for the first time. There are two reasons that optics offers a particularly fertile ground for EPs [52]: On one hand, the formal equivalence between the quantum-mechanical Schrödinger

equation and the optical wave equation; on the other hand, the possibility to manipulate loss and gain with a complex refractive index distribution  $n_0 + n_R(x) + in_I(x)$ , where  $n_0$  represents a constant background,  $n_R(x)$  is the real index profile of structure, and  $n_I(x)$  stands for gain and loss terms [53–55]. The real part of index is an even function of position  $n_R(x) = n_R(-x)$  and the imaginary part is odd i.e.,  $n_I(x) = -n_I(-x)$ , which satisfy the  $\mathcal{PT}$ -symmetry condition for the potential of Hamiltonian  $V(x) = V^*(-x)$  [56]. In addition to optical physics, there are other areas of physics where EPs play an important role, which we mention briefly.

### **Microwave Cavity**

Observation of transferring between two eigenvalues by encircling of the square-root branch point was accomplished in a microwave cavity for the first time [57]. In this experiment the complex eigenvalue was implemented by two real parameters and many properties of the EP such as fourfold encirclement, and phase transition were measured. A recent experiment [58] provides the direct proof of  $\mathcal{PT}$ -symmetry phase transition and shows that it is not reciprocal. This experiment used two coupled microwave resonators which simulate the gain/loss system. Other experiments with microwave cavities are discussed in [59,60], where the effects of EPs feature prominently.

### **Quantum Phase transition and Chaos**

The Lipkin model is a toy model which often used to study the quantum phase transition [61–63]. The interaction term reduces or increases the energy of Fermion pair between

two levels.

$$H(\lambda) = J_z + \frac{\lambda}{N} (J_+^2 + J_-^2) \quad (1.64)$$

where  $J_z, J_{\pm}$  are the  $N$ -dimensional representation of the  $SU(2)$  operators. A phase transition can occur if  $\lambda > 1$ , and by approaching to thermodynamic limit ( $N \rightarrow \infty$ ) it moves to  $\lambda = 1$ . If  $\lambda < 1$ , we are in the *normal* phase and we do not have singularity. In the *deformed* phase  $\lambda > 1$ , the symmetry is broken and even and odd numbers  $k$  of the  $E_k$  become degenerate. In this procedure EPs have a significant role [64,65]. A perturbation changes the pattern of EPs and also the spectrum. The concurrence of chaos and high density of EPs, which shows the region of phase transition, can be seen clearly, while the model remains robust outside the critical region for reasonable amplitude of perturbation.

In addition these physical phenomena, the role of EPs can be found in atomic physics, especially on Feshbach resonance. Also it has strong effect on behavior of laser system as well as open quantum systems. In Chap. 3, we discuss the EPs of two coupled harmonic oscillators, and investigate how they can affect the ground-state energy. Moreover we expand this model to quantum field theory. Accordingly we study different potentials, to discover the role of EPs on vacuum-state energy.

## Chapter 2

# Time-independent Hamiltonian for any linear constant-coefficient evolution equation

*This chapter contains the materials published in a paper [\[66\]](#), which represents work performed by me under the supervision of my advisor, C. M. Bender.*

## 2.1 Introduction

It seems unlikely that the equation for the damped classical harmonic oscillator

$$\ddot{x} + \alpha \dot{x} + \lambda x = 0, \quad (2.1)$$

a dissipative system, could be derived from a Hamiltonian. This is because  $E = \frac{1}{2}\dot{x}^2 + \frac{1}{2}\lambda x^2$ , the standard expression for the total energy, is not conserved for  $\alpha \neq 0$ . Indeed, it satisfies the equation

$$\frac{d}{dt} \left( \frac{1}{2}\dot{x}^2 + \frac{1}{2}\lambda x^2 \right) = -\alpha \dot{x}^2 \quad (2.2)$$

showing that it decreases with time. So, one might think that (2.1) cannot be derived from a time-independent Hamiltonian. Actually, it was shown [67–69] that the time-independent Hamiltonian for a damped harmonic oscillator is only possible when the rate of dissipation is equal to the mass or coefficient of acceleration term.

Nonetheless, Bateman [70] made the remarkable observation that if one appends the time-reversal oscillator equation with undamping (gain) instead of damping,

$$\ddot{y} - \alpha \dot{y} + \lambda y = 0 \quad (\alpha > 0), \quad (2.3)$$

then even though the two oscillators are independent and noninteracting, the two equations of motion (2.1) and (2.3) can be derived from the time-independent quadratic Hamiltonian

$$H = pq + \frac{\alpha}{2}(yq - xp) + \left(\lambda - \frac{\alpha^2}{4}\right)xy. \quad (2.4)$$

The two oscillator equations follow directly from Hamiltonian's equations of motion

$$\dot{x} = \frac{\partial H}{\partial p} = q - \frac{\alpha}{2}x, \quad (2.5)$$

$$\dot{y} = \frac{\partial H}{\partial q} = p + \frac{\alpha}{2}y, \quad (2.6)$$

$$\dot{p} = -\frac{\partial H}{\partial x} = \frac{\alpha}{2}p - \left(\lambda - \frac{\alpha^2}{4}\right)y, \quad (2.7)$$

$$\dot{q} = -\frac{\partial H}{\partial y} = -\frac{\alpha}{2}q - \left(\lambda - \frac{\alpha^2}{4}\right)x. \quad (2.8)$$

To derive (2.1) we differentiate (2.5) with respect to  $t$ , eliminate  $\dot{q}$  by using (2.8), and eliminate  $q$  by using (2.5). Similarly, to derive (2.3), we differentiate (2.6) with respect to  $t$ , eliminate  $\dot{p}$  by using (2.7), and eliminate  $p$  by using (2.6).

The Hamiltonian (2.4) is  $\mathcal{PT}$  symmetric; under parity reflection the oscillator with loss and gain are interchanged,

$$\mathcal{P} : x \rightarrow y, \quad y \rightarrow x, \quad p \rightarrow q, \quad q \rightarrow p, \quad (2.9)$$

and under time reversal  $T$  the signs of the momenta are reversed,

$$\mathcal{T} : x \rightarrow x, \quad y \rightarrow y, \quad p \rightarrow -p, \quad q \rightarrow -q. \quad (2.10)$$

The  $\mathcal{PT}$  symmetry of  $H$  in (2.4) and the success of Batman's strategy depend crucially on the gain and loss terms in (2.1) and (2.3) being exactly balanced. As a consequence of the gain/loss balance, the system possesses a conserved quantity, namely the value of  $H$ . However, the energy has the complicated form (2.4) and is not simple sum of kinetic and potential energies.

recently it was shown [71] that the equation of motion (2.1) of the damped oscillator can be derived from a (non-quadratic) time-independent Hamiltonian depending on only a *single canonical pair*  $(x, p)$ . This remarkable result was proved by using a modification of the *Prelle-Singer method* approach to identify integrals of motion of dynamical system, which explained by detailed in Sec. 2.2.

In [71] different forms of the Hamiltonian were given depending on whether the system was overdamped, underdamped, or critically damped. In particular, for the overdamped case  $(\alpha/2 > \lambda)$  the Hamiltonian takes the unconventional form

$$H = Axp + Bp^\delta, \quad (2.11)$$

where  $A, B$  and  $\delta$  are constants that we will specify later. Different functional forms were given for the other cases in order to have a real Hamiltonian. However, since this is not a concern for us, the functional form of (2.11) serves for all cases (apart from an obvious modification in the case of critical damping).

In addition to that, we show how to construct the Hamiltonian for an arbitrary homogeneous linear constant-coefficient differential equation of *any* order with new method. First, we do so for the second-order equation (2.1) and we demonstrate the procedure for a general third-order equation. An interesting special case of such an equation is the equation that describe the nonrelativistic self-acceleration of charged oscillator particle and it is quite remarkable that even though there are runaway modes, the energy of such a system is conserved. Then, we generalize our procedure to an arbitrary  $n$ th-order

constant-coefficient equation. In the last section we discuss about the problem of quantization and we show that quantizing the classical Hamiltonian is quite difficult in this procedure.

## 2.2 Hamiltonian Description of the Damped Linear Harmonic Oscillator

Counterintuitively, time independent Hamiltonian for dissipative equation with constant coefficient exists [71]. Naturally, it was believed that the damped linear harmonic oscillator

$$\ddot{x} + \alpha\dot{x} + \lambda x = 0 , \tag{2.12}$$

can only possess a time dependent Hamiltonian [72–76] which is  $H = (1/2)p^2e^{-\alpha t} + (\lambda/2)x^2e^{\alpha t}$  and consequently the Lagrangian  $L = e^{\alpha t}((1/2)\dot{x}^2 - (\lambda/2)x^2)$ . For the past several decades there has been a number of attempts to quantize the damped linear harmonic oscillator [77–81] from different points of view, but it appears that the problem still eludes a completely satisfactory resolution. Obviously, the major conceptual difficulty was the lack of time independent Hamiltonian formalism. What made this formalism possible is a method called the modified Prolle-Singer approach, which identifies integral of motion and integrability of dynamical systems [82–84]. This was the main point that interested us for further research on this topic. We rederive almost the same result using a completely different method; this is the content of this chapter. To be familiar with the Prolle-Singer procedure, in the next section we give a detailed calculation of the time independent Hamiltonian for the linear damped harmonic oscillator.

## 2.2.1 Prelle-Singer Procedure for Damped Harmonic Oscillator

We begin with this assumption that the (2.12) admits a first integral  $I(t, x, \dot{x}) = C$ , with  $C$  constant, so that the total differential becomes

$$dI = I_t dt + I_x dx + I_{\dot{x}} d\dot{x} = 0 , \quad (2.13)$$

where each subscript denotes partial differentiation with respect to that variable. Rewriting (2.12) in the form of  $\phi dt - d\dot{x} = 0$  with  $\phi(x, \dot{x}) = -(\alpha\dot{x} + \lambda x)$  and adding a null term  $S(t, x, \dot{x})\dot{x}dt - S(t, x, \dot{x})dx$ , we obtain

$$(\phi + S\dot{x}) dt - Sdx - d\dot{x} = 0 . \quad (2.14)$$

Hence, for the solutions the 1-forms (2.12) and (2.14) must be proportional. Multiplying (2.14) by the factor  $R(t, x, \dot{x})$  which acts as the integrating factor for (2.14), we get

$$dI = R(\phi + S\dot{x}) - RSdx - Rd\dot{x} = 0 . \quad (2.15)$$

Comparing (2.13) with (2.14) we get the relations

$$I_t = R(\phi + S\dot{x}), \quad I_x = -RS, \quad I_{\dot{x}} = -R . \quad (2.16)$$

Applying the compatibility equations,  $I_{tx} = I_{xt}$ ,  $I_{t\dot{x}} = I_{\dot{x}t}$ , and  $I_{\dot{x}x} = I_{x\dot{x}}$  on the (2.16) provides us

$$S_t + \dot{x}S_x + \phi S_{\dot{x}} = -\phi_x + \phi_{\dot{x}}S + S^2 , \quad (2.17a)$$

$$R_t + \dot{x}R_x + \phi R_{\dot{x}} = -(\phi_{\dot{x}+S})R , \quad (2.17b)$$

$$R_x - SR_{\dot{x}} - RS_{\dot{x}} = 0 . \quad (2.17c)$$

With solving (2.17a)-(2.17c), one can obtain expressions for  $S$  and  $R$ . It may be noted that any set of special solutions  $(S, R)$  is sufficient for our purpose. From knowing them the integral of motion  $I(t, x, \dot{x})$  can be deduced via the relation

$$I = I_1 - I_2 - \int \left[ R + \frac{d}{d\dot{x}} (I_1 - I_2) \right] d\dot{x} , \quad (2.18)$$

where

$$I_1 = \int R(\phi + \dot{x}S) dt, \quad I_2 = \int \left( RS + \frac{d}{dx} I_1 \right) dx . \quad (2.19)$$

Since we are interested in a time-independent Hamiltonian, we choose;  $I_t = 0$ . Hence, one can easily fix the null term  $S$  from first (2.16) as

$$S = -\frac{\phi}{\dot{x}} = \frac{\alpha\dot{x} + \lambda x}{\dot{x}} . \quad (2.20)$$

Substituting this into the (2.17b) we get

$$\dot{x}R_x - (\alpha\dot{x} + \lambda x) R_{\dot{x}} = -\frac{\lambda x}{\dot{x}} R . \quad (2.21)$$

(2.21) is a first-order linear partial differential equation with variable coefficients. As we mentioned earlier, any particular solution is sufficient to construct the integral of motion. Therefore, we choose a suitable *ansatz* for  $R$  instead of solving the general solution. We assume  $R$  to be of the form

$$R = \frac{\dot{x}}{(A(x) + B(x)\dot{x} + C(x)\dot{x}^2)^r} , \quad (2.22)$$

where  $A, B,$  and  $C$  are functions of  $x$  only. We demand the above form to deduce the first integral  $I$  has a rational form, that is,  $I = f(x, \dot{x})/g(x, \dot{x})$ , where  $f,$  and  $g$  are arbitrary function of  $x,$  and  $\dot{x}$ , from which we get  $I_x = (f_x g - f g_x)/g^2$  and  $I_{\dot{x}} = (f_{\dot{x}} g - f g_{\dot{x}})/g^2$ . From 2.16 one can see that  $R = I_{\dot{x}} = (f_{\dot{x}} g - f g_{\dot{x}})/g^2, S = I_x/I_{\dot{x}} = (f_x g - f g_x)/(f_{\dot{x}} g - f g_{\dot{x}})$ , and  $RS = I_x$ . Hence, the denominator of  $S$  should be the numerator of the function  $R$ . Since the denominator  $S$  is  $\dot{x}$ , we fix the numerator of  $R$  as  $\dot{x}$ . For simplicity we choose the denominator of  $R$  to be a polynomial of  $\dot{x}$ , because it has a rational form, and differentiating or integrating changes the power of the denominator by one and its form remains the same. Because of that we consider a constant power  $r$  for denominator of  $R$ , which as we see play an important role.

Substituting (2.22) into (2.21) in addition to simple calculation, we arrive at the relation

$$r \left[ \dot{x} \left( A_x + B_x \dot{x} + C_x \dot{x}^2 \right) - (\alpha \dot{x} + \lambda x)(B + 2C\dot{x}) \right] = -\alpha(A + B\dot{x} + 2C\dot{x}) . \quad (2.23)$$

Solving (2.23), we can fix the forms of  $A, B, C$  and  $r$ , and we find that

$$R = \begin{cases} \dot{x} / (\lambda x^2 + \alpha x \dot{x} + \dot{x}^2) & (\alpha^2 < 4\lambda), \\ \dot{x} / (\dot{x} + [(r-1)/r]\alpha x)^r & (\alpha^2 < 4\lambda), \\ \dot{x}, & (\alpha = 0), \end{cases} \quad (2.24)$$

where

$$r = \frac{\alpha}{2\lambda} [\alpha \pm \sqrt{\alpha^2 - 4\lambda}] . \quad (2.25)$$

Finally, substituting  $R$ , and  $S$  into the integral of (2.18) we get

$$I = \begin{cases} \frac{1}{2} \log(\dot{x}^2 + \alpha x \dot{x} + \lambda x^2) + (\alpha/2\omega) \tan^{-1}[(\alpha \dot{x} + 2\lambda x)/2\omega \dot{x}] & \alpha^2 < 4\lambda (\lambda, \alpha \neq 0) \text{ under-damped ,} \\ \frac{r-1}{r-2} (\dot{x} + \frac{\alpha}{r} x) (\dot{x} + \frac{r-1}{r} \alpha x)^{(1-r)}, & \alpha^2 > 4\lambda (\lambda, \alpha \neq 0) \text{ over-damped ,} \\ \frac{\dot{x}}{\dot{x} + (1/2)\alpha x} - \log(\dot{x} + \frac{1}{2}\alpha x), & \alpha^2 = 4\lambda (\lambda, \alpha \neq 0) \text{ critically damped ,} \\ \dot{x} + \alpha x, & \lambda = 0 (\alpha \neq 0) \text{ pure damping ,} \\ \dot{x}^2 + \lambda x^2, & \alpha = 0 (\lambda \neq 0) \text{ no damping ,} \end{cases} \quad (2.26)$$

with  $\omega = 1/2\sqrt{4\lambda - \alpha^2}$ . One can easily check that  $dI/dt = 0$  for each of the cases in (2.26). This equation demonstrates that the damped linear harmonic oscillator admits a time-independent integral of motion for all values of  $\alpha$  and  $\lambda$ . Now the integral of motion is time independent so we can find a Hamiltonian description for the damped equation of motion.

Assuming the existence of a Hamiltonian

$$I(x, \dot{x}) = H(x, p) = p\dot{x} - L(x, \dot{x}) , \quad (2.27)$$

where  $L(x, \dot{x})$  is the Lagrangian and  $p$  is the canonically conjugate momentum. Accordingly we have

$$\frac{\partial I}{\partial \dot{x}} = \frac{\partial H}{\partial \dot{x}} = \frac{\partial p}{\partial \dot{x}} \dot{x} + p - \frac{\partial L}{\partial \dot{x}} = \frac{\partial p}{\partial \dot{x}} \dot{x} , \quad (2.28)$$

that shows the conjugate momentum is the result of following integral

$$p = \int \frac{I_{\dot{x}}}{\dot{x}} d\dot{x} + f(x) , \quad (2.29)$$

where  $f(x)$  is an arbitrary function of  $x$ , and without loss of generality we take  $f(x) = 0$ .

By substituting (2.26) into (2.29) we obtain the conjugate momentum

$$p = \begin{cases} \tan^{-1}[(2\dot{x} + \alpha x)/2\omega x] & (\alpha^2 < 4\lambda), \\ (\dot{x} + [(r-1)/r]\alpha x)^{(1-r)} & (\alpha^2 \geq 4\lambda), \\ \log(\dot{x}) & (\lambda = 0), \\ \dot{x} & (\alpha = 0). \end{cases} \quad (2.30)$$

Substituting back of (2.30) into (2.28) we arrive at the following Hamiltonian

$$H = \begin{cases} (1/2) \log [x^2 \sec^2(\omega x p)] - (\alpha/2) x p & (\alpha^2 < 4\lambda) \\ [(r-1)/(r-2)] p^{(r-2)/(r-1)} - [(r-1)/r] \alpha x p & (\alpha^2 > 4\lambda) \\ \log(p) - (1/2) \alpha x p & (\alpha^2 = 4\lambda) \\ e^p + \alpha x & (\lambda = 0) \\ (1/2) p^2 + (\lambda/2) x^2 & (\alpha = 0). \end{cases} \quad (2.31)$$

One can easily check that the canonical equations of motion for the above Hamiltonian are exactly the (2.12) in appropriate parametric regimes. At this point we finish the introduction part for this topic and will come back to this issue in next section, where we derive the similar Hamiltonian for damped equation of motion and generalize it to higher order.

## 2.3 New Method of Derivation of Hamiltonian of Linear Constant-Coefficient Second-Order Differential Equation

In this section we present a new simple procedure that confirms the result of previous section. We start from the equation (2.12) and for sake of simplification in our calculation we assign  $\alpha = 2\gamma$  and  $\lambda = \omega^2$ . As a result the new equation reads

$$\ddot{x} + 2\gamma\dot{x} + \omega^2 = 0 . \quad (2.32)$$

By substituting  $x(t) = e^{-ivt}$ , we obtain a quadratic equation for the frequency  $v$ :

$$v^2 + 2i\gamma v - \omega^2 = 0 . \quad (2.33)$$

This equation factors

$$(v - \omega_1)(v - \omega_2) = 0 , \quad (2.34)$$

where

$$\omega_1 + \omega_2 = -2i\gamma, \quad \omega_1\omega_2 = -\omega^2 , \quad (2.35)$$

and thus

$$\omega_{1,2} = -i\gamma \pm \Omega = -i\gamma \pm \sqrt{\omega^2 - \gamma^2} . \quad (2.36)$$

The generic form of a Hamiltonian  $H(x, p)$  that can generate the evolution equation (2.32) is given in (2.11). There are two such Hamiltonian, corresponding to the two eigenfrequencies in (2.36). The first is

$$H_1 = -i\omega_1 xp + \frac{\omega_1}{\omega_1 - \omega_2} p^{1 - \frac{\omega_2}{\omega_1}} . \quad (2.37)$$

A second and equally effective Hamiltonian is obtained by interchanging the subscripts 1 and 2:

$$H_2 = -i\omega_2 xp + \frac{\omega_2}{\omega_2 - \omega_1} p^{1 - \frac{\omega_1}{\omega_2}} . \quad (2.38)$$

These Hamiltonians appear in (2.31) for the case of over-damping ( $\gamma^2 > \omega^2$ ), in which case they are real, but they apply equally well when ( $\gamma^2 < \omega^2$ ) if we are not concerned with the reality of the Hamiltonian. Indeed, the Hamiltonian is no longer the standard real energy, which is not conserved. Rather, it is a complex quantity which is conserved and from which the equations of motion can be derived in the standard way.

For the Hamiltonian  $H_1$ , Hamilton's equations read

$$\dot{x} = \frac{\partial H_1}{\partial p} = -i\omega_1 x + p^{-\frac{\omega_2}{\omega_1}} , \quad (2.39)$$

$$\dot{p} = -\frac{\partial H_1}{\partial x} = i\omega_1 p . \quad (2.40)$$

We then take a time derivative of (2.39) and simplify the resulting equation first by using (2.40) and then by using (2.39):

$$\begin{aligned}
\ddot{x} + i\omega_1\dot{x} &= -\frac{\omega_2}{\omega_1}\dot{p}p^{-1-\frac{\omega_2}{\omega_1}} \\
&= -i\omega_2p^{-\frac{\omega_2}{\omega_1}} \\
&= -i\omega_2(\dot{x} + i\omega_1x) .
\end{aligned} \tag{2.41}$$

Thus

$$\ddot{x} + i(\omega_1 + \omega_2)\dot{x} - \omega_1\omega_2x = 0 \tag{2.42}$$

which reduces to (2.32) upon using (2.35).

The equation of motion (2.32) has one conserved (time-independent) quantity, and this quantity can be expressed in terms of the function  $x(t)$  only. To find this quantity, we begin with (2.39) and solve for  $p$ :

$$p = (\dot{x} + i\omega_1x)^{-\frac{\omega_1}{\omega_2}} \tag{2.43}$$

We then use this result to eliminate  $p$  from the Hamiltonian  $H_1$ . Since  $H_1$  is time-independent, we conclude that

$$C_1 = \frac{(\dot{x} + i\omega_2x)^{\omega_2}}{(\dot{x} + i\omega_1x)^{\omega_1}} \tag{2.44}$$

is conserved. Had we started with the Hamiltonian  $H_2$  we would have obtained quantity

$$C_2 = \frac{(\dot{x} + i\omega_1x)^{\omega_1}}{(\dot{x} + i\omega_2x)^{\omega_2}} , \tag{2.45}$$

but this is not an independent conserved quantity because  $C_1 = 1/C_2$ . These conserved quantities were also found in [71] for the case of over-damping.

When  $\gamma = 0$ , these results reduce to the familiar expressions in the case of simple harmonic oscillator. In this case we let  $\omega = \omega_1 = -\omega_2$  so that  $H_1$  becomes

$$H_1 = -i\omega xp + \frac{1}{2}p^2, \quad (2.46)$$

which is related to the standard simple harmonic oscillator Hamiltonian by the change of variable  $p \rightarrow p - i\omega x$ . The conserved quantities  $C_2$  and  $C_1$  become simply  $(\dot{x} + \omega^2 x^2)^{\pm\omega}$ , in which we recognize usual conserved total energy.

### Hamiltonian for a Constant-Coefficient Third-Order Equation

In this section we show how to construct a Hamiltonian that gives rise to the general third-order constant-coefficient evolution equation

$$(D + i\omega_1)(D + i\omega_2)(D + i\omega_3) = 0, \quad (2.47)$$

where  $D = \frac{d}{dt}$ . The Hamiltonian that we will construct has just one degree of freedom.

An interesting physical example of such different equation is the third-order differential equation

$$m\ddot{x} + kx - m\tau\ddot{\dot{x}} = 0 \quad (2.48)$$

that describe an oscillating charged particle subject to a radiative back reaction force [85]. Following Batemans's approach for the damped harmonic oscillator [70], Englert [86]

showed that the pair of noninteracting equation (2.48) and

$$m\ddot{y} + ky + m\tau\ddot{y} = 0 \quad (2.49)$$

can be derived from the quadratic Hamiltonian

$$H = \frac{(ps - rq)}{m\tau} + \frac{2rs}{m\tau^2} + \frac{pz + qw}{2} - \frac{mzw}{2} + kxy . \quad (2.50)$$

This Hamiltonian contains the four degree of freedom  $(x, p)$ ,  $(y, q)$ ,  $(z, r)$ , and  $(w, s)$ . An interacting version of this model was studied in [87]. In fact, it was found that the two equations of motion (2.48) and (2.49) can be derived from the simpler quadratic Hamiltonian

$$H = \frac{pr + qz}{\sqrt{m\tau}} - \frac{rz}{\tau} + kxy , \quad (2.51)$$

which has only the three degree of freedom  $(x, p)$ ,  $(y, q)$ , and  $(z, r)$ . A similar three-degree of freedom Hamiltonian was also found in [87].

Our objective here is to find a *one*-degree of freedom Hamiltonian that can be used to derive the third-order differential equation (2.47). Note that the general solution to (2.47) is

$$x = a_1 e^{-i\omega_1 t} + a_2 e^{-i\omega_2 t} + a_3 e^{-i\omega_3 t} , \quad (2.52)$$

where  $a_k$  are arbitrary constants. If we form  $(D + i\omega_2)(D + i\omega_3)x$ , that is,  $\ddot{x} + i(\omega_2 + \omega_3)\dot{x} - \omega_2\omega_3x$ , we obtain

$$a_1 e^{-i\omega_1 t} = -\frac{(D + i\omega_2)(D + i\omega_3)x}{(\omega_1 - \omega_2)(\omega_1 - \omega_3)} , \quad (2.53)$$

in which the constants  $a_2$  and  $a_3$  do not appear. Similarly, we have

$$\begin{aligned} a_2 e^{-i\omega_2 t} &= -\frac{(D + i\omega_3)(D + i\omega_1)x}{(\omega_2 - \omega_3)(\omega_2 - \omega_1)}, \\ a_3 e^{-i\omega_3 t} &= -\frac{(D + i\omega_1)(D + i\omega_2)x}{(\omega_3 - \omega_1)(\omega_3 - \omega_2)}. \end{aligned} \quad (2.54)$$

So, assuming that the frequencies  $\omega_k$  are all distinct, there are two independent conserved quantities, namely

$$\begin{aligned} C_2 &= \frac{[\ddot{x} + i(\omega_2 + \omega_3)\dot{x} - \omega_2\omega_3x]^{\frac{\omega_1}{\omega_3}}}{[\dot{x} + i(\omega_1 + \omega_2)x - \omega_1\omega_2x]^{\frac{\omega_1}{\omega_3}}}, \\ C_3 &= \frac{[\ddot{x} + i(\omega_2 + \omega_3)\dot{x} - \omega_2\omega_3x]^{\frac{\omega_1}{\omega_2}}}{[\dot{x} + i(\omega_1 + \omega_3)\dot{x} - \omega_1\omega_3x]^{\frac{\omega_1}{\omega_2}}}. \end{aligned} \quad (2.55)$$

These expressions and the equation of motion can be derived from the Hamiltonian

$$H = -i\omega_1 x p + \frac{b_2 \omega_1}{\omega_1 - \omega_2} p^{1 - \frac{\omega_2}{\omega_1}} + \frac{b_3 \omega_1}{\omega_1 - \omega_3} p^{1 - \frac{\omega_3}{\omega_1}}, \quad (2.56)$$

where  $b_2$  and  $b_3$  are arbitrary constants. Thus,  $\dot{p} \equiv -\frac{\partial H}{\partial x} = i\omega_1 p$ . This means that  $p \propto e^{i\omega_1 t}$ , so that  $1/p$  is directly related to combination in (2.53).

Then, from Hamiltonian's equation  $\dot{x} \equiv \frac{\partial H}{\partial p}$  and from further differentiation with respect to  $t$ , we obtain

$$\begin{aligned} \dot{x} &= -i\omega_1 x + b_2 p^{-\frac{\omega_2}{\omega_1}} + b_3 p^{-\frac{\omega_3}{\omega_1}}, \\ \ddot{x} &= -i\omega_1 \dot{x} - i\omega_2 b_2 p^{-\frac{\omega_2}{\omega_1}} - i\omega_3 b_3 p^{-\frac{\omega_3}{\omega_1}}, \\ \dddot{x} &= -i\omega_1 \ddot{x} - \omega_2^2 b_2 p^{-\frac{\omega_2}{\omega_1}} - \omega_3^2 b_3 p^{-\frac{\omega_3}{\omega_1}}. \end{aligned} \quad (2.57)$$

These equations depend on the constants  $b_2$  and  $b_3$ . Nevertheless, after we combine these equations and perform some simplifying algebra, we obtain

$$\ddot{x} + i(\omega_1 + \omega_2 + \omega_3)\dot{x} - (\omega_1\omega_2 + \omega_2\omega_3 + \omega_3\omega_1)x - i\omega_1\omega_2\omega_3 = 0 . \quad (2.58)$$

The constants  $b_2$  and  $b_3$  have disappeared in this combination and we have reconstructed the equation of motion (2.47). These constants are reminiscent of Lagrange multipliers, but they are unlike Lagrange multipliers in that we do not vary the Hamiltonian with respect to them. Rather, we require that the equations of motion be *independent* of these constants.

Using only derivatives up to the second order, we can find expressions for  $b_2 p^{-\omega_2/\omega_1}$  and  $b_3 p^{-\omega_3/\omega_1}$ , namely

$$\begin{aligned} i(\omega_3 - \omega_2)b_2 p^{-\frac{\omega_2}{\omega_1}} &= \ddot{x} + i(\omega_1 + \omega_3)\dot{x} - \omega_1\omega_3 x , \\ i(\omega_2 - \omega_3)b_3 p^{-\frac{\omega_3}{\omega_1}} &= \ddot{x} + i(\omega_1 + \omega_2)\dot{x} - \omega_1\omega_2 x . \end{aligned} \quad (2.59)$$

in which we recognize two of the quantities that appear in (2.55). The third such quantity, namely  $\ddot{x} + i(\omega_1 + \omega_2)\dot{x} - \omega_1\omega_2 x$ , is closely related to  $H$ ,

$$\begin{aligned} \ddot{x} + i(\omega_2 + \omega_3)\dot{x} - \omega_2\omega_3 x &= -(\omega_1 - \omega_2)(\omega_1 - \omega_3)x + ib_2(\omega_3 - \omega_1)p^{-\omega_2/\omega_1} + ib_3(\omega_2 - \omega_1)p^{-\omega_3/\omega_1} \\ &= i(\omega_1 - \omega_2)(\omega_3 - \omega_1)\frac{H}{\omega_1 p} . \end{aligned}$$

We conclude that

$$C_2 = \frac{i(\omega_1 - \omega_2)(\omega_3 - \omega_1)p}{[i(\omega_2 - \omega_3)b_3]^{\omega_1/\omega_3}} \frac{H}{\omega_1 p} \propto H b_3^{-\omega_1/\omega_3} . \quad (2.60)$$

Similarly, we have

$$C_3 \propto H b_2^{-\omega_1/\omega_2} . \quad (2.61)$$

Thus  $C_2$  and  $C_3$  are constants of the motion because they are both proportional to the Hamiltonian, with proportionality constants given by powers of  $b_2$  and  $b_3$ , respectively.

To summarize, by eliminating the parameters  $b_2$  and  $b_3$  the evolution equation (2.47) can be derived from the unusual time-independent Hamiltonian (2.56) containing the single coordinate variable  $x$  and its conjugate momentum  $p$ . This Hamiltonian is a conserved quantity, which can be expressed as

$$H = i\omega_1 p \frac{\ddot{x} + i(\omega_2 + \omega_3)\dot{x} - \omega_2\omega_3 x}{(\omega_1 - \omega_2)(\omega_1 - \omega_3)} \quad (2.62)$$

The conserved quantities  $C_2$  and  $C_3$  are both proportional to  $H$ .

Before moving on, we must explain how a Hamiltonian with a single degree of freedom can give rise to a differential equation whose order is greater than two. The problem is as follows. Our Hamiltonian has the general form

$$H = axp + f(p) . \quad (2.63)$$

Therefore, the equations of motion are simply

$$\dot{x} = ax + g(p) , \quad (2.64)$$

where  $g(p) = f'(p)$ , and

$$\dot{p} = -ap \quad (2.65)$$

We solve (2.65) first,

$$p(t) = Ce^{-at} \quad (2.66)$$

where  $C$  is an arbitrary constant. Next, we return to (2.64), which becomes

$$\dot{x} = ax + g(Ce^{-xt}) \quad (2.67)$$

after we eliminate  $p$  by using (2.66). This is a *first-order* equation. Thus, its solution has only *two* arbitrary constants:

$$x(t) = \phi(t, C, D) \quad (2.68)$$

We obtained the higher-order differential equation (2.58) by the sequence of differentiation in (2.57) that were required to eliminate the constants  $b_2$  and  $b_3$ . Of course, the solution to an  $n$ th-order equation can incorporate  $n$  pieces of data such as  $n$  initial conditions:  $x(0)$ ,  $\dot{x}(0)$ ,  $\ddot{x}(0)$ ,  $\ddot{\ddot{x}}(0)$ , and so on. How is it possible to incorporate  $n$  pieces of data with only two arbitrary constants  $C$ , and  $D$ ? There appear to be  $n - 2$  missing arbitrary constants.

The answer is that the  $n - 2$  pieces of initial data determine  $n - 2$  parameters  $b_k$  multiplying each of the fractional powers of  $p$  in  $H$ . (One parameter can always be removed by a scaling.) We can incorporate the initial data into the Hamiltonian in the form of parameters. These parameters specify an ensemble of Hamiltonian, all of which gives a unique  $n$ th-order field equation that is independent of these parameters and is capable of accepting  $n$  pieces of initial data.

For the triplet equation, we can see from (2.59) that the ratio  $b_2^{1/\omega_2}/b_3^{1/\omega_3}$  is related to the initial conditions. So, for the case of the third-order equation, the three arbitrary constants are  $C$ ,  $D$  and  $b_2^{1/\omega_2}/b_3^{1/\omega_3}$ . We emphasize that the Hamiltonian gives the higher-order

equations of motion precisely because of the requirement that the parameters  $b_k$  drop out from the equation of motion. The parameters  $b_k$  in the Hamiltonian are crucial because they incorporate the initial data and are determined by the initial data. The nonzero parameter  $b_3$  forces the evolution equation to be third order. Without  $b_3$  the Hamiltonian does not know about the third frequency  $\omega_3$ . Indeed, if  $b_3 = 0$ , (2.56) reduces to (2.37) (with  $b_2 = 1$ ). [This is consistent with (2.59) because setting  $b_3 = 0$  there implies that  $\ddot{x} + i(\omega_1 + \omega_2) - \omega_1\omega_2x = 0$ ]

Finally, one may ask what would happen if we followed the standard procedure for deriving the equations of motion for  $x(t)$  from the Hamiltonian equations of motion  $\dot{p} = -\partial H/\partial x$  and  $\dot{x} = \partial H/\partial p$ . This would mean solving the second equation for  $p$  in terms of  $x$  and  $\dot{x}$  and then substituting back in the first to obtain a second-order equation for  $x(t)$ . In our case that would mean solving the first equation of (2.57) for  $p$ , which is not possible for general values of the parameters. However, it is instructive to see how this procedure works if we choose the parameters so that an explicit solution is possible. For example, if we choose  $\omega_1 = 1, \omega_2 = -2, \omega_3 = 4, b_2 = 2$  and  $b_3 = 1$ , the equation can be solved to give  $p^2 = -1 + \sqrt{\dot{x} + ix + 1}$ . Substituting back into the equation  $\dot{p} = ip$  gives, after some algebra, the nonlinear second-order equation

$$(\ddot{x} - 3i\dot{x} + 4x - 4i)^2 = -16(\dot{x} + ix + 1) . \quad (2.69)$$

Further manipulation shows this to be equivalent to the constancy of  $C_2/C_3$ .

So, in the cases where the standard procedure can be followed in practice, the resulting nonlinear second-order equations is equivalent to an equation for a constant of motion (which of course depends on the parameters  $b_2$  and/or  $b_3$ )

## 2.4 Hamiltonian for a Constant-Coefficient $n$ th-Order Equation

It is straightforward to generalize to the case of an arbitrary  $n$ th-order constant-coefficient evolution equation

$$\left[ \prod_{r=1}^n (D + i\omega_r) \right] x(t) = 0, \quad (2.70)$$

whose general solution is

$$x(t) = \sum_{r=1}^n a_r e^{-i\omega_r t}. \quad (2.71)$$

For simplicity, we assume that the frequencies  $\omega_r$  are all distinct; at the end of this section we explain what happens if some of the frequencies are degenerate.

Corresponding to (2.54) and (2.55), we have

$$e^{-i\omega_s t} \propto \left[ \prod_{r \neq s}^n (D + i\omega_r) \right] x(t). \quad (2.72)$$

Thus, the quantity

$$Q_s \equiv \left\{ \left[ \prod_{r \neq s}^n (D + i\omega_r) \right] \right\}^{\frac{1}{\omega_s}} \quad (2.73)$$

is proportional to  $e^{-it}$  for all  $s$ . Hence, the  $n - 1$  independent ratios  $Q_s/Q_1$  ( $s > 1$ ) are all conserved. Any other conserved quantity can be expressed in terms of these ratios.

The equation of motion and the conserved quantities can be derived from the Hamiltonian

$$H = -i\omega_1 x p + \sum_{r \neq 1}^n \frac{b_r \omega_1 p^{1 - \frac{\omega_r}{\omega_1}}}{\omega_1 - \omega_r}, \quad (2.74)$$

which is the  $n$ th order generalization of (2.56) for the cubic case. In this expression the  $n - 1$  coefficients  $b_r$  are arbitrary. Note that in constructing the Hamiltonian  $H$  there is nothing special about the subscript “1” and it may be replaced by the subscript “ $s$ ” ( $1 < s \leq n$ ).

### 2.4.1 Degenerate Frequencies

Until now, we have assumed that the frequencies  $\omega_r$  are all distinct. However, if some of the frequencies are degenerate, there is a simple way to construct the the appropriate Hamiltonian: If the frequencies  $\omega_1$  and  $\omega_2$  are equal, we make the replacement

$$\frac{\omega_1}{\omega_1 - \omega_2} p^{1 - \frac{\omega_2}{\omega_1}} \rightarrow \log(p). \quad (2.75)$$

(In making this replacement we are shifting the Hamiltonian by an infinite constant.)

Thus, for  $\omega_1 = \omega_2$  the Hamiltonian  $H_1$  in (2.37) reduces to

$$H_1 = -i\omega_1 xp + \log p. \quad (2.76)$$

Hamilton’s equations for this Hamiltonian immediately simplify to (2.42) with  $\omega_1 = \omega_2$ .

Similarly, for the case  $\omega_1 = \omega_2$  the Hamiltonian (2.56) reduces to

$$H = -i\omega_1 xp + b_2 \log p + \frac{b_3 \omega_1}{\omega_1 - \omega_3} p^{1 - \frac{\omega_3}{\omega_1}} \quad (2.77)$$

and Hamiltonian’s equations for this Hamiltonian readily simplify to (2.58) with  $\omega_1 = \omega_2$ .

Also, if the frequencies are triply degenerate,  $\omega_1 = \omega_2 = \omega_3 = \omega$ , the Hamiltonian in (2.56) is replaced by

$$H = -i\omega xp + b \log p + \frac{1}{2}c (\log p)^2 , \quad (2.78)$$

where  $b$  and  $c$  are two parameters that are determined by the initial data. Once again, Hamilton's equation's for this Hamiltonian combine to give (2.58) with  $\omega_1 = \omega_2 = \omega_3 = \omega$ .

## 2.5 Quantization

The obvious question to be addressed next is whether it is possible to use the Hamiltonians that we have constructed to *quantize* classical systems that obey a linear constant-coefficient evolution equation. Let us begin by discussing the simple case of the quantum harmonic oscillator (QHO), whose Hamiltonian  $H_1$  is given in (2.46).

One possibility is to quantize Hamiltonian in  $p$ -space by setting  $x = id/dp$ . Then the time-independent Schrödinger eigenvalue equation is, by shifting  $E$  by  $\omega$

$$H_1 \tilde{\psi}(p) = \left( \omega p \frac{d}{dp} + \frac{1}{2} p^2 \right) \tilde{\psi}(p) = E \tilde{\psi}(p) , \quad (2.79)$$

whose solution is

$$\tilde{\psi}(p) \propto p^{\frac{E}{\omega}} e^{-\frac{p^2}{(4\omega)^2}} . \quad (2.80)$$

In this way of doing things we can derive the quantization condition by demanding that  $\tilde{\psi}$  be a well-defined, nonsingular function, which requires that  $E = n\omega$ , where  $n$  is a

nonnegative integer [1]. However, these “momentum-space” eigenfunctions are problematical because  $p$  has no clear physical interpretation as a momentum, and it is not a Hermitian operator. The  $p$ -space eigenfunctions are certainly not orthonormal in any simple sense because they do not solve a Sturm-Liouville boundary value problem [88].

However, we can calculate the corresponding  $x$ -space eigenfunctions by Fourier transform using the formula [89]

$$H_n(z) = \frac{(-i)^n}{2\sqrt{\pi}} e^{z^2} \int_{-\infty}^{\infty} dp e^{ipz} p^n e^{-p^2} \quad (2.81)$$

We find that

$$\psi_n(x) \propto e^{-\frac{1}{2}\omega^2 x^2} \phi_n(x) , \quad (2.82)$$

where  $\phi_n(x)$  is the  $n$ th eigenfunction of the QHO. This is consistent with our remark above that  $H_1$  is related to the standard QHO Hamiltonian by the transformation  $p \rightarrow p - i\omega x$ . This transformation is achieved at the operator level by the similarity transformation  $p \rightarrow e^{-\omega^2 x^2} p e^{\omega^2 x^2}$  [90]. Because of this additional factor, our eigenfunctions are orthonormal with respect to the metric  $\eta = e^{\omega^2 x^2}$ . As an alternative approach, we can cast (2.46) in  $x$ -space as

$$H_1 = -\frac{1}{2} \frac{d^2}{dx^2} - \omega^2 \left( 1 + x \frac{d}{dx} \right) , \quad (2.83)$$

from which we can obtain the  $\psi_n(x)$  directly.

To summarize, the quantized version of (2.46) corresponds to a transformed version of the QHO, where the  $x$ -space eigenfunctions are simply related to the standard eigenfunction, and are orthonormal with respect to an additional weight function. The  $p$ -space eigenfunctions can be written down but their interpretation is not at all obvious (the operator  $p$  corresponds to the conventional raising operator  $a^\dagger$ ) and are not orthogonal in any simple

way. Moreover,  $p$ , represented as  $-id/dx$ , is not Hermitian because the overlap integral between two wave functions has to be calculated with the inclusion of the metric  $\eta(x)$ , so integration by parts is no longer simply a matter of a minus sign. Instead,  $p$  is *pseudo-Hermitian* [12,26,91] with respect to  $\eta$ , i.e.,  $p^\dagger = \eta p \eta^{-1}$ . In  $p$  space the weight function  $e^{\omega^2 x^2}$  becomes the highly nonlocal operator  $e^{-\omega^2 d^2/dp^2}$ .

If we now generalize to the damped harmonic oscillator, we can still find a solution  $\tilde{\psi}(p)$  to the time-independent Schrödinger equation, namely [71]

$$\tilde{\psi}(p) \propto p^{\frac{E}{\omega_1}} \exp \left[ -\frac{\omega_1}{(\omega_1 - \omega_2)^2} p^{1 - \frac{\omega_1}{\omega_2}} \right], \quad (2.84)$$

but even if we take  $E = n\omega_1$  in order to make the prefactor nonsingular, we are still left with a nonintegral, and in general complex, power of  $p$  in the exponential. (See also the comments in [71]). This, in addition to the previously discussed problem with  $\tilde{\psi}(p)$ , we would now have to consider it to be a function in a cut plane. Moreover, there is no simple formula like (2.81) whereby one could obtain the  $x$ -space eigenfunction. Furthermore, if we cast the equation in  $x$ -space we obtain

$$H_1 = \frac{1}{1 - \frac{\omega_2}{\omega_1}} \left\{ -i \frac{d}{dx} \left[ \left( -i \frac{d}{dx} \right)^{-\frac{\omega_2}{\omega_1}} - i(\omega_1 - \omega_2)x \right] \right\} \quad (2.85)$$

in which the difficulty associated with a fractional derivative is manifest.

Evidently, quantizing Hamiltonian of the form in (2.63) is nontrivial. The problem of quantizing the cubic equation describing the back-reaction force on a charged particle was solved in [87]. However, the system that was actually quantized was a *pair of coupled* cubic equations in the *unbroken*  $\mathcal{PT}$ -symmetric region. Thus, it may be that the most

effective approach for quantizing a Hamiltonian of the form (2.63) is to introduce a large number of additional degrees of freedom.

## 2.6 Conclusion

We have shown that any  $n$ th-order linear constant-coefficient evolution equation can be derived from a nonconventional but simple Hamiltonian of the form (2.63). Remarkably, this Hamiltonian has only one degree of freedom, that is, one pair of dynamical variables  $(x, p)$ . Furthermore, we have shown that for such a system there are  $n - 1$  independent constants of the motion and we have constructed these conserved quantities in terms of  $x(t)$  and its time derivatives. However, we find that it is not easy to formulate a general procedure to quantize the system described by the Hamiltonian, and this remains an extremely interesting but difficult open problem.

## Chapter 3

# Analytic Structure of Eigenvalue of Coupled quantum Systems

*This chapter contains the materials published in a paper [\[92\]](#), which represents work performed by me under the supervision of my advisor, C. M. Bender.*

## 3.1 Introduction

The analytic structure of self-coupled systems, such as the quantum anharmonic oscillator, has been studied in great depth. Singularities in the coupling-constant plane have been identified as the cause of the divergence of perturbation theory [93,94]. These singularities are typically square-root branch points and are associated with phenomenon of level crossing. These singularities are sometimes referred to as exceptional points [95]. Studies of coupling-constant analyticity have revealed a remarkable and generic phenomenon, namely, that the eigenvalues belonging to the spectrum of the Hamiltonian are analytic continuations of one another as functions of the complex coupling constant. Thus, the energy levels of a quantum system, which are discrete when the coupling constant is real and positive, are actually smooth continuations of one another in the complex-coupling-constant plane [1], and a simple geometric picture of quantization emerges: The discrete eigenvalues of a quantum system are in one-to-one correspondence with the sheets of the Riemann surface. The different energy levels of the Hamiltonian are merely different branches of a multivalued energy function.

While this picture of quantization has emerged from studies of coupling-constant singularities of self-coupled systems, this chapter argues that an even more elaborate picture arises from studies of coupled quantum systems. Consider, for example, the simple case of two coupled quantum harmonic oscillator, one having natural frequency  $\nu > 0$  and the other having natural natural frequency  $\omega > 0$ . For definiteness, we assume that  $\nu > \omega$ . The Hamiltonian for such a system has the form

$$H = p^2 + \nu^2 x^2 + q^2 + \omega^2 y^2 + gxy , \quad (3.1)$$

where  $g$  is the coupling parameter. For sufficiently large  $|g|$  the eigenvalues of  $H$  become singular. To demonstrate this rewrite the potential  $V(x, y) = v^2x^2 + \omega^2y^2 + gxy$  as

$$V(x, y) = v^2 \left( x + \frac{gy}{2v^2} \right)^2 + y^2 \left( \omega^2 - \frac{g^2}{4v^2} \right) \quad (3.2)$$

We see immediately that on the line  $x + gy/2v^2 = 0$  in the  $(x, y)$  plane  $V(x, y)$  becomes unbounded below if  $g^2 > 4v^2\omega^2$ . Thus, while the potential has a positive discrete spectrum when the coupling constant  $g$  lies in the range

$$-2v\omega < g < 2v\omega \quad (3.3)$$

we expect there to be singular points at  $g = \pm 2v\omega$  in the coupling-constant plane. This result raises the question, what is the nature of the singular points at  $\pm 2v\omega$ ?

Coupling-oscillator models have been studied in great detail in many papers [70,96–101] and in particular for oscillator models of the type in (3.1). The presence of singularities at  $g = \pm 2v\omega$  was noted in [96]; however, the nature of singularities and the Riemann sheet structure was not identified in any of these papers.

In this chapter we show that the Riemann surface for the coupled-oscillator Hamiltonian (3.1) consists of four sheets. The singularities at  $g = \pm 2v\omega$  are square-root singularities, like the exceptional-point singularities of self-coupling oscillators. However, if we cross either of the square-root branch cuts, we enter a second sheet of the Riemann surface on which two new square-root branch points appear. These branch points are located at  $g = \pm i(v^2 - \omega^2)^{1/2}$ . If we cross either of the branch cuts emanating from these new branch points, we enter a third sheet of the Riemann surface where there are yet another pair of square-root exceptional points at  $g = \pm 2v\omega$ , unconnected with the singularities on

sheets one and two. Crossing either of the branch cuts emanating from these singularities at  $g = \pm 2\nu\omega$  takes us to a fourth sheet of the Riemann surface. Not all energy levels of the coupled harmonic oscillator mix among themselves as  $g$  varies on this four-sheeted Riemann surface. Rather, each energy level belongs to quarter of energies that are analytic continuation of one another. We find the fourth sheet of the Riemann surface corresponds to four distinct *spectral phases* of the coupled oscillator system (3.1)

We give a detailed description of these spectral phases in the next section. We explain below how such spectral phases arise. Let us consider a single harmonic oscillator, whose dynamics are defined by the Hamiltonian

$$H = p^2 + \nu^2 x^2 . \quad (3.4)$$

This simple quantum system actually has two spectral phases characterized by two distinct spectra. To understand why, we assume that  $\nu$  is a positive parameter and we note that the  $n$ th eigenvalue  $E_n$ , which is defined by the eigenvalue problem

$$-\frac{d^2}{dx^2}\psi(x) + \nu^2 x^2 \psi(x) = E_n \psi(x) \quad (\psi \rightarrow 0 \text{ as } x \rightarrow \pm\infty) , \quad (3.5)$$

is given by

$$E_n = (2n + 1)\nu \quad (n = 0, 1, 2, 3, \dots). \quad (3.6)$$

In [102] it was observed that if we analytically continue  $\nu$  in a semicircle in the complex- $\nu$  plane, that is, if we let  $\nu = re^{i\phi}$  ( $r$  real) and allow  $\phi$  to run from 0 to  $\pi$ , the eigenvalues change sign even though the Hamiltonian remains unchanged. By this analytic continuation we reach a new phase of the harmonic oscillator whose spectrum is *negative* and

*unbounded below*. Thus, the Hamiltonian (3.4) of the harmonic oscillator has two distinct and independent real spectra that are related by analytic continuation in the natural frequency  $\nu$  of the oscillator.

How can one Hamiltonian (3.4) have two different spectra? The answer to this question is that the positive spectrum is obtained by imposing the boundary condition in (3.5) in a pair of Stokes wedges [1, 2, 23, 103] centered about the positive-real- $x$  and negative-real- $x$  axis. We refer to the positive spectrum as the *conventional* one. These wedges have angular opening  $\pi/2$ . The negative spectrum is defined by imposing the boundary condition in a pair of Stokes wedges containing and centered about the upper and lower imaginary- $x$  axes. We refer to the negative spectrum as the *unconventional* spectrum of the harmonic oscillator. These Stokes wedges also have angular opening of  $\pi/2$ . To understand the configuration of the wedges we examine the WKB geometrical approximation

$$\psi \sim e^{\pm\nu x^2/2} \tag{3.7}$$

to the solution of the harmonic oscillator eigenvalue equation (3.5). On the basis of (3.7) we can see that the  $90^\circ$  wedges in which the eigenfunctions vanish rotate clockwise through an angle of  $\pi/2$  as  $\nu$  rotate anticlockwise through an angle of  $\pi$ . Thus, those two phases are analytic continuation of one another and are analytically connected by rotations in the complex frequency plane.

A principal result of this chapter is that if we analytically continue the physical system consisting of two coupled harmonic oscillators described by the Hamiltonian in (3.1) in the coupling-constant parameter  $g$ , we obtain all four possibilities for the phases of the two oscillators in which each possibilities for the two oscillators in which each oscillator

is in a conventional or unconventional phase. Thus, all four phases are analytically connected on the Riemann surface of the complex coupling  $g$ , even though the frequencies  $\nu$  and  $\omega$  are held fixed and positive.

## 3.2 Analytic Continuation of Eigenvalue Problem for Harmonic Oscillator

Analytic continuation of the coupling-constant parameter in some quantum-mechanical potential may cause a paradox [102]. To illustrate the problem we consider the potential

$$V(x) = a^2x^6 - 3ax^2, \quad (3.8)$$

which the Schrödinger equation corresponding to this potential has the form

$$-\psi''(x) + (a^2x^6 - 3ax^2)\psi(x) = E\psi(x). \quad (3.9)$$

When  $a > 0$ , the ground-state wave function  $\psi_0$  is exactly

$$\psi_0(x) = e^{-\frac{1}{4}ax^4}. \quad (3.10)$$

This is indeed the ground-state eigenfunction because it has no nodes. By substituting (3.10) into (3.9) and applying simple algebra we obtain  $E_0(a) = 0$ . Now suppose we analytically continue the equation of ground-state energy from positive to negative values of parameter  $a$ . Accordingly, the ground-state energy is still  $E_0(a) = 0$ . However, this conclusion is wrong! For the case of  $a < 0$  the Schrödinger differential equation (3.9) can

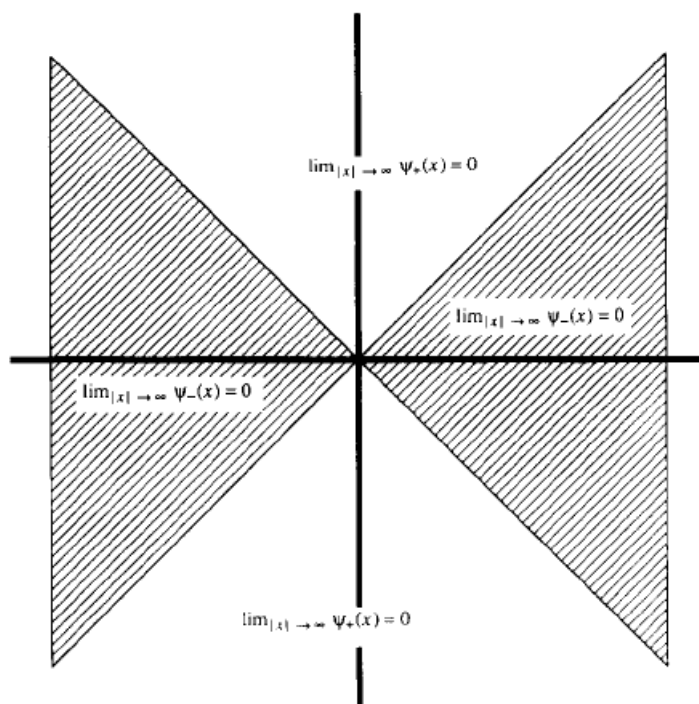


Figure 3.1: Regions (shaded) in the complex- $x$  plane where the boundary condition  $\psi(x) \rightarrow 0$  is satisfied as  $|x| \rightarrow \infty$  for the eigenvalue problem in (3.12). Note that the harmonic oscillator is actually *two* problems, one on the real axis and the other along the imaginary axis.

be solved numerically, and indeed the lowest eigenvalue is a positive number

$$E_0(a) = 1.9333\dots\sqrt{|a|} \tag{3.11}$$

How is it possible that an analytic continuation of the zero function is nonzero? To address this question we need to define very carefully the procedure of analytic continuation of the eigenvalue problem [102]. Obviously, the ground-state wave function  $\psi_0 = \exp\left(-\frac{1}{4}ax^4\right)$  is nonnormalizable after continuation of  $a$  to negative values, which indicates a simple replacement of  $a$  by  $-a$  is not the correct procedure.

In order to provide an illustrative explanation, we describe the correct procedure of analytic continuation of coupling constant for harmonic oscillator, which has the potential  $V(x) = 1/4a^2x^2$ . Accordingly, the Schrödinger differential equation reads

$$\left(-\frac{d^2}{dx^2} + \frac{1}{4}a^2x^2 - E\right) = 0, \quad (3.12)$$

with the associate boundary condition

$$\lim_{|x| \rightarrow \infty} \psi(x) = 0. \quad (3.13)$$

To continue the parameter  $a$  into the complex plane we need to generalize the Schrödinger eigenvalue problem (3.12) from the real- $x$  axis to the complex- $x$  plane. As we explained comprehensively in chap. 1, WKB approximation solution for this differential equation is  $\psi_{\pm} \sim \exp\left(\pm\frac{1}{4}ax^2\right)$  which determine the Stokes wedges. As can be seen in Fig. 3.1 in the shaded region  $\psi_-$  goes to zero for large value of  $x$  in complex plane and in the unshaded region  $\psi_+$  approaches to zero as  $|x| \rightarrow \infty$ . Thus, if we extend the differential equation into the complex plane we actually obtain two completely independent eigenvalue problems.

With these arrangements we can discuss the analytic continuation of the eigenvalue problem. If we let

$$a = \rho e^{i\theta}, \quad (3.14)$$

and allow  $\theta$  to increase from 0 to  $\pi$ , then the centerlines of the shaded regions in fig. 3.1 also rotate in the complex plane but in the clockwise in order to retain the quantization condition  $\psi_- \rightarrow 0$  as  $x \rightarrow \infty$ . In our case that  $\psi_-(x) = \exp\left(-\frac{1}{4}ax^2\right)$ , the centerline rotates  $90^\circ$  clockwise. Before analytic continuation of  $a$  the ground state energy  $E_0 = \frac{1}{2}a$ . After continuation the Schrödinger differential equation and the quantization conditions

read

$$\left(-\frac{d^2}{dx^2} + \frac{1}{4}a^2x^2 - E\right)\psi(x) = 0, \quad (3.15)$$

$$\lim_{x \rightarrow \pm i\infty} \psi(x) = 0. \quad (3.16)$$

To solve this problem we set  $x = ir$  and get

$$\left(-\frac{d^2}{dr^2} + \frac{1}{4}a^2r^2 + E\right)\psi(r) = 0, \quad (3.17)$$

$$\lim_{r \rightarrow \pm\infty} \psi(r) = 0. \quad (3.18)$$

Notice that (3.17) is the same as (3.12) except that the sign of  $E$  is reverse, which means after analytic continuation of  $a$  to  $-a$  the energy of ground state is

$$E = -\frac{a}{2}, \quad (3.19)$$

as it was expected to be. This result can be generalized to a polynomial potential  $V(x)$  whose highest power in  $x$  term is  $\lambda x^{2n}$  and there are  $n + 1$  independent eigenvalue problems in the complex- $x$  plane. As  $\lambda$  rotates to an angle  $\theta$  in a counterclockwise direction into the complex plane, the array of eigenvalue problem, rotates in a clockwise direction by an angle of  $\theta/(2n + 2)$ .

This simple example shows the basic idea of analytic continuation of a parameter in differential equation, and how it causes change in the eigenvalues of a system. In next sections we investigate the effect of analytic continuation on the ground state of two coupled harmonic oscillators.

### 3.3 Energy levels of the Coupled Harmonic Oscillator

In this section we examine the analytic structure of the eigenvalues of the coupled harmonic oscillator Hamiltonian (3.1). We begin by the ground-state eigenfunction, which has the general form

$$\psi(x, y) = e^{-\frac{1}{2}ax^2 - \frac{1}{2}by^2 + cxy} , \quad (3.20)$$

where  $a, b$  and  $c$  are constants to be determined. We substitute (3.20) into the time-independent Schrödinger eigenvalue equation  $H\psi = E\psi$ , which has the explicit form

$$-\psi_{xx} + v^2x^2\psi - \psi_{yy} + \omega^2y^2\psi + gxy\psi = E\psi . \quad (3.21)$$

We then equate the coefficient of  $x^2, y^2, xy$ , and  $x^0y^0$  and obtain the four equations

$$v^2 = a^2 + c^2 , \quad (3.22)$$

$$\omega^2 = b^2 + c^2 , \quad (3.23)$$

$$0 = 2ac + 2bc + g , \quad (3.24)$$

$$E = a + b . \quad (3.25)$$

Subtracting the first equation from the second and combining the result with the third equations allows us to calculate  $a, b$ , and  $c$ , which we then eliminate in favor of a single quartic polynomial equation for the eigenvalue  $E$ :

$$E^4 - 2(v^2 + \omega^2)E^2 + (v^2 - \omega^2)^2 + g^2 = 0 . \quad (3.26)$$

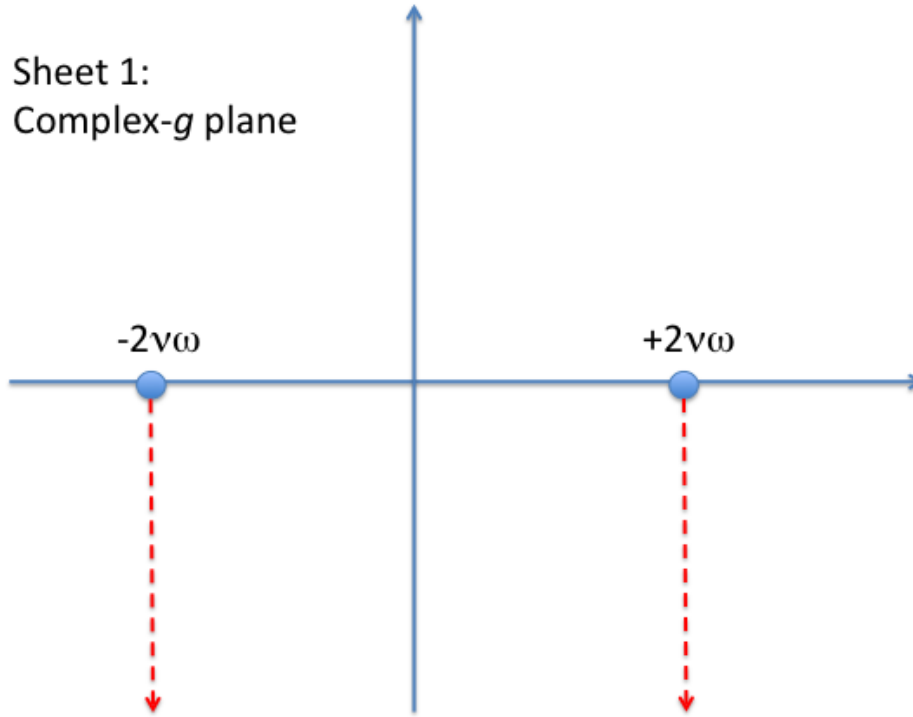


Figure 3.2: Sheet 1 of the complex Riemann surface of  $E(g)$  in (3.27). On this sheet both the inner and outer square roots are positive when their argument are positive. Branch points are indicated by blue dots and branch cuts by red dashed lines. On this sheet  $E(0) = v + \omega$ .

The solution to this equation involves square roots,

$$E(g) = \left[ v^2 + \omega^2 + \left( 4v^2\omega^2 - g^2 \right)^{\frac{1}{2}} \right]^{\frac{1}{2}} \quad (3.27)$$

and from this equation we see that  $E(g)$  is a four-valued function of the coupling constant  $g$ .

Let us make a grand tour of the Riemann surface on which  $E(g)$  is defined. We begin on sheet 1, where both square-root functions are real and positive when their argument are real and positive. There are two obvious square-root branch points (zeros of the inner square root) and these are located at  $g = \pm 2\nu\omega$ . Square-root branch cuts emerge from each of these branch points and, as shown on Fig. 3.2, we have chosen to draw these branch cuts as vertical lines going downward. On sheet 1, we have chosen to draw these branch cuts as vertical lines going downward. On sheet 1

$$E(0) = \nu + \omega \quad (3.28)$$

and because we assume that  $\nu$  and  $\omega$  are real and positive we see that both oscillators are in their conventional ground states.

There are no other singularities on sheet 1 that allow us to change the sign of the outer square root. This is because at such a singular point the argument of the outer square root function would have to vanish:

$$\nu^2 + \omega^2 + \sqrt{4\nu^2\omega^2 - g^2} = 0 \quad (3.29)$$

The solution of this equation is obtained by squaring  $\nu^2 + \omega^2 = -\sqrt{4\nu^2\omega^2 - g^2}$ :

$$-g^2 = (\nu^2 - \omega^2) , \quad (3.30)$$

So  $-g^2$  is positive. The solution in (3.30) is *spurious* because both terms in (3.29) are positive.

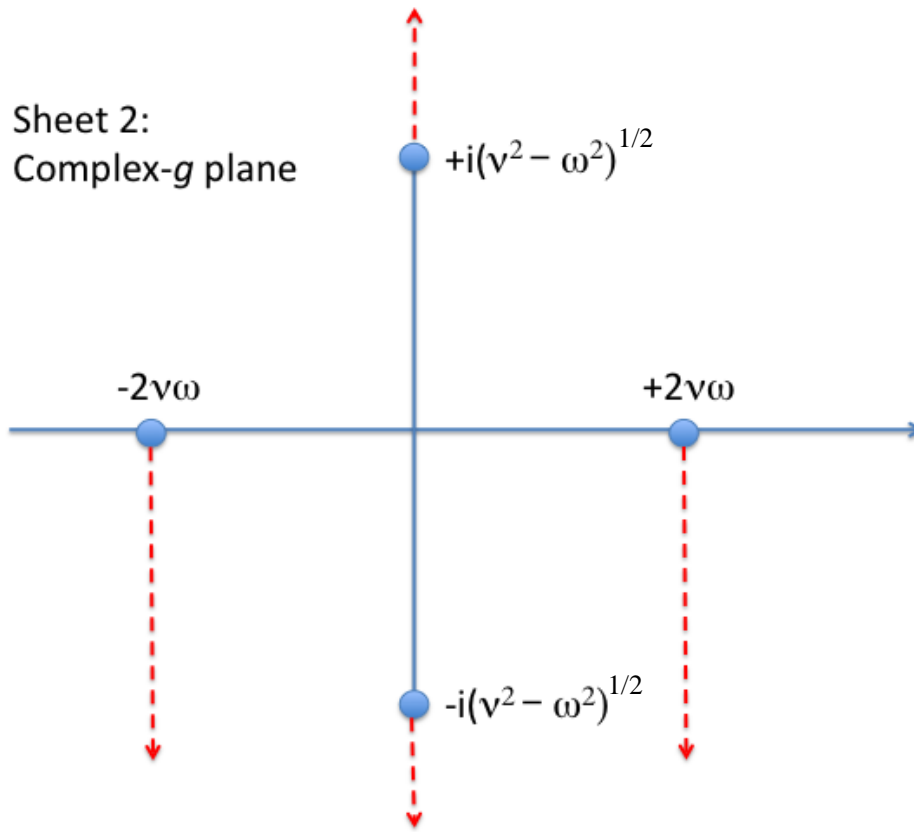


Figure 3.3: Sheet 2 of the complex Riemann surface of  $E(g)$  in (3.27). On this sheet the inner square root in (3.27) is negative and the outer square root is positive when their argument are positive. On this sheet  $E(0)$  is  $\nu - \omega$  (assuming that  $\nu - \omega$  is positive).

If we analytically continue  $E(g)$  through either of the branch cuts on sheet 1, we arrive on sheet 2, where the inner square root changes sign. Therefore, on this sheet

$$E(0) = \nu - \omega \tag{3.31}$$

assuming that  $\nu > \omega$ . Thus, the  $x$  oscillator is in its conventional ground state but the  $y$  oscillator is in its unconventional ground state. Because the inner square root returns

negative values when its argument is positive, the solution for  $-g^2$  in (3.30) is *not* spurious. Therefore, there are new branch cuts associated with the sign change of the outer square root; these branch cuts emanate from branch points located at

$$g = \pm i \left( \nu^2 - \omega^2 \right)^{1/2} . \quad (3.32)$$

All four branch cuts on sheet 2 are shown on Fig. 3.3. If we now pass through a branch cut emanating from  $\pm 2\nu\omega$ , we return to sheet 1 but if we pass through a branch cut emanating from either branch point in (3.32), we enter sheet 3.

On sheet 3 there are two pairs of square-root branch cuts. The branch points on the imaginary axis coincide with those on sheet 2. However, there is a new pair of branch points on the real axis at  $g = \pm 2\nu\omega$ . Although these branch points appear at the same locations as on sheet 1 and 2, they are unrelated to those branch points. We show this explicitly in figure (3.4) by drawing the associated branch cuts differently. On this sheet both the inner and outer square-root functions in (3.27) are negative and

$$E(0) = -\nu + \omega \quad (3.33)$$

when  $\nu - \omega$  is positive. Now the  $x$  oscillator is in an unconventional ground state and the  $y$  oscillator is in a conventional ground state.

If we now pass through a branch cut emanating from (3.32), we return from sheet 3 to 2. However, if pass through a branch cut emanating from  $\pm 2\nu\omega$ , we enter sheet 4. On this sheet there are only branch points, which located at  $\pm 2\nu\omega$  (see Fig. 3.5). On sheet 4

$$E(0) = -\nu - \omega \quad (3.34)$$

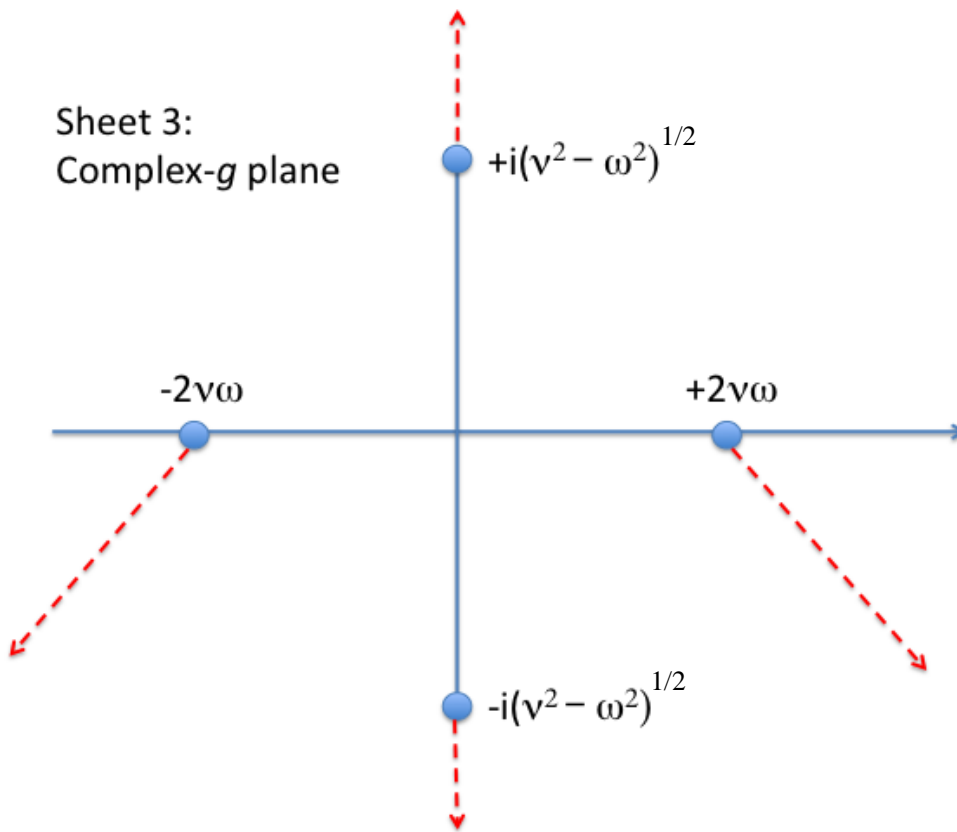


Figure 3.4: Sheet 3 of the complex Riemann surface of  $E(g)$  in (3.27). On this sheet both the inner and outer square roots are negative when their arguments are positive and thus  $E(0) = -v + \omega$ .

Both oscillators are now in unconventional ground states. To summarize, Figs. 3.2-3.5 describe each of the four branches of the function  $E(g)$  in 3.27. On these four branches  $E(0)$  takes the values given in (3.28), (3.31), (3.33), and (3.34). From these four values of  $E(0)$  we infer that by analytically continuing the two-coupled-oscillator system in (3.1) through the entire Riemann surface we access both phases, conventional and unconventional, of both oscillators, even though the two frequency parameter  $v$  and  $\omega$  are held fixed.

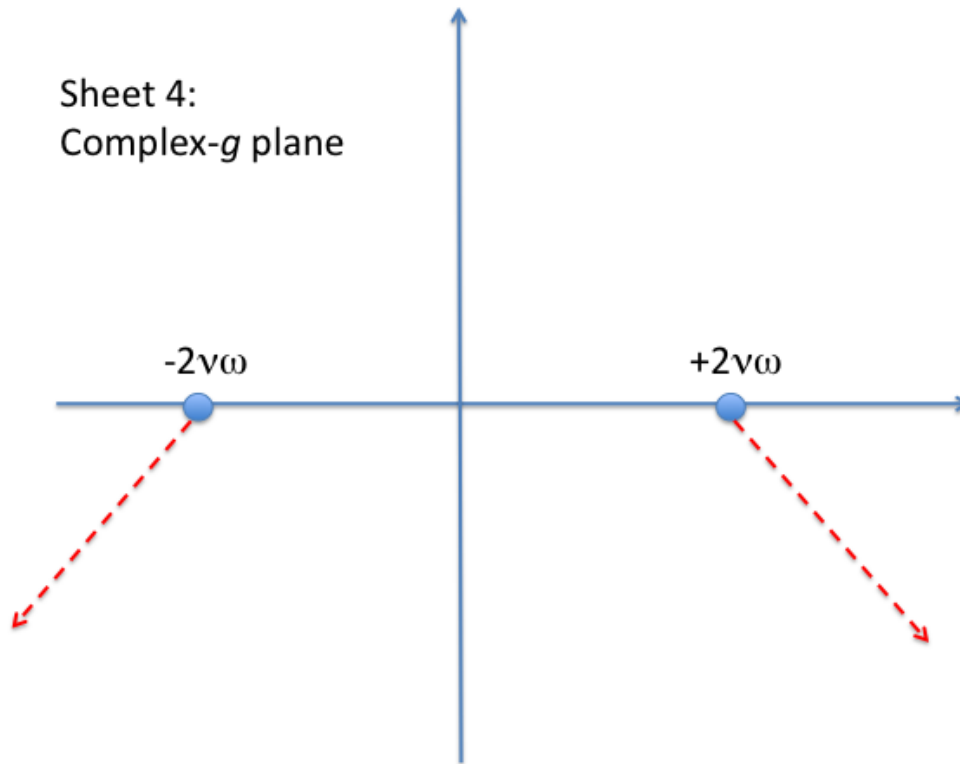


Figure 3.5: Sheet 4 of the complex Reimann surface of  $E(g)$  in (3.27). On this sheet the inner square root is positive and while the outer square root is negative when their argument are positive. On this sheet  $E(0) = \nu - \omega$ .

The four-fold structure of the ground-state energy is repeated for all of the energy levels. To verify this, we construct the eigenfunctions associated with the other energy levels of the theory. These eigenfunctions consist of the exponential in (3.20) multiplied by a polynomial  $P(x, y)$ . If  $P(x, y)$  has the form

$$P(x, y) = Ax + By + Cxy + D, \quad (3.35)$$

the eigenvalue equation (3.21) leads to the three coupled equations (3.22), (3.23), and (3.24) together with four alternative for  $E$ :

$$ED = (a + b)D , \quad (3.36)$$

$$EA = A(3a + b) - 2Bc , \quad (3.37)$$

$$EB = B(a + 3b) - 2Ac , \quad (3.38)$$

$$EC = D(g + 2bc + 2ac) + 3C(a + b) . \quad (3.39)$$

For the quartet of ground-state energy levels described above,  $D = 1$ ,  $A = B = C = 0$ , so that  $P(x, y) = 1$ . We assign the label  $(0, 0)$  to this quartet because it reduces to the (conventional and unconventional) ground states of the  $x$  and  $y$  oscillators when  $g = 0$  and  $c = 0$ . We use the designation  $(0, 1)$  for the quartet  $P(x, y) = y$ ,  $(1, 0)$  for the quartet  $P(x, y) = x$ , and  $(1, 1)$  for the quartet  $P(x, y) = xy$  that give rise to spectra in the decoupling limit  $g = 0, c = 0$ . In this limit, it follows again that  $a^2 = \nu^2$  and  $b^2 = \omega^2$ , leading to four quartets with the additional three spectra arising from (3.37) for  $(1, 0)$  when  $B = C = D = 0$ , (3.38) for  $(0, 1)$  when  $A = C = D = 0$  and (3.39) for  $(1, 1)$  when  $A = B = D = 0$ . These four quartets are illustrated in Fig. 3.6 for the case  $\nu = 2$  and  $\omega = 1$ . We emphasize that the energy levels of different quartets are *not* analytic continuation of one another but the elements of each quartet are analytic continuation of one another and branches of a four-valued function defined on exactly the same the Riemann surface pictured in Figs. 3.2-3.5.

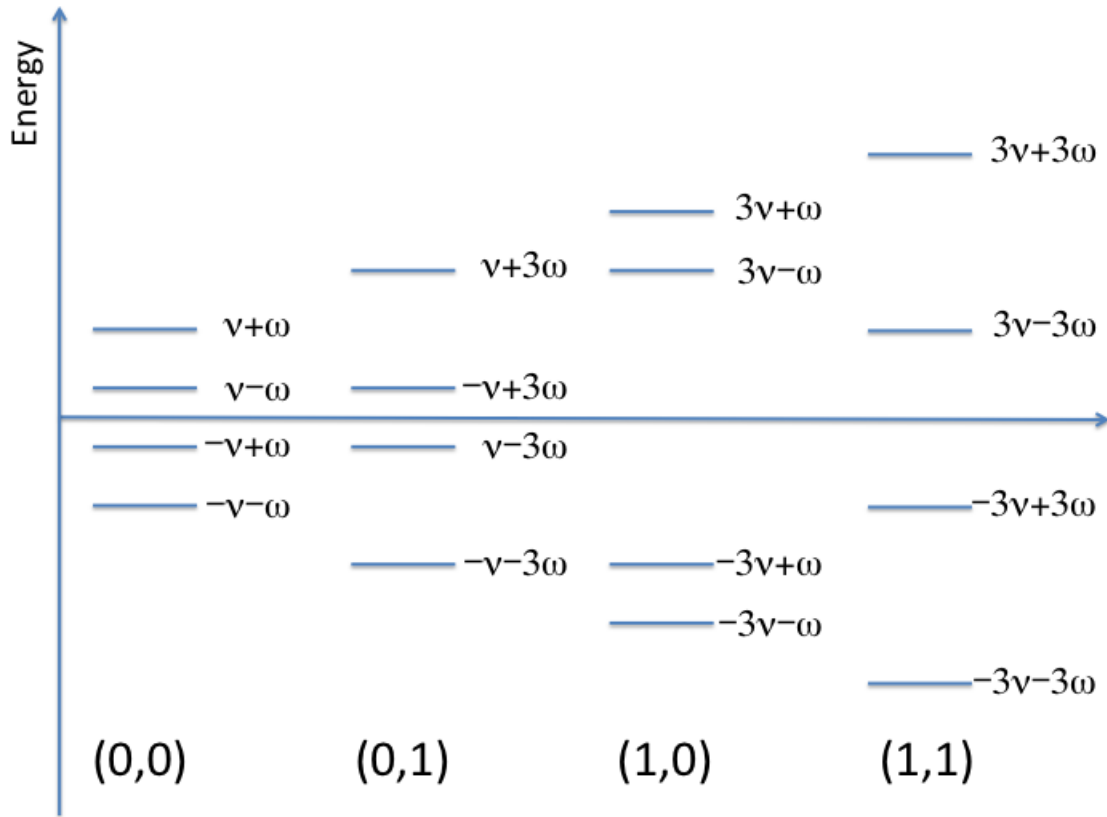


Figure 3.6: First four quartets of energy levels associated with the Hamiltonian (3.1). The quartets are labeled  $(m, n)$ , and the quartets shown are for  $m = 0, 1$  and have  $n = 0, 1$ . We have chosen the values  $\nu = 2$  and  $\omega = 1$  and have plotted the values of  $E(0)$  to scale. Note that each energy eigenvalue corresponds to the lowest such state on a different Riemann sheet.

## 3.4 Partition Function for Zero-Dimensional Field Theories

### 3.4.1 Interacting Quadratic Field Theory

Let us examine the zero-dimensional field-theoretic equivalent of the Hamiltonian (3.1). The partition function for this field theory is given by the integral

$$Z(g) = \int \int dx dy e^{-v^2x^2 - \omega^2y^2 - gxy} \quad (3.40)$$

where both integration paths run from  $-\infty$  to  $\infty$ . We can evaluate the integral exactly by rearranging the terms in the exponential as we did in (3.2):

$$Z(g) = \int \int dx dy e^{-v^2[x+gy(2v^2)]^2 - y^2[\omega^2 - g^2/(4v^2)]} . \quad (3.41)$$

Simple transformation then reduce this to a product of two gaussian integrals,

$$Z(g) = \int \int \frac{2dx dy}{\sqrt{4v^2\omega^2 - g^2}} e^{-x^2 - y^2} , \quad (3.42)$$

which evaluate to

$$Z(g) = \frac{2\pi}{\sqrt{4v^2\omega^2 - g^2}} . \quad (3.43)$$

This partition function is a *double*-valued function of  $g$  and is defined on a two-sheeted Riemann surface. Like the coupled harmonic oscillator discussed in section 3.3 the square-root singularities are located at  $g = \pm 2v\omega$ . However, unlike the case of the coupled

harmonic oscillator, the Reimann surface two sheets and not four; these sheets correspond to the possible signs of  $Z(g)$  and these sheets correspond to the analogs of the conventional-conventional theory and unconventional-unconventional theory. (To obtain the unconventional-unconventional theory from the conventional-conventional theory we replace  $x$  by  $ix$  and  $y$  by  $iy$  and this changes the sign of the partition function.) There is no analytic continuation to the partition function for a mixed unconventional-conventional theory. This is because the path of integration is included with the integral that defines the partition function. Given an eigenvalue differential equation we are free to choose the boundary conditions (we can require that the eigenfunctions vanish as  $x \rightarrow \pm\infty$  or as  $x \rightarrow \pm i\infty$ ) but there is no such freedom in the case of an integral. To obtain other phase we would have to change the path of integration in the definition of the partition function.

We can generalize this calculation by including in the partition function external fields  $J$  and  $K$  coupled on the  $x$  and  $y$  fields:

$$Z(J, K; g) = \int \int dx dy e^{-v^2 x^2 - \omega^2 y^2 - gxy + Jx + Ky} . \quad (3.44)$$

Evaluating this integral by following the same procedure as above, we now find a more elaborate singularity structure,

$$Z(g) = \frac{2\pi}{\sqrt{4v^2\omega^2 - g^2}} \exp\left(\frac{J^2\omega^2 + K^2v^2 - gKL}{4\omega^2v^2}\right) , \quad (3.45)$$

which is again defined on the two-sheeted Reimann surface but in addition has essential singularities at the square-root branch points. Consequently, all of the Green's functions,

which are obtained by taking derivatives with respect to the external sources, have increasingly stronger singularities at  $g = \pm 2\nu\omega$ .

### 3.4.2 Interacting Sextic Field Theory

A higher-power selfinteracting field theory that possesses a conventional real spectrum and in addition possesses a real  $\mathcal{PT}$ -symmetric spectrum has a sextic interaction of the form  $\phi^6$ . We thus examine a field theory that describes the coupling of two sextic oscillators and we choose a symmetric form for the coupling. The partition function for the zero-dimensional version of this coupled quantum field theory is

$$Z(g) = \int \int dx dy e^{-x^6 - y^6 - gx^3y^3} . \quad (3.46)$$

This sextic theory is more difficult to examine analytically. We begin by expanding the coupling term as a series in powers of  $g$ :

$$Z(g) = \sum_{n=0}^{\infty} \frac{(-g)^n}{n!} \int \int dx dy e^{-x^6 - y^6} x^{3n} y^{3n} . \quad (3.47)$$

Since the  $x$  and  $y$  integrals run from  $-\infty$  to  $\infty$ , only even values of  $n$  contribute to the partition function. When  $n$  is even, we have

$$\int_{-\infty}^{\infty} dx e^{-x^6} x^{3n} = \frac{1}{3} \Gamma \left( \frac{n}{2} + \frac{1}{6} \right) , \quad (3.48)$$

but if  $n$  is odd, the integral vanishes. Thus, we make the replacement  $n = 2m$  and re-express the partition function as a sum over  $m$ :

$$Z(g) = \frac{1}{9} \sum_{m=0}^{\infty} \frac{g^{2m}}{(2m)!} \Gamma\left(m + \frac{1}{6}\right). \quad (3.49)$$

This sum is a hypergeometric series:

$$Z(g) = \frac{1}{9} \Gamma^2\left(\frac{1}{6}\right) {}_2F_1\left(\frac{1}{6}, \frac{1}{6}; \frac{1}{2}; \frac{g^2}{4}\right). \quad (3.50)$$

In general, the hypergeometric series has a radius of convergence of 1. (This is easy to verify by using the Stirling approximation for the Gamma function.) This implies that  $Z(g)$  has a singularity on the circle  $|g| = 2$ .

It is important to identify the precise location and nature of this singularity. To do so we use the linear transformation formula [89]

$$\begin{aligned} {}_2F_1(a, d; c; z) &= \frac{\Gamma(c)\Gamma(c-a-b)}{\Gamma(c-a)\Gamma(c-b)} {}_2F_1(a, b; a+b-c+1; 1-z) \\ &+ (1-z)^{c-a-b} \frac{\Gamma(c)\Gamma(a+b-c)}{\Gamma(a)\Gamma(b)} {}_2F_1(c-a, c-b; c-a-b+1; 1-z) \end{aligned} \quad (3.51)$$

This transformation makes the singularity explicit because the hypergeometric function is analytic in the circle. Applying this transformation gives

$$Z(g) = \frac{\sqrt{\pi}\Gamma^3\left(\frac{1}{6}\right)}{9\Gamma^2\left(\frac{1}{3}\right)} {}_2F_1\left(\frac{1}{6}, \frac{1}{6}; \frac{5}{6}; 1 - \frac{g^2}{4}\right) + \left(1 - \frac{g^2}{4}\right)^{\frac{1}{6}} \frac{\sqrt{\pi}\Gamma\left(-\frac{1}{6}\right)}{9} {}_2F_1\left(\frac{1}{3}, \frac{1}{3}; \frac{7}{6}; 1 - \frac{g^2}{4}\right) \quad (3.52)$$

from which we conclude that  $Z(g)$  is defined on a six-sheeted Reimann surface and that the branch points on all six sheets of the Reimann surface are located at  $g = \pm 2$ , which corresponds with the singularities of the coupled harmonic oscillator model at  $\pm 2\nu\omega$  with  $\nu = \omega = 1$ .

More generally, we can examine the green's functions  $G_{\alpha,\beta}$  of the theory, which are defined as integrals of the form

$$G_{\alpha,\beta} \equiv \int \int dx dy x^\alpha y^\beta e^{-x^6 - y^6 - gx^3y^3} \quad (3.53)$$

where  $\alpha$  and  $\beta$  are integers. It is necessary that  $\alpha + \beta$  is even for the Green's function to be nonvanishing. Following the same analysis as above, we find that all Green's functions are defined on a six-sheeted Reimann surface and that the singularity in the complex- $g$  plane has the form

$$\left(1 - \frac{g^2}{4}\right)^{\frac{1-\alpha-\beta}{6}} \quad (3.54)$$

Thus, like the Green's function for the coupled harmonic oscillator we see that the singularity becomes stronger with increasing  $\alpha$  and  $\beta$ , but the Green's functions are always six-valued functions of  $g$ .

## 3.5 Conclusions

We have shown that a coupled quantum theory has a rich analytic structure as a function of the coupling constant. By analytically continuing in the coupling constant we can obtain different spectral phases of the *uncoupled* theory. Indeed, if we think the coupling constant as an external classical source, then by varying this external source in a closed loop in the complex-coupling-constant plane we can even imagine extracting energy from the conventional ground state of such theory, at least in principle. For example, we can begin with the uncoupled harmonic-oscillator system (3.1) in its conventional ground state (3.28). We then turn on the source  $g$ , smoothly and continuously vary  $g$ , and finally turn off  $g$  again when the system is in the unconventional ground state (3.31). Such a process appears to be exothermic because it extracts an amount of energy equal to be  $2\nu + 2\omega$ . However, varying the coupling constant requires that we do work on the system. Until now, it is not clear what it means to vary a coupling constant through complex values. However, remarkable progress on this is currently being made from an experimental point of a system and by doing so to analytically continue from one energy state to another. Such a process has actually been achieved in the laboratory by smoothly varying the parameters of a microwave cavity [13] and, in doing so, going continuously from one frequency mode to another. More recently, experiments have been performed in which an exceptional point is *dynamically* encircled [49, 50]. That is, a combination of physical parameters is varied in real time, and the system response is measured, allowing one to access different Riemann surfaces. While [49] emphasizes robust switching, [50] concerns itself with energy transfer between different states of a system, such as has been considered here in our illustrative prototypical system. An experimental approach, whether

optomechanical or using light, acoustics, matter waves, or microwaves may in the future yield experimental verification of the analytic continuation discussed in this work.

Finally, these studies have been performed for *linear* couplings between the oscillators, which led to the four-fold structure shown here. It is to be expected that other types of couplings lead to different, possibly more complicated Riemann surfaces.

# Chapter 4

## Behavior of eigenvalues in a region of broken- $\mathcal{PT}$ symmetry

*This chapter contains the materials published in a paper [\[104\]](#), which represents work performed by me under the supervision of my advisor, C. M. Bender.*

## 4.1 Introduction

$\mathcal{PT}$ -symmetric quantum theory has its roots in a series of papers that proposed a new perturbative approach to scalar quantum field theory: Instead of a conventional expansion in powers of a coupling constant, it was proposed that a perturbation parameter  $\delta$  be introduced that measures the nonlinearity of the theory. Thus, to solve a  $g\phi^4$  field theory one studies a  $g\phi^2 (\phi^2)^\delta$  theory and treats  $\delta$  as a small parameter. After developing a perturbation expansion in powers of  $\delta$ , the parameter  $\delta$  is set to one to obtain the results for the  $g\phi^4$  theory. This perturbative calculation is impressively accurate and does not require the coupling constant  $g$  to be small [105, 106]. A crucial technical feature of this idea is that  $\phi^2$  and not  $\phi$  be raised to the power  $\delta$  in order to avoid raising a negative number to a noninteger power and thereby generating complex number as an artifact of the procedure.

Subsequently, the  $\delta$  expansion was used to solve an array of nonlinear classical differential equations taken from various areas of physics: The Thomas-Fermi equation (nuclear charge density)  $y''(x) = [y(x)]^{3/2} / \sqrt{x}$  is modified to  $y''(x) = y(x) [y(x)/x]^\delta$ ; the Lane-Emdon equation (stellar structure)  $y''(x) + 2y'(x)/x + [y(x)]^n = 0$  is modified to  $y''(x) + 2y'(x)/x + [y(x)]^{1+\delta}$ ; the Blasius equation (fluid dynamics)  $y'''(x) + y''(x)y(x) = 0$  is modified to  $y'''(x) + y''(x)[y(x)]^\delta = 0$ ; the Korteweg-de Vries equation (nonlinear waves)  $u_t + uu_x + u_{xxx} = 0$  is modified to  $u_t + u^\delta u_x + u_{xxx} = 0$ . In each of these cases the quantity raised to power delta is positive and when  $\delta = 0$  the equation becomes linear. Just a few terms in the  $\delta$  expansion gives an accurate numerical result [107].

The breakthrough of  $\mathcal{PT}$ -symmetric quantum theory was the surprising discovery that to avoid the appearance of spurious complex numbers it is actually not necessary to raise

a positive quantity to the power  $\delta$  so long as the quantity is symmetric under combined space and time reflection. This fact is highly nontrivial and was totally unexpected. For example, a quantum-mechanical potential of the form  $x^2 (ix)^\epsilon$  does not necessarily lead to complex eigenvalues because the quantity  $ix$  is  $\mathcal{PT}$  invariant. Indeed, the non-Hermitian  $\mathcal{PT}$ -symmetric Hamiltonian

$$H = p^2 + x^2 (ix)^\epsilon \quad (4.1)$$

has the property that its eigenvalues are entirely real, positive, and discrete when  $\epsilon \geq 0$  (see Fig. 4.1) The reality of the spectrum was noted in [2, 108] and was attributed to the  $\mathcal{PT}$  symmetry of  $H$ . Doery, Dunning, and Tateo proved that the spectrum is real when  $\epsilon > 0$  [24, 109]. Following the observation that the eigenvalues of non-Hermitian  $\mathcal{PT}$ -symmetric Hamiltonians could be real, many papers were published in which various  $\mathcal{PT}$ -symmetric model Hamiltonian were studied [6].

A particularly interesting feature of  $\mathcal{PT}$ -symmetric Hamiltonian is that they often exhibit a transition from a parametric region of *unbroken*  $\mathcal{PT}$  symmetry in which all of the eigenvalues are real to a region of *broken*  $\mathcal{PT}$  symmetry in which some of the eigenvalues are real and the rest of the eigenvalues occurs in complex-conjugate pairs. The  $\mathcal{PT}$  transition occurs in both the classical and quantized versions of a  $\mathcal{PT}$ -symmetric Hamiltonian [108] and this transition has been observed in numerous laboratory experiments [13, 14, 56, 58, 110–117].

There have been many studies of the real spectrum of  $H$  in (4.1) but essentially nothing has been published regarding the analytic behavior of the complex eigenvalues as functions of  $\epsilon$  in the region of broken  $\mathcal{PT}$  symmetry. However, it is known that there is sequence of negative-real values of  $\epsilon$  lying between  $-1$  and  $0$  at which pairs of real wigenvalues become degenerate and split into pairs of complex-conjugate eigenvalues.

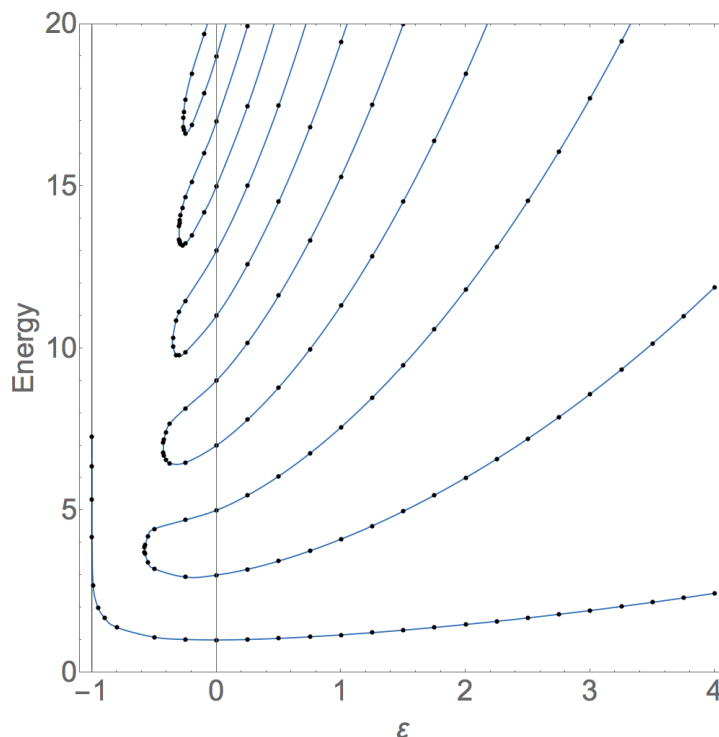


Figure 4.1: Real eigenvalues of the Hamiltonian  $H = p^2 + x^2(ix)^\epsilon$  plotted as function of the parameter  $\epsilon$ . When  $\epsilon \geq 0$  (the region of unbroken  $\mathcal{PT}$  symmetry), the spectrum is real, positive, and discrete. However, as  $\epsilon$  goes below 0 ( $\epsilon < 0$  is known as the region of *broken  $\mathcal{PT}$  symmetry*) the real eigenvalues begin to merge pairwise and from complex-conjugate pair. When  $-1 < \epsilon < 0$ , there are only a finite number of real positive eigenvalues and an infinite number of complex-conjugate pairs of eigenvalues. When  $\epsilon \leq -0.57793$ , only one real eigenvalue survives and as  $\epsilon$  approaches  $-1^+$ , this real eigenvalue becomes infinite. The behavior of the complex eigenvalues in the region of broken  $\mathcal{PT}$  symmetry is not shown in this graph and has not been explored until now.

These special values of  $\epsilon$  are often called *exceptional points* [95]. In general, eigenvalues usually have square-root branch-point singularities at exceptional points.

Exceptional points in the complex plane, sometimes called *Bender-Wu Singularities*, explain the divergence of perturbation expansions [93, 94]. The appearance of exceptional points is a generic phenomenon. In these early studies of coupling-constant analyticity, it

was shown that the energy levels of a Hamiltonian, such as the Hamiltonian for the quantum anharmonic oscillator  $H = p^2 + x^2 + gx^4$ , are analytic continuations of one another as functions of the complex coupling constant  $g$  due to the phenomenon of level crossing at the exceptional points. Thus, the energy levels of a quantum system, which are discrete when  $g$  is real and positive, are actually smooth analytic continuations of one another in the complex- $g$  plane [1]. A simple topological picture of quantization emerges: The discrete energy levels of a Hamiltonian for  $g > 0$  are all branches of a multivalued energy function  $E(g)$  and the distinct eigenvalues of this Hamiltonian correspond with the sheet of the Riemann surface on which  $E(g)$  is defined. Interestingly, it is possible to vary the parameter of a Hamiltonian in laboratory experiments and thus to observe *experimentally* the effect of encircling exceptional points [13, 49, 50].

The purpose of this chapter is to study the analytic continuation of the real eigenvalues shown in Fig. 4.1 as  $\epsilon$  moves down the negative- $\epsilon$  axis. We discuss the Stokes wedges that characterize the eigenvalue problem as  $\epsilon$  goes below  $-1$  and we show that there is an *infinite-order* exceptional point at  $\epsilon = -1$  where there is an elaborate logarithmic spiral (a double helix) of eigenvalues. The real part of each complex-conjugate pair of eigenvalues that is formed at exceptional points between  $\epsilon = -1$  and  $\epsilon = 0$  approaches  $\infty$  like  $|\ln(\epsilon + 1)|^{2/3}$  as  $\epsilon$  approaches  $-1$ . In contrast, the imaginary parts of each pair of eigenvalues vanish logarithmically at  $\epsilon = -1$ . As  $\epsilon$  goes below  $-1$ , the real parts of the eigenvalues rise up from 0. As  $\epsilon$  goes from just above to just below  $-1$ , the imaginary parts of the eigenvalues appear to undergo discrete jumps but in fact they vary continuously as functions of  $\epsilon$ .

In Sec. 4.3 we give plot of the eigenvalues in the region  $-2 < \epsilon < -1$  and perform an asymptotic analysis of the eigenvalues near  $\epsilon = -2$ . As  $\epsilon$  approaches  $-2$ , the entire

spectrum becomes degenerate; the real parts of all the eigenvalues approach  $-1$  and the imaginary parts coalesce to  $0$ .

Section 4.4 presents a numerical study of the eigenvalues in the region  $-4 < \epsilon < -2$ . We show that a transition occurs at  $\epsilon = -2$  in which the eigenspectrum goes from being discrete to become partially discrete and partially *continuous*. The continuous part of the spectrum lies on complex-conjugate pairs of curves in the complex- $\epsilon$  plane. Another transition occurs at  $\epsilon = -3$  (the  $\mathcal{PT}$ -symmetric Coulomb potential); below  $\epsilon = -3$  some of the discrete eigenvalues become real. As  $\epsilon$  approaches the conformal point  $\epsilon = -4$ , the eigenvalues collapse to the single value  $0$ . Sec. 4.5 gives brief concluding remarks.

## 4.2 Eigenvalue Behavior as $\epsilon \rightarrow -1$

### 4.2.1 Stokes wedges

The time-dependent Schrödinger eigenvalue problem for the Hamiltonian  $H$  in (4.1) is characterized by the differential equation

$$-y''(x) + x^2(ix)^\epsilon y(x) = Ey(x) . \quad (4.2)$$

The boundary condition imposed on the eigenfunctions require that  $y(x) \rightarrow 0$  exponentially rapidly as  $|x| \rightarrow \infty$  in a pair of Stokes wedges in the complex- $x$  plane. This subsection explains the location of these Stokes wedges.

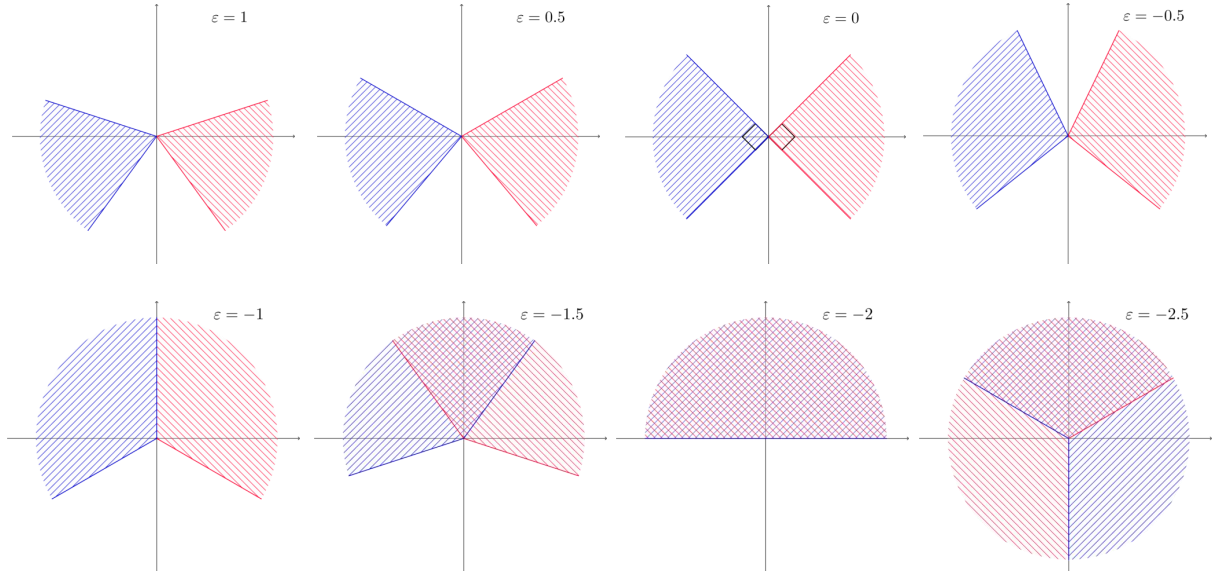


Figure 4.2: Stokes wedges associated with the eigenvalue problem for the Hamiltonian  $H = p^2 + x^2 (ix)^\epsilon$  for eight values of  $\epsilon$ . The location of center lines, the upper edges, and the lower edges of the Stokes wedges are given in (4.3)-(4.8). The left wedge is colored blue and the right wedge is colored red. As  $\epsilon$  decreases, the wedges get wider and rotate upwards. At  $\epsilon = -1$  the two wedges touch and fuse into one wedge. However, when  $\epsilon$  goes below  $-1$ , the sheets are again distinct; the left wedge rotates clockwise into sheet  $-1$  and the right wedge rotates anticlockwise into sheet  $1$ .

As has been previously discussed at length, the potential  $x^2 (ix)^\epsilon$  has a logarithmic singularity in the complex- $x$  plane when  $\epsilon$  is not an integer. Thus, it is necessary to introduce a branch cut. This branch cut is chosen to run from  $0$  to  $\infty$  in the complex- $x$  plane along the positive-imaginary axis because this choice respects the  $\mathcal{PT}$  symmetry of the Hamiltonian. This is because  $\mathcal{PT}$  symmetry translates into left-right symmetry in the complex- $x$  plane (that is, mirror symmetry with respect to the imaginary- $x$  axis) [2, 108]. The argument of  $x$  on the principal sheet (sheet  $0$  of the Riemann surface) runs from  $-3\pi/2$  to  $\pi/2$ . On sheet  $1$ ,  $\pi/2 < \arg x < 5\pi/2$ ; on sheet  $-1$ ,  $-7\pi/2 < \arg x < -3\pi/2$ ; and so on.

As explained in [2, 108], the Stokes wedges in which the boundary condition on  $y(x)$  are imposed are located in the complex- $x$  plane in a  $\mathcal{PT}$ -symmetric fashion. If  $\epsilon = 0$ , the Stokes sedges have angular opening  $\pi/2$  and are centered about the positive  $x$  and negative  $x$  axis on the principal sheet of the Reimann surface. As  $\epsilon$  increases from 0, the wedges get narrower and rotate downwards; as  $\epsilon$  decreases from 0, the Stokes wedges get wider and rotate upwards. Wentzel-Kramers-Brillouin (WKB) analysis provides precise formulas for the location of the center line of the Stokes wedges,

$$\theta_{\text{right wedge, center}} = -\frac{\epsilon}{8 + 2\epsilon}\pi, \quad (4.3)$$

$$\theta_{\text{left wedge, center}} = -\pi + \frac{\epsilon}{8 + 2\epsilon}\pi, \quad (4.4)$$

the upper edges of the Stokes wedges,

$$\theta_{\text{right wedge, upper edge}} = \frac{2 - \epsilon}{8 + 2\epsilon}\pi, \quad (4.5)$$

$$\theta_{\text{left wedge, upper edge}} = -\pi - \frac{2 - \epsilon}{8 + 2\epsilon}\pi, \quad (4.6)$$

and the lower edges of the Stokes wedges,

$$\theta_{\text{right wedge, lower edge}} = -\frac{2 + \epsilon}{8 + 2\epsilon}\pi, \quad (4.7)$$

$$\theta_{\text{left wedge, lower edge}} = -\pi + \frac{2 + \epsilon}{8 + 2\epsilon}\pi. \quad (4.8)$$

The location of the Stokes wedges for eight values of  $\epsilon$  are shown in Fig. 4.2 . As  $\epsilon$  decreases to  $-1$ , the opening angles of the wedges increases to  $120^\circ$  and the upper edges of the wedges touch. At the special value  $\epsilon = -1$  the logarithmic Riemann surface collapses to a single sheet; the wedges fuse and are no longer separated. As a result, there are no

eigenvalues at all (the spectrum is null) [118]. When  $\epsilon$  goes below  $-1$ , the wedges are again distinct and no longer touch; the left wedge rotates in the negative direction and enters sheet  $-1$  while the right wedge rotates in the positive direction and enters sheet  $1$ .

## 4.2.2 Numerical Behavior of the Eigenvalues as $\epsilon$ decreases below 0

Previous numerical studies of the (real) eigenvalues for  $\epsilon \geq 0$  were done by using the shooting method. However, when the eigenvalues become complex, the shooting method is not effective and we have used the finite-element method and several variational methods. We have checked that the eigenvalues produced by these different methods all agree to at least five decimal places.

Figure 4.1 may seem to suggest that the real eigenvalues disappear pairwise at special isolated values of  $\epsilon$ . However, the eigenvalues do not actually disappear; rather, as each pair of real eigenvalues fuse, these eigenvalues convert into a complex-conjugate pair of eigenvalues. At this transformation point, both the real and imaginary parts of each pair of eigenvalues vary *continuously*; the real parts remain nonzero and the imaginary parts move away from zero as  $\epsilon$  goes below the transition point. A more complete plot of the eigenvalues in Fig. 4.3 shows that the real parts of each pair of eigenvalues decay slightly as  $\epsilon$  decreases toward  $-1$ , while the imaginary parts grow slowly in magnitude. However, just as  $\epsilon$  reaches  $-1$  the real parts of the eigenvalues suddenly diverge logarithmically to  $+\infty$  and the imaginary parts of the eigenvalues suddenly vanish logarithmically. Below  $\epsilon = -1$  the real parts of the eigenvalues rapidly descend from  $+\infty$  and the imaginary part of the eigenvalues rise up from  $0$ . This behavior is depicted in Fig. 4.3 and a detailed description of the region  $-1.05 < \epsilon < -0.95$  is shown in Fig. 4.4.

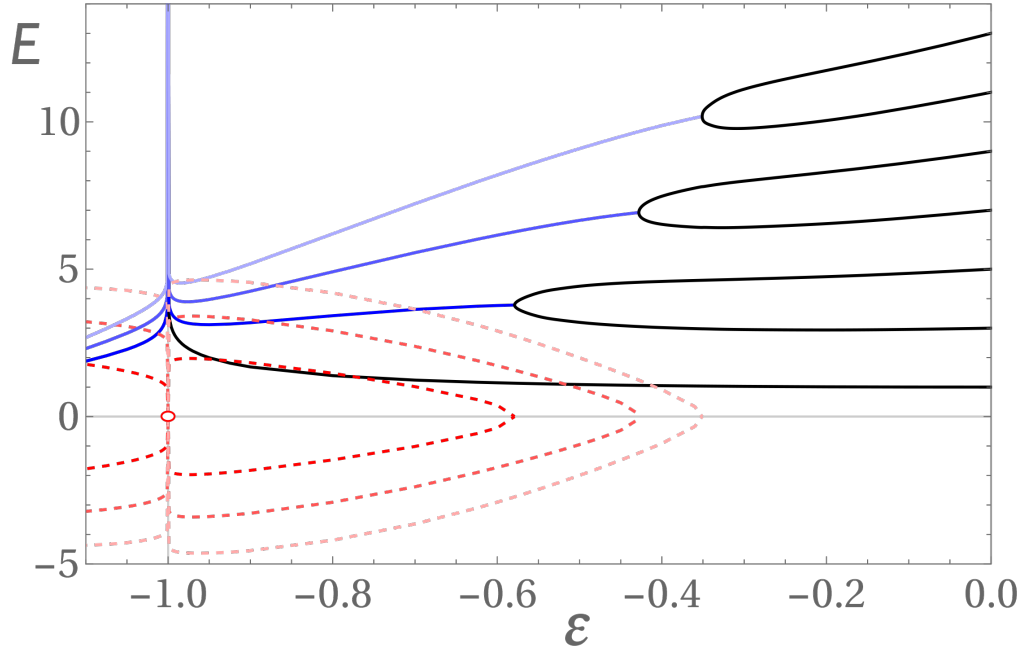


Figure 4.3: Eigenvalues of the Hamiltonian  $H = p^2 + x^2(ix)^\epsilon$  plotted as functions of the parameter  $\epsilon$  for  $-1.1 < \epsilon < 0$ . This graph is a continuation of the graph in Fig. 4.3. As  $\epsilon$  decreases below 0 and enters the region of broken  $\mathcal{PT}$  symmetry, real eigenvalues (solid black lines) become degenerate and then form complex-conjugate pairs. The real parts of these pairs of eigenvalues (solid blue lines) initially decrease as  $\epsilon$  decreases but blow up suddenly as  $\epsilon$  approaches  $-1$ . The real parts then decrease as  $\epsilon$  decreases below  $-1$ . The imaginary parts of the eigenvalue pairs (dashed red lines) remain finite and appear to suffer discontinuous jumps at  $\epsilon = -1$ . However, a closer look shows that these dashed lines rapidly decay to 0 near  $\epsilon = -1$  and then rapidly come back up to different values as  $\epsilon$  passes through  $-1$ . A blow-up of the region near  $\epsilon = -1$  is given in Fig. 4.4.

### 4.2.3 Asymptotic Study of the Eigenvalues near $\epsilon = -1$

Figure 4.3 shows that the eigenvalues are singular at  $\epsilon = -1$  and suggests that this singularity is more complicated than the square-root branch-point singularities that occur at standard exceptional points [119]. To identify the singularity we perform a local asymptotic about the point  $\epsilon = -1$ . We begin by letting  $\epsilon = -1 + \delta$  and we treat  $\delta$  as small

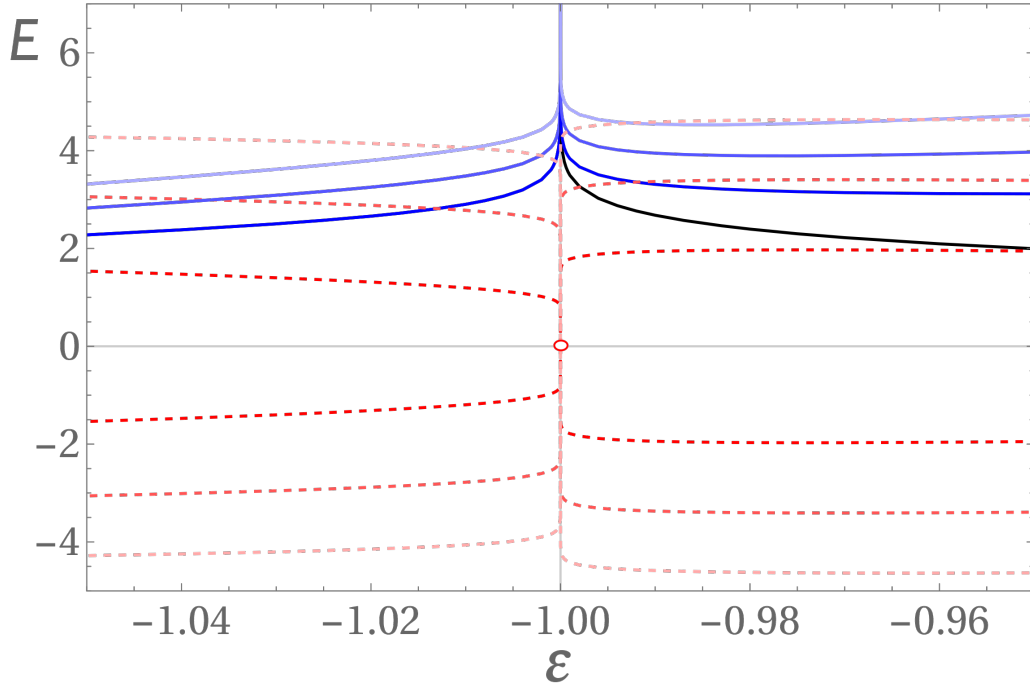


Figure 4.4: Detailed view of Fig. 4.3 showing the behavior of the eigenvalues of the Hamiltonian  $H = p^2 + x^2(ix)^\epsilon$  plotted as functions of the parameter  $\epsilon$  for  $-1.05 \leq \epsilon \leq -0.95$ . There is one real eigenvalue for  $\epsilon > -1$  (solid black line). The real parts of the complex eigenvalues (blue solid lines) and the real eigenvalue diverge at  $\epsilon = -1$ . The complex eigenvalues occur in complex-conjugate pairs and the imaginary parts of the eigenvalues rapidly go to 0 at  $\epsilon = -1$ . These behaviors are expressed quantitatively in (4.24).

( $\delta \ll 1$ ). This allows us to approximate the potential  $x^2(ix)^\epsilon$  in (4.1) as

$$-ix \left[ 1 + \delta \ln(ix) + \mathcal{O}(\delta^2) \right] \quad (4.9)$$

We also expand the eigenfunctions in powers of  $\delta$ :

$$\psi(x) = y_0(x) + \delta y_1(x) + \mathcal{O}(\delta^2) . \quad (4.10)$$

Because we are treating  $\delta$  as small, the Stokes wedges have an angular opening close to  $2\pi/3$  and are approximately centered about the angles  $\theta_L = -7\pi/6$  and  $\theta_R = \pi/6$ . We construct solutions  $\psi_L(x)$  and  $\psi_R(x)$  in the left and right Stokes wedges. We then patch together these eigenfunctions and their first derivatives at the origin  $x = 0$ . The patching condition is

$$0 = \psi_R(x)\psi_L'(x) - \psi_R'(x)\psi_L(x)|_{x=0} . \quad (4.11)$$

To zeroth order in power of  $\delta$  the Schrödinger eigenvalue equation  $H\psi(x) = E\psi(x)$  reads

$$y_0''(x) + ix y_0(x) + E y_0(x) = 0 . \quad (4.12)$$

Substituting  $x = r e^{i\theta_{L,R}}$  reduces this equation to an Airy equation [89] for the zeroth-order eigenfunctions  $y_{0,(L,R)}(r)$  in the left and right wedges:

$$y_{0,(L,R)}''(r) - \left( r - E^{\mp i\pi/3} \right) y_{0,(L,R)}(r) = 0 , \quad (4.13)$$

where the derivatives are now taken with respect to  $r$ .

The boundary condition on the eigenfunctions in each wedge require that  $y_{0,(L,R)}(r) \rightarrow 0$  as  $r \rightarrow \infty$ , so the solutions to (4.13) are Airy function [89]:

$$y_{0,(L,R)}(x) = C_{L,R} \text{Ai} \left( r - E e^{\mp i\pi/3} \right) = C_{L,R} \text{Ai} \left( \mp x e^{\pm i\pi/6} + E e^{\pm 2i\pi/3} \right) , \quad (4.14)$$

where  $C_{L,R}$  are multiplicative constants.

The right side of the patching condition (4.11) for the zeroth-order solutions is calculated from the Wronskian identity for Airy functions [89]:

$$\begin{aligned}
& \psi_{0,R}(x)\psi'_{0,L}(x) - \psi'_{0,R}(x)\psi_{0,L}(x)|_{x=0} \\
&= -C_L C_R \left[ e^{-i\pi/6} \text{Ai} \left( Ee^{-2i\pi/3} \right) \text{Ai}' \left( Ee^{2i\pi/3} \right) + e^{i\pi/6} \text{Ai} \left( Ee^{2i\pi/3} \right) \text{Ai}' \left( Ee^{-2i\pi/3} \right) \right] \\
&= -iC_L C_R W \left[ \text{Ai} \left( Ee^{2i\pi/3} \right), \text{Ai} \left( Ee^{-2i\pi/3} \right) \right] = \frac{1}{2\pi} C_L C_R \neq 0 . \quad (4.15)
\end{aligned}$$

When  $\delta$  is exactly 0, the potential is linear in  $x$  and  $y_{0,(L,R)}(x)$  are the *exact* solutions to the Schrödinger equation. The above calculation shows that these solutions cannot be patched, and thus there are no eigenvalues at all when  $\epsilon = -1$  ( $\delta = 0$ ). This conclusion is consistent with Fig. 4.3, which shows that the real parts of all of the eigenvalues become infinite as  $\epsilon$  approaches  $-1$ . The fact that the spectrum is empty at  $\epsilon = -1$  is not a new result; the absence of eigenvalues of a linear potential was established in [120].

Next, we perform a first-order  $\mathcal{O}(\delta^1)$  analysis. We set  $y_1(x) = Q(x)y_0(x)$ . (This substitution is motivated and explained in detail in [1].) The first-order Schrödinger equation now reads

$$y_1''(x) + ix y_1(x) + ix \ln(ix) y_0(x) + E y_1(x) = 0 . \quad (4.16)$$

We multiply this equation by the integrating factor  $y_0(x)$  and insert the leading-order approximation to eigenfunction and obtain

$$\left[ y_0^2(x) Q'(x) \right]' = -ix \ln(ix) y_0^2(x) . \quad (4.17)$$

We then integrate this equation along the center ray of each Stokes wedge:

$$\begin{aligned}
Q'_{L,R}(x) &= i \int_0^{\mp \exp(\mp i\pi/6)\infty} dt t \ln(it) \left[ \frac{y_{0,(L,R)}(t)}{y_{0,(L,R)}(x)} \right]^2 \\
&= ie^{\mp i\pi/3} \int_0^\infty ds s \ln(\mp se^{\mp i\pi/6}) \left[ \frac{y_{0,(L,R)}(\mp se^{\mp i\pi/6})}{y_{0,(L,R)}(x)} \right]^2 \\
&= ie^{\mp i\pi/3} \int_0^\infty ds s \ln(se^{\mp 2i\pi/6}) \left[ \frac{\text{Ai}(s + Ee^{\pm 2i\pi/3})}{\text{Ai}(\mp xe^{\pm i\pi/6} + Ee^{\pm 2i\pi/3})} \right]^2 . \tag{4.18}
\end{aligned}$$

Thus, to first order in  $\delta$  with  $\psi(x) = y_0(x) [1 + \delta Q(x)]$  the patching condition (4.11) becomes

$$\begin{aligned}
0 &= [1 + \delta Q_R(0) + \delta Q_L(0)] [y_{0,R}(x)y'_{0,L}(x) - y'_{0,R}(x)y_{0,L}(x)]_{x=0} + \delta y_{0,L}(x)y_{0,R}(x) [Q'_L(0) - Q'_R(0)] \\
&= C_L C_R \left\{ -\frac{1}{2\pi} + \delta \text{Ai}(Ee^{-2i\pi/3}) \text{Ai}(Ee^{2i\pi/3}) [Q'_L(0) - Q'_R(0)] \right\} \tag{4.19}
\end{aligned}$$

where we have used the zeroth-order patching condition (4.11) and the leading-order eigenfunction (4.14). Note that because the Schrödinger equation is linear we are free to choose  $Q_L(0) + Q_R(0) = 0$ .

For large  $E$ , we use the asymptotic expansion of the Airy function [89]

$$\text{Ai}(x) \sim \frac{1}{2\sqrt{\pi}} x^{-\frac{1}{4}} \exp\left(-\frac{2}{3}x^{3/2}\right) \quad (|x| \rightarrow \infty, |\arg x| < \pi) . \tag{4.20}$$

Thus, the patching condition for  $|E| \rightarrow \infty$  becomes

$$\frac{2}{\delta} \sim \frac{1}{\sqrt{E}} \exp\left(\frac{4}{3}E^{3/2}\right) [Q'_R(0) - Q'_L(0)] . \tag{4.21}$$

Note that because we are treating  $\delta$  as small, the difference  $Q'_R(0) - Q'_L(0)$  is approximately a positive real number. For real  $E$  this difference is exactly real because  $Q'_R(0)$  and  $-Q'_L(0)$  are complex conjugates.

We expand the right side of (4.21) to first order in  $\beta/\alpha$ , where  $\alpha = \text{Re}E > 0$  and  $\beta = \text{Im}E$ . This expansion is justified because, as we can see in Fig. 4.3, the imaginary parts are small compared with the real parts near  $\epsilon = -1$ . The patching condition (4.21) then becomes

$$\begin{aligned} \frac{2}{\delta} &\sim \alpha^{-1/2} \left(1 + i\frac{\beta}{\alpha}\right)^{-1/2} \exp\left[\frac{4}{3}\alpha^{3/2} \left(1 + i\frac{\beta}{\alpha}\right)^{3/2}\right] \\ &= \alpha^{-1/2} \left(1 - i\frac{\beta}{2\alpha}\right) \exp\left(\frac{4}{3}\alpha^{3/2}\right) \exp\left(-2i\alpha^{1/2}\beta\right) + \mathcal{O}\left(\frac{\beta^2}{\alpha^2}\right). \end{aligned} \quad (4.22)$$

Hence, when  $\delta$  is positive, we obtain the condition

$$\arg \frac{2}{\delta} = \arctan\left(-\frac{\beta}{2\alpha} - 2\alpha^{1/2}\beta = 2m\pi\right), \quad (4.23)$$

where  $m$  is an integer. This result simplifies because the arctangent term is small; to leading-order we obtain  $2\alpha^{1/2}\beta = 2m\pi$ . Similarly when  $\delta < 0$ , we find that  $2\alpha^{1/2}\beta = (2m + 1)\pi$ .

We conclude that for either sign of  $\delta$  we obtain a simple formula for the real part of the eigenvalues. Specifically, if we combine the above three equations, we obtain  $\frac{2}{|\delta|} \sim \alpha^{-1/2} \exp\left(\frac{4}{3}\alpha^{3/2}\right)$ . Hence, in the neighborhood of  $\epsilon = -1$  (that is, when  $\delta$  is near 0), the real parts of the eigenvalues are logarithmically divergent while the imaginary parts of the eigenvalues remain finite:

$$\text{Re}E \sim \left(-\frac{3}{4} \ln |\delta|\right)^{2/3}, \quad \text{Im}E \sim \frac{n\pi}{2\sqrt{\text{Re}E}}, \quad (4.24)$$

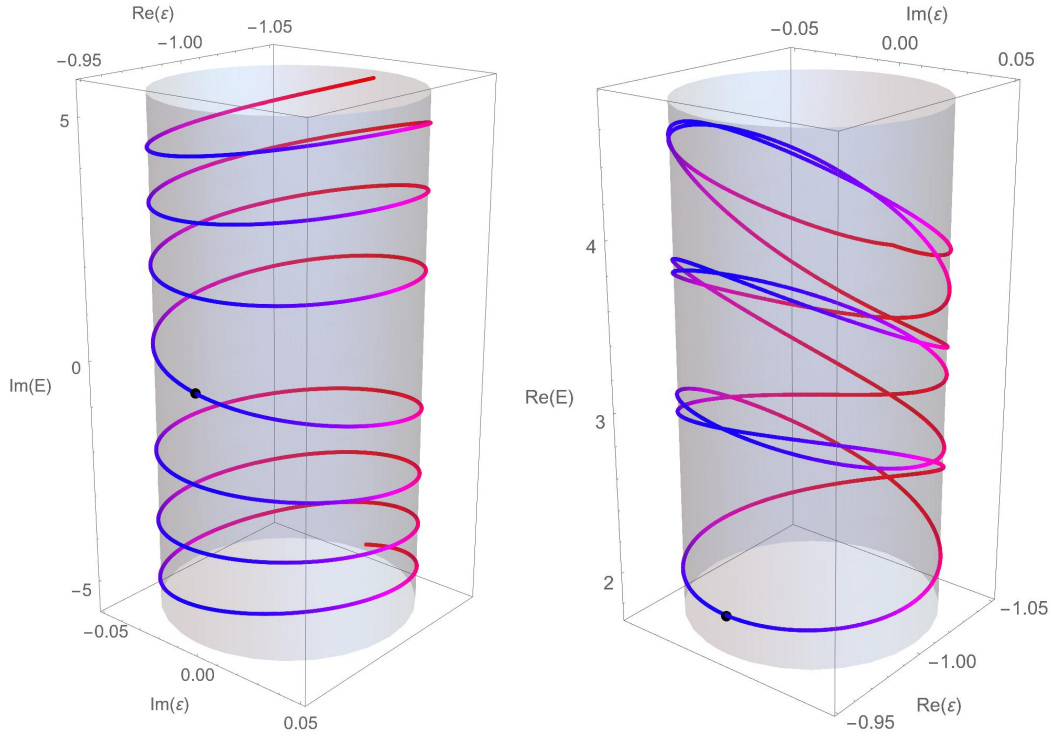


Figure 4.5: Behavior of eigenvalues of the Hamiltonian  $H = p^2 + x^2(ix)^\epsilon$  as the parameter  $\epsilon$  winds around the exceptional point at  $\epsilon = -1$  in a circle of radius 0.05 in the complex- $\epsilon$  plane. This singular point is an infinit-order exceptional point, and all of the complex eigenvalues analytically continue into one another as one encircles the exceptional point. The lines are shaded blue when  $\text{Re}\epsilon > 0$  and red line  $\text{Im}\epsilon < 0$ . The behavior of the imaginary parts of the eigenvalues (left panel) are easier to visualize because they exhibit a simple logarithmic spiral. The dot shows that the imaginary part of an eigenvalue (the eigenvalue shown in black in Figs. 4.3 and 4.4) vanishes (the eigenvalue is real) when  $\text{Re}\epsilon > 0$ . However, as we wind in one direction the imaginary parts of the eigenvalues increases in a helical fashion and as we wind in the opposite direction the imaginary parts of the eigenvalues decrease in a helical fashion. As we pass the real- $\epsilon$  axis we pass through the values plotted on the red dashed line shown in Figs. 4.3 and 4.4. A shaded cylinder has been drawn to assist the eye in following this helix. The two helices intersect four times each time the singular point at  $\epsilon = -1$  is encircled, and they intersect at  $90^\circ$  intervals. If we begin at the dot, we see that the real parts of the eigenvalues increase as we rotate about  $\epsilon = -1$  in either direction. Each time  $\epsilon$  crosses the real axis in the complex- $\epsilon$  plane the curves pass through the values shown at the left and right edges of Fig. 4.4

where  $n$  is an even integer for  $\delta > 0$  and  $n$  is odd integer for  $\delta < 0$ . Evidently, the imaginary parts of the eigenvalues vary rapidly as  $\epsilon$  passes through  $-1$  because there is a *logarithmic* singularity at  $\epsilon = -1$ . A blow-up of the region  $-1.05 < \epsilon < 1.05$  is given in Fig. 4.4.

To visualize the behavior of the eigenvalues near  $\epsilon = -1$  more clearly, we have plotted the imaginary and real parts of the eigenvalues in the *complex- $\epsilon$*  plane in the left and right panels of Fig. 4.5. Observe that the imaginary parts of the eigenvalues lie on a helix and that the real parts of the eigenvalues lie on a double helix as  $\epsilon$  winds around the logarithmic singularity at  $\epsilon = -1$ . This logarithmic singularity is an *infinite-order* exceptional point, which one discovers only very rarely in studies of the analytic structure of eigenvalue problems.

### 4.3 Eigenvalue Behavior as $\epsilon \rightarrow -2$

In Fig. 4.6 we plot the first three complex-conjugate pairs of eigenvalues in the range  $-2.0 \leq \epsilon \leq -1.1$ . Note that the eigenvalues  $E_k$  coalesce to the value  $-1$  as  $\epsilon$  approaches  $-2$ . As  $\epsilon$  decreases towards  $-2$  the real part of  $E_k$  becomes more negative as  $k$  increases, and the spectrum becomes *inverted*; that is, the higher-lying real parts of the eigenvalues when  $\epsilon$  is near  $-1.7$  (for example) decrease as  $\epsilon$  decreases and they cross when  $\epsilon$  is near  $-1.3$ . This crossing region is shown in detail in Fig. 4.7.

The objective of this section is to explain the behavior of the eigenvalues as approaches  $-2$  by performing a local analysis near  $\epsilon = -2$ . To do so we let

$$\epsilon = -2 + \delta \tag{4.25}$$

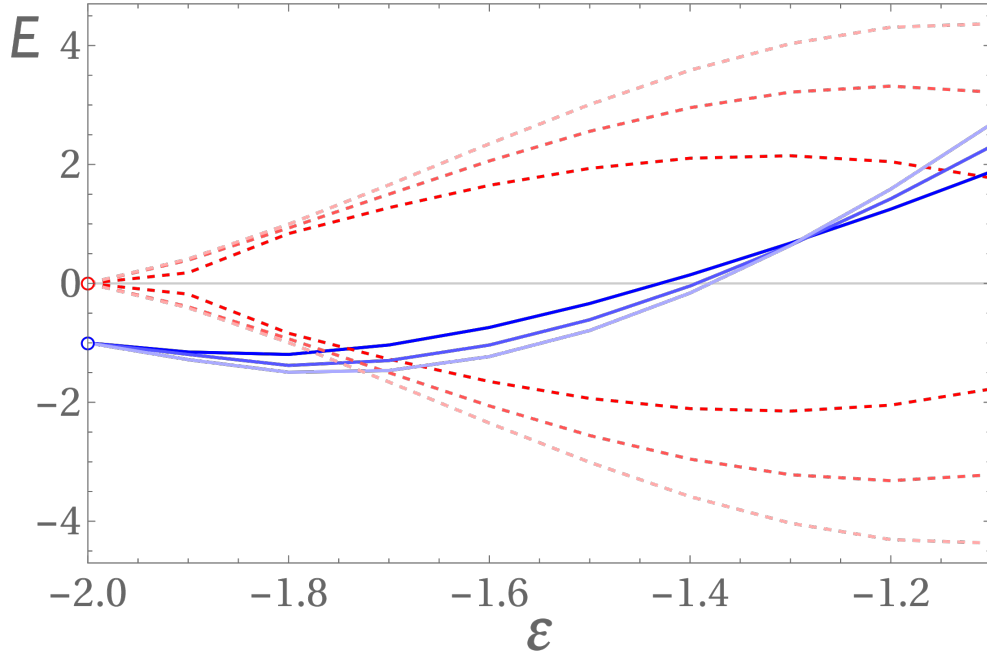


Figure 4.6: First three complex-conjugate pairs of eigenvalues of the Hamiltonian  $H = p^2 + x^2(ix)^\epsilon$  plotted as of Fig. 4.3. Note that the real parts of the eigenvalues coalesce to  $-1$  and the imaginary parts coalesce to  $0$  as  $\epsilon$  approaches  $-2$ . The results of a WKB calculation of these eigenvalues near  $\epsilon = -2$  is given in (4.46). Note that the real parts of the eigenvalues near  $\epsilon = -1.3$ , but they do not all cross at the same point as can be seen in Fig. 4.7

and treat  $\delta$  small ( $\delta \ll 1$ ) and positive. With this change of parameter (4.2) becomes

$$-y''(x) - (ix)^\delta y(x) = Ey(x). \quad (4.26)$$

The boundary condition on  $y(x)$ , which we can deduce from Fig. 4.2, are that the eigenfunctions  $y(x)$  must vanish asymptotically at the ends of a path that originates at  $e^{-3\pi i/2\infty}$  in the complex- $x$  plane, goes down to the origin along the imaginary axis, encircles the origin in the positive direction, goes back up the imaginary axis, and terminate at  $e^{\pi i/2\infty}$ . The eigenfunctions are required to vanish at the endpoints  $e^{-3\pi i/2\infty}$  and  $e^{\pi i/2\infty}$ .

We now make the crucial assumption that it is valid to expand the potential term in (4.26) as series in powers of  $\delta$ . To second order in  $\delta$ , we then have

$$-y''(x) - \delta \ln(ix)y(x) - \frac{1}{2}\delta^2 [\ln(ix)]^2 y(x) = (E + 1)y(x). \quad (4.27)$$

In this form, one can see that to every order in powers of  $\delta$  the potential terms in the Schrödinger equation are singular at  $x = 0$ . As a consequence, the solution  $y(x)$  vanishes at  $x = 0$ . (One can verify that  $y(0) = 0$  by examining the WKB approximation to  $y(x)$ ; the prefactor  $[V(x) - E]^{-1/4}$  vanishes logarithmically.)

We then make the change of independent variable  $t = -ix$ . In term of  $t$ , (4.27) becomes

$$-y''(t) + \delta \ln(-t)y(t) + \frac{1}{2}\delta^2 [\ln(-t)]^2 y(t) = -(E + 1)y(t). \quad (4.28)$$

This eigenvalue equation is posed on a contour on the real- $t$  axis that originates at  $t = +\infty$ , goes down the positive-real  $t$  axis, encircles the origin in the positive direction, and goes back up to  $e^{2i\pi}\infty$ , and  $y(t)$  is required to vanish at the end points of this contour. We then replace  $\ln(-t)$  with  $\ln(t) \pm i\pi$ :

$$-y''(t) + \delta [\ln(t) \pm i\pi] y(t) + \frac{1}{2}\delta^2 [\ln(t) \pm i\pi]^2 y(t) = -(E + 1)y(t) . \quad (4.29)$$

Next, we make the scale change

$$t = s/\sqrt{\delta} \quad (4.30)$$

This converts (4.29) into the Schrödinger equation

$$-y''(s) + \ln(s)y(s) + \delta U(s)y(s) = Fy(s) , \quad (4.31)$$

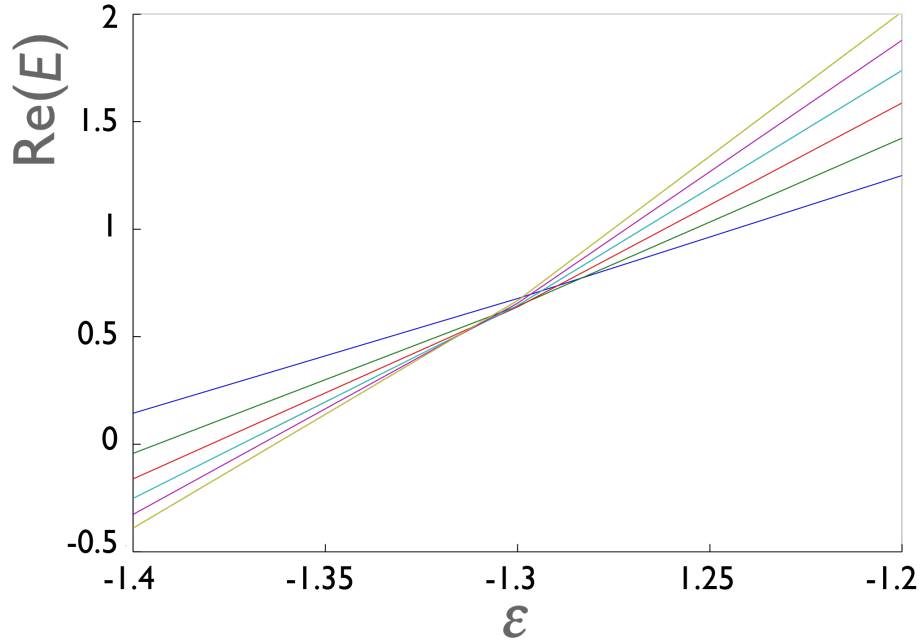


Figure 4.7: Detail of Fig. 4.6 showing the behavior of the real parts of the first six eigenvalues of the Hamiltonian  $H = p^2 + x^2(ix)^\epsilon$  for  $-1.4 \leq \epsilon \leq -1.2$ . The real parts of the eigenvalues cross almost at the same value of  $\epsilon$  but the imaginary parts of the eigenvalues remain well separated.

where the energy term  $F$  is given by

$$F = -(E + 1)/\delta + \frac{1}{2} \ln(\delta) \mp i\pi - \frac{1}{8} \delta [\ln(\delta)]^2 + \frac{1}{2} \delta \pi^2 \pm \frac{1}{2} \delta i\pi \ln(\delta) \quad (4.32)$$

and the order  $\delta$  term in the potential is given by

$$U(s) = \frac{1}{2} [\ln(s)]^2 - \frac{1}{2} \ln(\delta) \ln(s) \pm i\pi \ln(s) . \quad (4.33)$$

Our procedure will be as follows. First, we neglect the  $U(s)$  term in (4.31) because  $\delta$  is small and we use WKB theory to solve the simpler Schrödinger equation

$$-y_0''(s) + \ln(s)y_0(s) = F_0y_0(s) \quad (4.34)$$

Second, we find the energy shift  $\Delta F$  due to the  $U(s)$  term in (4.31) by using first-order Rayleigh-Schrödinger theory [1]; to wit; we calculate the expectation value of  $U(s)$  in the WKB approximation to  $y_0(s)$  in (4.34). Having found  $F = F_0 + \Delta F$ , we obtain the energy  $E$  from (4.32):

$$E = -1 - F\delta + \frac{1}{2}\delta \ln(\delta) \mp i\pi\delta - \frac{1}{8}\delta^2 [\ln(\delta)]^2 + \frac{1}{2}\pi^2\delta^2 \pm \frac{1}{2}i\pi\delta^2 \ln(\delta) . \quad (4.35)$$

This approach gives a very good numerical approximation to the energies shown in Fig. 4.6.

The standard WKB quantization formula for the eigenvalues  $F_0$  in a single-well potential  $V(s)$  (the two-turning-point problem) is

$$\left(n + \frac{1}{2}\right) \pi = \int_{s_1}^{s_2} ds \sqrt{F_0 - V(s)} \quad (n \gg 1) . \quad (4.36)$$

For (4.34) the potential  $V(s)$  is  $\ln(s)$  and the boundary conditions on  $y_0(s)$  are given on the positive half line:  $y_0(s)$  vanishes at  $s = 0$  and at  $s = +\infty$ . In order to apply (4.36), we extend the differential equation to the whole line  $-\infty < s < +\infty$  by replacing  $\ln(s)$  with  $\ln(|s|)$  and consider only the *odd-parity* solutions. Thus, we must replace the integer  $n$  in (4.36) when  $2k + 1$ , where  $k = 0, 1, \dots$ . The turning points are given by  $s_1 = -e^{F_0}$  and

$s_2 = e^{F_0}$ . Hence, the WKB formula (4.36) becomes

$$\left(2k + 1 + \frac{1}{2}\right) \pi = \int_{-e^{F_0}}^{e^{F_0}} ds \sqrt{F_0 - \ln(|s|)} = 2 \int_0^{e^{F_0}} ds \sqrt{F_0 - \ln(|s|)} \quad (k \gg 1) \quad (4.37)$$

The substitution  $s = ue^{F_0}$  simplifies this equation to

$$\left(2k + \frac{3}{2}\right) \pi = 2e^{F_0} \int_0^1 du \sqrt{-\ln(u)}, \quad (4.38)$$

and the further substitution  $v = -\ln(u)$  reduces the integral to a  $\Gamma$  function:

$$\int_0^1 du \sqrt{-\ln(u)} = \int_0^\infty dv e^{-v} v^{1/2} = \Gamma\left(\frac{3}{2}\right) = \frac{1}{2}\sqrt{\pi}. \quad (4.39)$$

Thus, the WKB approximation to the eigenvalues  $F_0$  is

$$F_0 = \ln \left[ \left(2k + \frac{3}{2}\right) \sqrt{\pi} \right], \quad (4.40)$$

which is valid for large  $k$ .

Next, we calculate the order- $\delta$  correction  $\Delta F$  to (4.40) due to the potential  $U(s)$  in (4.31).

To do so we calculate the expectation value of  $U(s)$  in the WKB eigenfunction  $y_0(s)$  of (4.34):

$$\Delta F = \delta \frac{\int_0^\infty ds U(s) [y_0(s)]^2}{\int_0^\infty ds [y_0(s)]^2}, \quad (4.41)$$

where  $U(s)$  is given in (4.33).

Integrals of this type are discussed in detail in Chap.9 of [1]. To summarize the procedure, in the classically forbidden region beyond the turning point,  $y_0(s)$  is exponentially small, and the contribution to the integral from this region is insignificant. In the classically

Table 4.1: Comparison of the real parts of the eigenvalues of the different equation (4.26) at  $\delta = 0.01$  with the asymptotic approximation in (4.46). The rate at which the accuracy increases with increasing  $k$  is similar to the increase in accuracy of the standard WKB approximation to the eigenvalues of the quartic anharmonic oscillator [1].

$k$	Numerical value of $\text{Re}E_k$ at $\delta = 0.01$	$\mathcal{O}(\delta^2)$ calculation of $\text{Re}E_k$ in (4.46)	Relative error
0	-1.0352	-1.0414	8.70 %
2	-1.0426	-1.0461	0.33%
4	-1.0469	-1.0493	0.30%
6	-1.0499	-1.0518	0.18%
8	-1.023	-1.0538	0.15%
10	-1.0542	-1.0555	0.12%
12	1.0559	-1.0569	0.10%

allowed region, the square of the eigenfunction has the general WKB from

$$[y_0(s)]^2 = \frac{C}{\sqrt{F_0 - V(s)}} \sin^2 \left[ \phi + \int^s dr \sqrt{F_0 - V(r)} \right], \quad (4.42)$$

where  $C$  is a multiplicative constant and  $\phi$  is a constant phase shift.

Making the replacement  $\sin^2 \theta = \frac{1}{2} - \frac{1}{2} \cos(2\theta)$ , we observe that because of the Reimann-Lebesgue lemma, the cosine term oscillates to zero for large quantum number  $k$ , and we may replace  $[y_0(s)]^2$  in the integrals in (4.41) by the simple function  $\frac{1}{2} [F_0 - V(s)]^{-1/2}$ . Thus, the shift in the eigenvalues is given by

$$\Delta F = \delta \frac{\int_0^{e^{F_0}} \frac{ds \ln(s)}{\sqrt{F_0 - \ln(s)}} \left[ \frac{1}{2} \ln(s) - \frac{1}{2} \ln(s) \pm i\pi \right]}{\int_0^{e^{F_0}} \frac{ds}{\sqrt{F_0 - \ln(s)}}}. \quad (4.43)$$

After making the previous changes of variable  $s = e^{F_0} u$  followed by  $v = -\ln(u)$ , we obtain

Table 4.2: Comparison of the imaginary parts of the eigenvalues of the differential equation (4.26) at  $\delta = 0.01$  with the asymptotic approximation in (4.46).

$k$	Numerical value of $\text{Im}E_k$ at $\delta = 0.01$	$\mathcal{O}(\delta^2)$ calculation of $\text{Im}E_k$ in (4.46)	Relative error
0	0.03397	0.03210	3.5 %
2	0.03352	0.03220	3.8%
4	0.03339	0.03224	3.4%
6	0.03334	0.03226	3.2%
8	0.03332	0.03228	3.1%
10	0.03332	0.03229	3.0%
12	0.03333	0.03231	3.0%

$$\Delta F = \delta \frac{\int_0^\infty dv e^{-\nu} (F_0 - \nu) \nu^{-1/2} \left[ \frac{1}{2} (F_0 - \nu) - \frac{1}{2} \ln(\delta) \pm i\pi \right]}{\int_0^\infty dv e^{-\nu} \nu^{-1/2}}, \quad (4.44)$$

which evaluates to

$$\Delta F = \frac{1}{8} \delta \left[ 4F_0^2 - 4F_0 + 3 - 4F_0 \ln(\delta) + 2 \ln(\delta) \pm i\pi(8F_0 - 4) \right]. \quad (4.45)$$

Finally, we substitute  $F = F_0 + \Delta F$  in (4.35) to obtain the eigenvalues  $E_k$ :

$$E_k = -1 + \delta \left[ \frac{1}{2} \ln(\delta) - F_0 \right] - \frac{1}{8} \delta^2 \left\{ [\ln(\delta)]^2 + 2 \ln(\delta) - 4 \ln(\delta) F_0 + 3 - 4\pi^2 - 4F_0 + 4F_0^2 \right\} \\ \pm i \left\{ -\delta\pi + \frac{1}{2} \delta^2 [\pi \ln(\delta) + \pi - 2F_0] \right\}, \quad (4.46)$$

where  $F_0$  is given in (4.40).

To verify these results, in Tables 4.1 and 4.2 we compare our numerical calculation of  $\text{Re}E_k$  and  $\text{Im}E_k$  with the asymptotic prediction in (4.46).

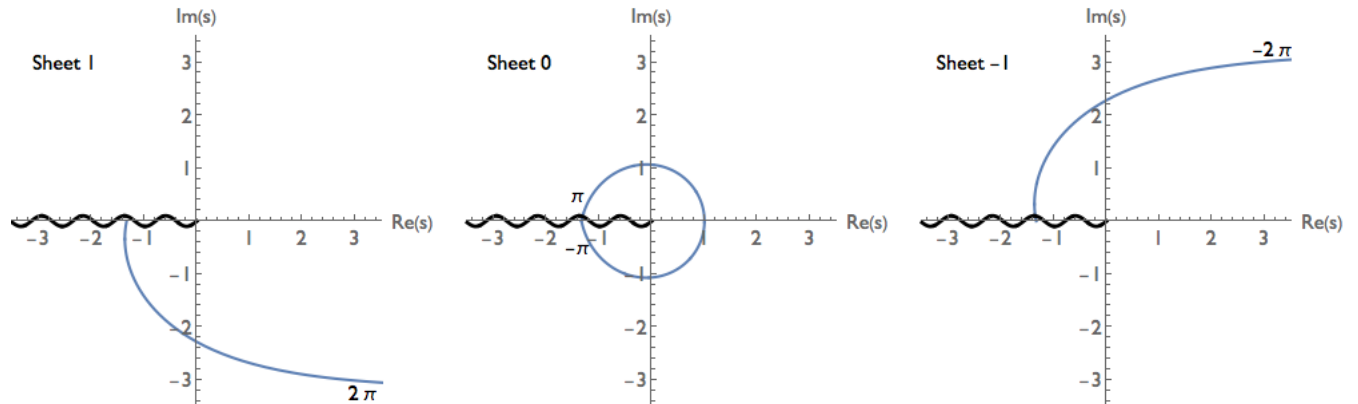


Figure 4.8: Contour in the complex- $s$  plane for the complex Coulomb potential  $\epsilon = -3$ . The contour comes in from  $\infty$  parallel to the positive-real axis at an angle of  $-2\pi$  in the center of the left Stokes wedge (right panel). Next, it loops around the origin in the positive direction (center panel). Finally, it goes back out to  $\infty$  parallel to the positive-real axis at an angle of  $2\pi$  in the center of the right Stokes wedge (left panel). The total rotation about the origin is  $4\pi$ .

#### 4.4 Eigenvalue Behavior for $-4 < \epsilon < -2$

This section reports our numerical calculations of the eigenvalues for  $\epsilon$  between  $-2$  and  $-4$ . We rotate in  $x$  in (4.2) by  $90^\circ$  by making the transformation  $s = ix$ . In the  $s$  variable, the eigenvalue equation (4.2) becomes

$$\psi''(s) - s^{2+\epsilon}\psi(s) = E\psi(s) . \quad (4.47)$$

In the  $x$  variable the center-of-wedge angles (4.3-4.4) are  $-\pi + \epsilon\pi/(8 + 2\epsilon)$  and  $-\epsilon\pi/(8 + 2\epsilon)$  but in the  $s$  variable these angles are simply  $\mp 2\pi/(4 + \epsilon)$ . Thus, the integration

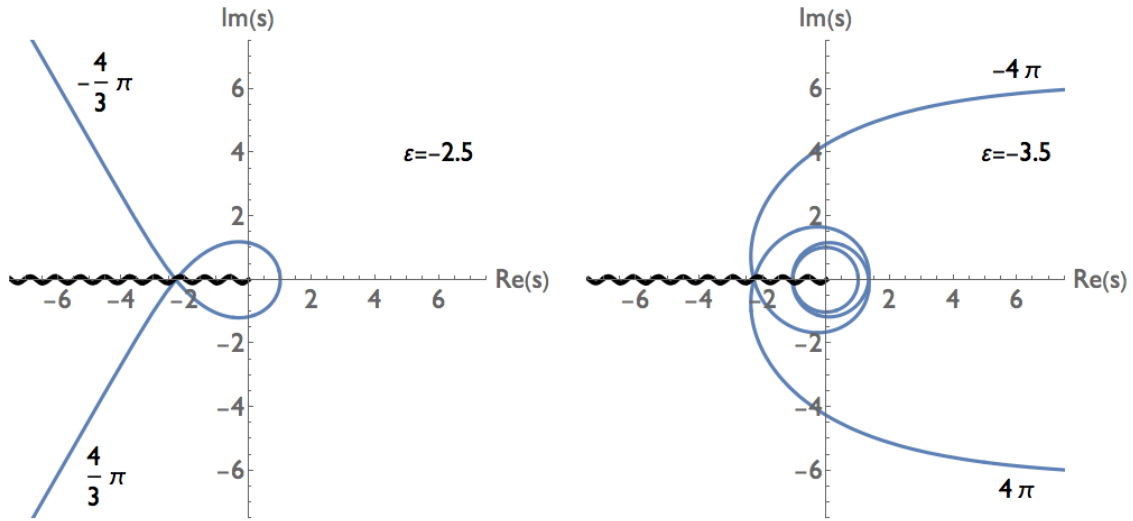


Figure 4.9: Eigenvalue contours in the complex- $s$  plane for the cases  $\epsilon = -2.5$  and  $\epsilon = -3.5$ .

contour makes  $2/(4 + \epsilon)$  loops around the logarithmic branch point at the origin in the complex- $s$  plane.

For example, if  $\epsilon = -3$  (this is the complex  $\mathcal{PT}$ -symmetric version of the Coulomb potential for which  $H = p^2 + i/x$  [121]), then the contour loops around the origin exactly twice; it goes from an angle  $-2\pi$  to the angle  $2\pi$ . Looping contours for other complex eigenvalue problem have been studied in the past and have been called “toboggan contours” [122]. In the  $\mathcal{PT}$ -symmetric Coulomb case the contour is shown in Fig. 4.8. Figure 4.9 shows the contours for the cases  $\epsilon = -2.5$  and  $\epsilon = -3.5$ .

To solve these eigenvalue problems with looping contours, we introduce the change of variable

$$s(t) = \frac{1}{1-t^2} \exp \frac{2\pi i t}{4+\epsilon} \quad (4.48)$$

which parametrizes the looping path in the complex- $s$  plane in terms of the real variable  $t$ . As  $t$  ranges from  $-1$  to  $+1$ , the path in the complex- $s$  plane comes in from infinity in the center of the left Stokes wedge, loops around the logarithmic branch-point singularity at the origin, and goes back out to infinity in the center of the right Stokes wedge. In terms of the  $t$  variable the eigenvalue equation (4.47) has the form

$$\frac{\psi''(t)}{[s'(t)]^2} - \frac{s''(t)}{[s'(t)]^3} \psi'(t) - [s(t)]^{2+\epsilon} \psi(t) = E\psi(t) \quad (4.49)$$

where  $\psi(t)$  satisfies  $\psi(-1) = \psi(1) = 0$ .

To solve this eigenvalue problem we use the Arnoldi algorithm, which has recently become available on Mathematica [123]. This algorithm finds low-lying eigenvalues, whether they are real. We apply the Arnoldi algorithm to (4.49) subject to homogeneous Dirichlet boundary conditions  $\psi(-1 + \eta) = \psi(1 - \eta) = 0$  and let  $\eta \rightarrow 0^+$ . There are two possible outcomes: (i) In this limit, some eigenvalues rapidly approach limiting values; these eigenvalues belong to the discrete part of the spectrum. (ii) Other eigenvalues become dense to curves in the complex plane as  $\eta \rightarrow 0^+$ ; these eigenvalues belong to the continuous part of spectrum.

#### 4.4.1 $\epsilon$ Slightly Below $-2$

As soon as  $\epsilon$  goes below  $-2$ , the eigenvalues explode away from the value  $-1$  (shown at the left side of Fig. 4.6). In Fig. 4.10 we plot about 100 eigenvalues for  $\epsilon = -2.0001$  and  $-2.001$ . In each plot, we see both discrete and continuous eigenvalues. The continuous eigenvalues lie on a complex-conjugate pair of curves in the left-half plane; the discrete eigenvalues also lie in the left-half but closer to the real axis.

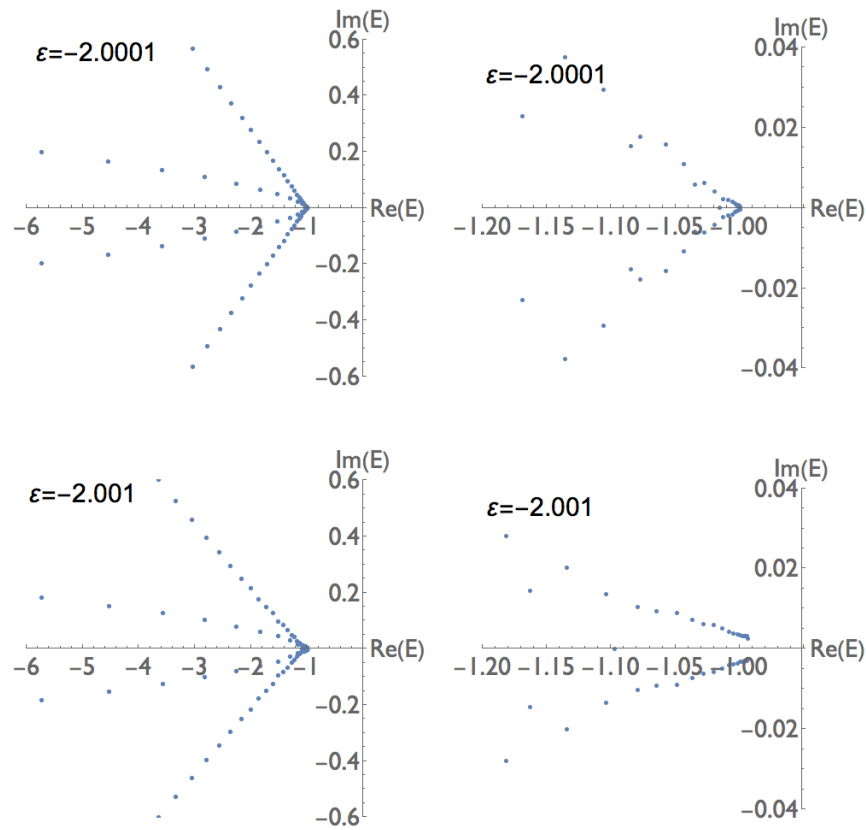


Figure 4.10: Eigenvalues of the Hamiltonian  $H = p^2 + x^2(ix)^\epsilon$  for  $\epsilon = -2.0001$  and  $-2.001$ . (The right panels are magnifications of the left panel.) The spectrum lies in the left-half complex plane and is partly continuous and partly discrete. The eigenvalues in the continuous part of the spectrum lie on a pair of complex-conjugate curves that radiate away from  $-1$  and as we calculate more eigenvalues, the points on these curves become denser. The discrete part of the spectrum consists of eigenvalues lying on two complex-conjugate curves that are much closer to the negative-real axis. There is an elaborate structure near  $\epsilon = -1$ . As  $\epsilon$  goes below  $-2$ , the eigenvalues move away from  $-1$ ; specially, for  $\epsilon = -2.0001$  the distance from  $-1$  to the nearest eigenvalue is about  $0.0005$  and for  $\epsilon = -2.001$  the distance to the nearest eigenvalue is about  $0.008$

## 4.4.2 Discrete and Continuous Eigenvalues

While the purpose of Fig. 4.10 is to show that the eigenvalues explode away from  $-1$  as  $\epsilon$  goes below  $-2$ , it is also important to show how to distinguish between discrete and continuous eigenvalues. To illustrate this, we apply the Arnoldi algorithm at  $\epsilon = -2.6$ . Our results are given in Fig. 4.11 for  $\eta = 0.01$ . The spectrum in this case differs qualitatively from the spectrum near  $\epsilon = -2$ ; there are now *two* pairs of curves of continuous eigenvalues, and these curves are now in the right-half complex plane. The discrete eigenvalues are still in the left-half complex plane but further from the negative real axis. There is an elaborate spectral structure near the origin, and this is shown in Fig. 4.12. (We do not investigate this structure in this paper and reserve it for future research.)

We emphasize that when the Arnoldi algorithm is used to study a spectrum, it can only return discrete values. Thus, one must determine whether an Arnoldi eigenvalue belongs to a discrete or a continuous part of the spectrum. To distinguish between these two possibilities, we study the associated eigenfunctions and observe how they obey the boundary conditions. Plots of discrete and continuous eigenfunctions associated with eigenvalues shown in Fig. 4.11 are given in Figs. 4.13 and 4.14.

In Fig. 4.13 we plot the absolute values of the eigenvalues of the eigenfunctions corresponding to the complex-conjugate pair of eigenvalues  $E = -1.79 \pm 4.31i$  for  $\epsilon = -2.6$ . Observe that as  $t$  approaches the boundaries  $-1$  and  $1$ , the eigenfunctions decay to 0 exponentially. We conclude from this that the eigenvalues are discrete. This result can then be verified by taking finer cell sizes in the Arnoldi algorithm. As the cell size decreases, the numerical values of  $E$  are stable. In contrast, in Fig. 4.14 in which the absolute values of the eigenfunctions corresponding to the pair of eigenvalues  $E = -0.01 \pm 0.18i$  are

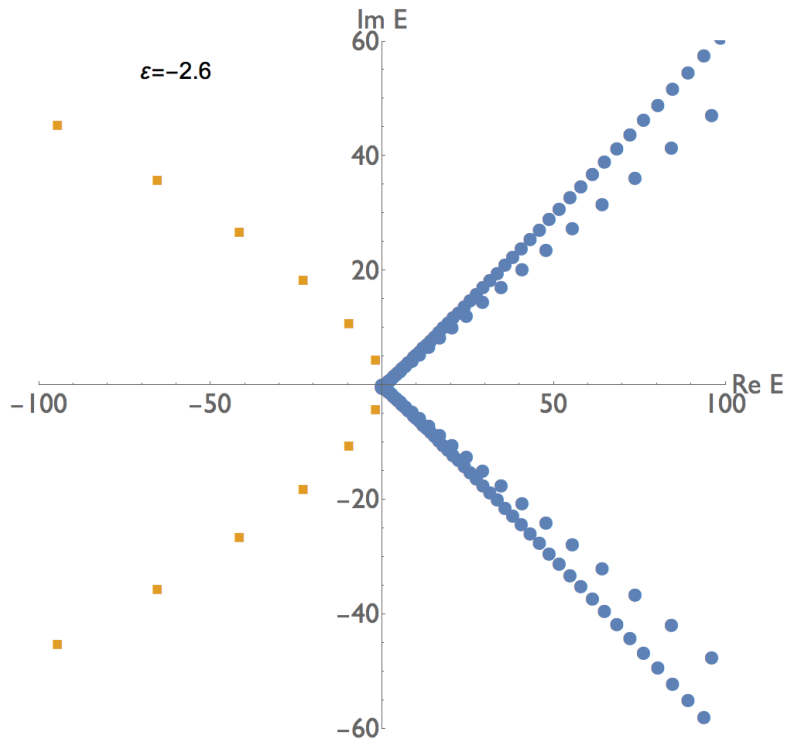


Figure 4.11: Discrete and continuous parts of the spectrum of the  $\mathcal{PT}$ -symmetric Hamiltonian  $H = p^2 + x^2(ix)^\epsilon$  for the case  $\epsilon = -2.6$ . The discrete eigenvalues (orange squares) occur in pairs the left-half complex plane. The continuous eigenvalues (blue dots) lie on two complex-conjugate pairs of curves in the right-half complex plane. As we decrease the cell size in the Arnoldi algorithm, the dots become dense on these curves. The continuous curves of eigenvalues originate slightly to the left of the origin.

plotted, we see that the eigenfunctions vanish exponentially at one end point but vanish sharply at the other end point. We therefore identify these eigenvalues as belonging to the continuous spectrum. Decreasing the Arnoldi cell size results in a denser set of eigenvalues along the same curve.

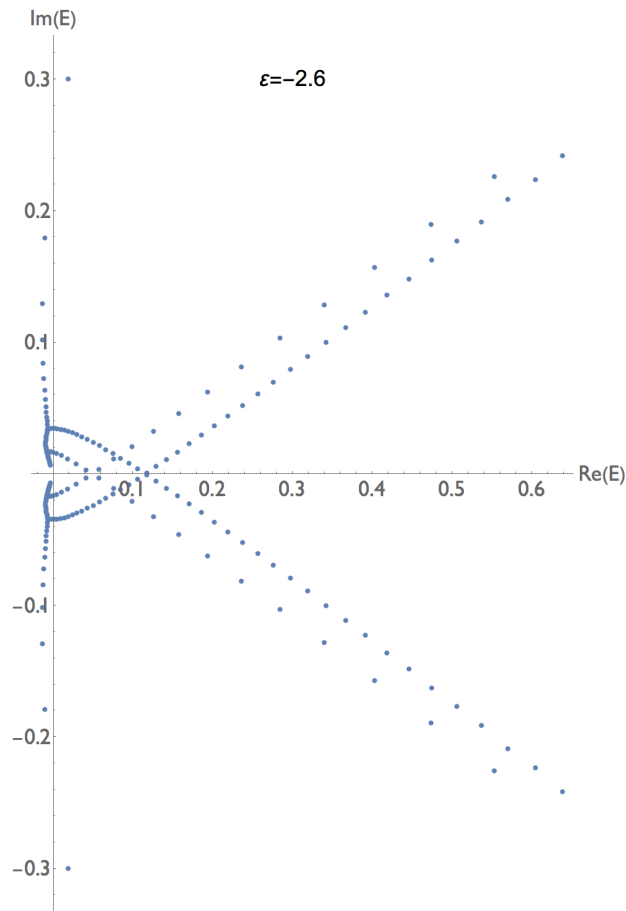


Figure 4.12: Detail of Fig. 4.11 showing the elaborate near the origin in the complex-eigenvalue plane for  $\epsilon = -2.6$

### 4.4.3 Complex Coulomb Potential $\epsilon = -3$

For the Coulomb potential  $\epsilon = -3$ , (4.47) becomes

$$\psi''(s) - \frac{1}{s}\psi(s) = E\psi(s), \quad (4.50)$$

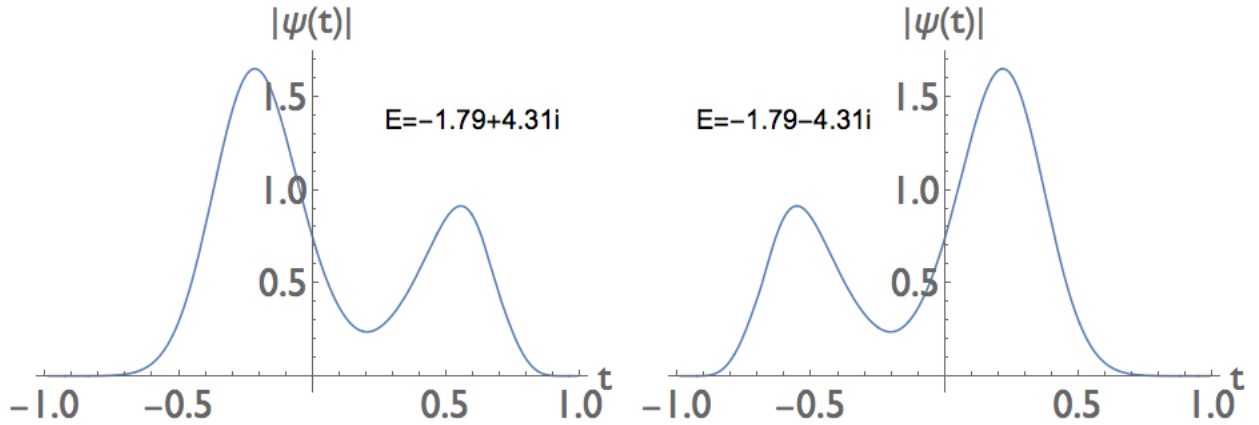


Figure 4.13: Absolute values of the the eigenfunction  $\psi(t)$  for the discrete eigenvalue  $-1.79 \pm 4.31i$  for  $\epsilon = -2.6$ . The eigenfunctions satisfy homogeneous boundary conditions at  $\pm(1 - \eta)$  for  $\eta = 0.01$  and look like bound-state eigenfunctions in the sense that the eigenfunctions decay to 0 exponentially fast at both boundary points. The left and right panels are interchanged under  $t \rightarrow -t$ , which corresponds to a  $\mathcal{PT}$  reflection.

which is a special case of the Whittaker equation

$$w''(z) + \left[ -\frac{1}{4} + \frac{\kappa}{z} + \frac{\frac{1}{4} - \mu^2}{z^2} \right] w(z) = 0, \quad (4.51)$$

with  $\mu^2 = \frac{1}{4}$  [89]. The boundary conditions are unusual (they differ from those in conventional atomic physics) in that  $\psi(s) \rightarrow 0$  as  $|s| \rightarrow \infty$  with  $\arg(s) = \pm 2\pi$ . Rather than performing an analytic solution to the eigenvalue problem, we simply present the numerical result, which are obtained by solving (4.49) with  $\epsilon = -3$ . Figure 4.15 displays about 100 eigenvalues, which lie on two pairs of complex-conjugate curves in the left-half plane. These eigenvalues are part of the continuous spectrum. A blow-up of the region around the origin is shown in Fig. 4.16.

The Coulomb case  $\epsilon = -3$  is a transition point between the regions  $\epsilon > -3$  and  $\epsilon < -3$ . In the first region, the discrete eigenvalues occur in complex-conjugate pairs and there are no

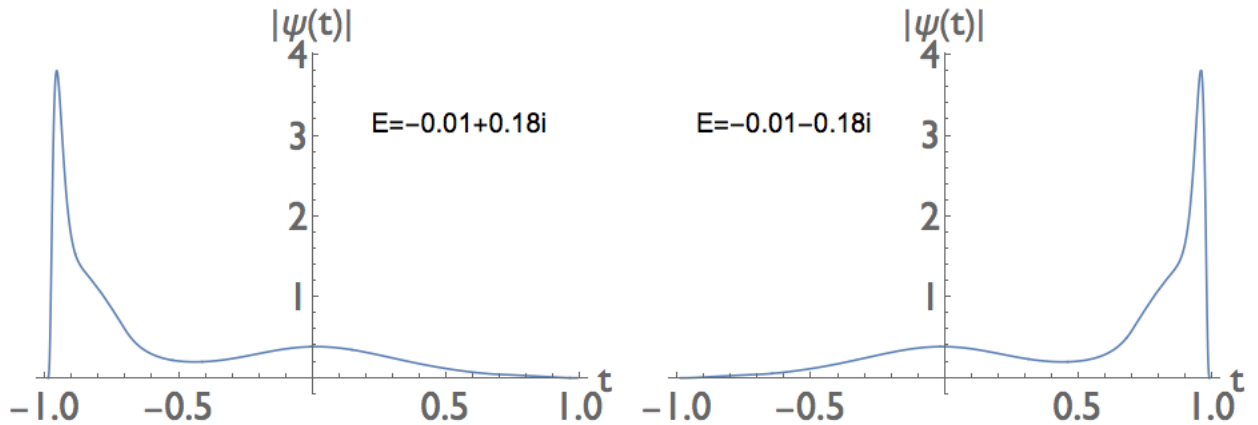


Figure 4.14: Absolute values of the eigenfunctions for the continuum eigenvalues  $-0.01 \pm 0.18i$  for  $\epsilon = -2.6$ . These eigenvalues belong to the continuous spectrum. The indication that they are part of the continuous spectrum is that at one of the boundary points the eigenfunctions suddenly drop to 0 rather than decaying exponentially to 0. As in Fig. 4.13, the left and right panels are interchanged under  $t \rightarrow -t$ , which corresponds to a  $\mathcal{PT}$  reflection.

discrete eigenvalues (as we see in Fig. 4.11). In discrete spectrum includes both real and complex-conjugate pairs of eigenvalues in addition to the continuous spectrum. Figure 4.17 illustrates the typical distribution of eigenvalues in the latter region for the choice  $\epsilon = -3.8$ . In Fig. 4.18 we display the eigenfunction for the real discrete eigenvalue  $E = 0.0804$ . Unlike the eigenfunctions in Figs. 4.13 and 4.14, this eigenfunction is symmetric in  $t$ .

#### 4.4.4 Conformal Limit $\epsilon \rightarrow -4$

The limit  $\epsilon$  to  $-4$  is the conformal limit of the theory and thus the behavior of the eigenvalues in this limit is interesting to determine. It is difficult to study this limit because the eigenvalue equation in the complex- $s$  plane follows a contour that loops around the origin many times when  $\epsilon$  is near  $-4$ . Indeed, the number of loops approaches  $\infty$  as  $\epsilon$  to  $-4$

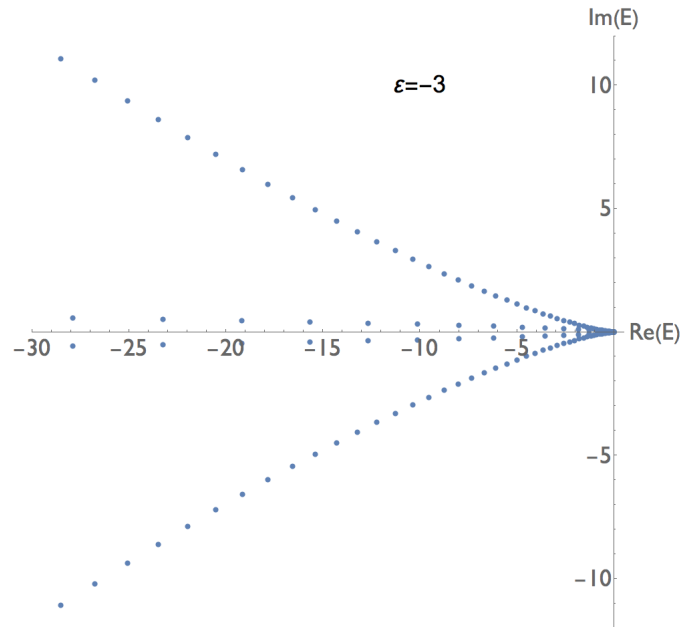


Figure 4.15: Eigenvalues for the Coulomb case  $\epsilon = -3$ . These are no discrete eigenvalues and the continuum eigenvalues lie on four curves in the left-half complex plane.

and, as a consequence, we are less confident about the dependability of the Arnoldi algorithm that we are using to obtain our numerical result. Nevertheless, we have studied the spectrum for values of  $\epsilon$  that are slightly greater than  $-4$  and examine the trend as  $\epsilon$  moves closer to  $-4$ . We find that in this limit the entire spectrum collapses to the origin. It is not easy to demonstrate this by studying the continuous part of the spectrum; these points merely become denser in the vicinity of the origin. However, the discrete eigenvalues move toward the origin as  $\epsilon \rightarrow -4$ . In Table 4.3 we show the behavior of the first three real eigenvalues as  $\delta \rightarrow 0$ , where  $\epsilon = -4 + \delta$ . These data are plotted in Fig. 4.19. This figure suggests that the eigenvalues vanish linearly with  $\delta$ .

Table 4.3: First three real discrete eigenvalues as a function of  $\delta$ , where  $\epsilon = -4 + \delta$ . All the eigenvalues approach 0 as  $\delta \rightarrow 0$ . In fact, Fig. 4.19 indicates that they approach zero in a linear fashion.

$\delta$	First real eigenvalue	Second real eigenvalue	Third real eigenvalue
0.15	0.173	0.440	0.807
0.12	0.114	0.321	0.628
0.08	0.080	0.230	0.454
0.06	0.060	0.177	0.351
0.04	0.035	0.116	0.236
0.02	0.012	0.049	0.106

## 4.5 Conclusion

In this paper we have studied the eigenvalues of  $H$  in 4.1 for  $-4 < \epsilon < 0$  and we have shown that there is a rich analytic structure as a function of the parameter  $\epsilon$ . We have identified transition points at the integer values  $\epsilon = 0, -1, -2, -3$ . Just above  $\epsilon = 0$  the eigenvalues are all real and positive but below  $\epsilon = 0$  the eigenvalues split sequentially into complex-conjugate pairs and all of the eigenvalues but one are complex below about  $\epsilon = -0.58$ . At  $\epsilon = -1$  the real parts of the eigenvalues approaches  $\infty$  but the imaginary parts of the eigenvalues all vanish.

At the Coulomb value  $\epsilon = -3$  the continuous parts of the spectrum swing around to the negative complex plane and the discrete eigenvalues disappear. Below the Coulomb transition the discrete eigenvalues reappear and some of the discrete eigenvalues are now *real*. As  $\epsilon$  approaches the conformal point  $-4$ , the spectrum appears to implode to the origin.

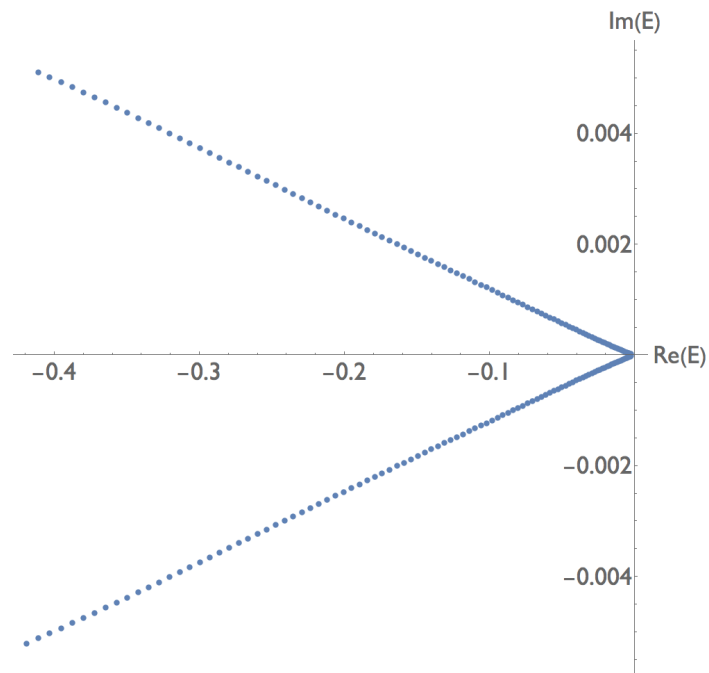


Figure 4.16: Detail of the region around the origin in the complex eigenvalue plane of Fig. 4.15 for  $\epsilon = -3$ . For this figure we have chosen  $\eta = 0.999$  and have taken the very small cell size 0.00001.

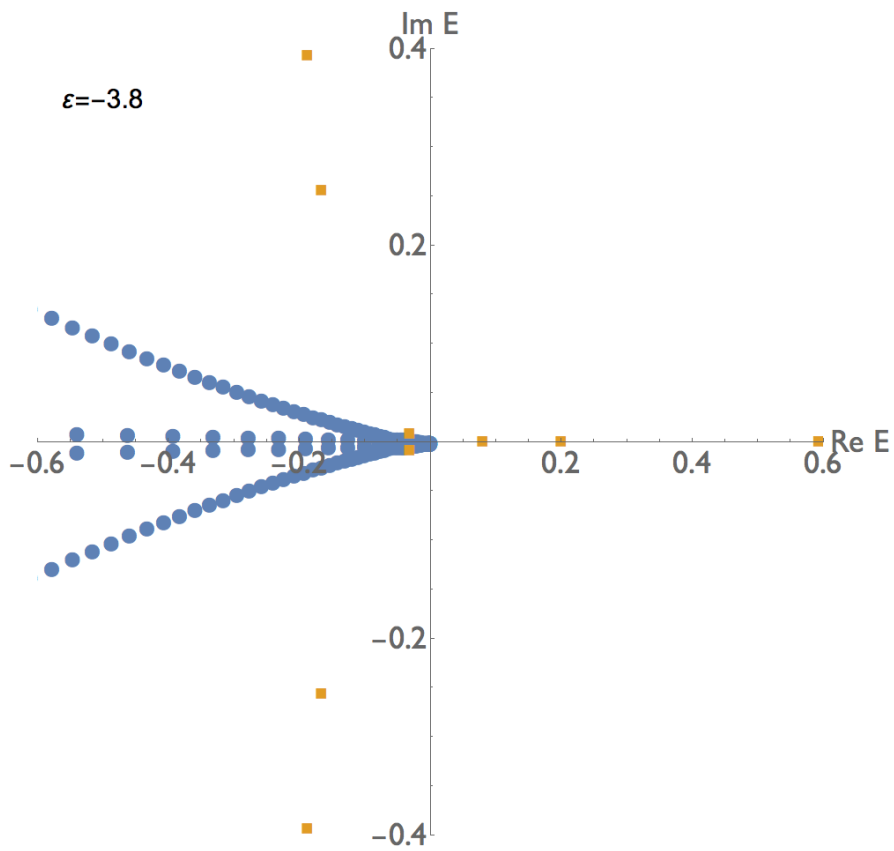


Figure 4.17: Eigenspectrum for  $\epsilon = -3.8$ . The continuous part of the spectrum (blue dots) lies on two complex-conjugate pairs of curves in the left-half plane and resembles that of the Coulomb case (see Fig. 4.15). The discrete part of the spectrum (orange squares) consists of complex-conjugate eigenvalues in the left-half plane and real eigenvalues on the positive-real axis.

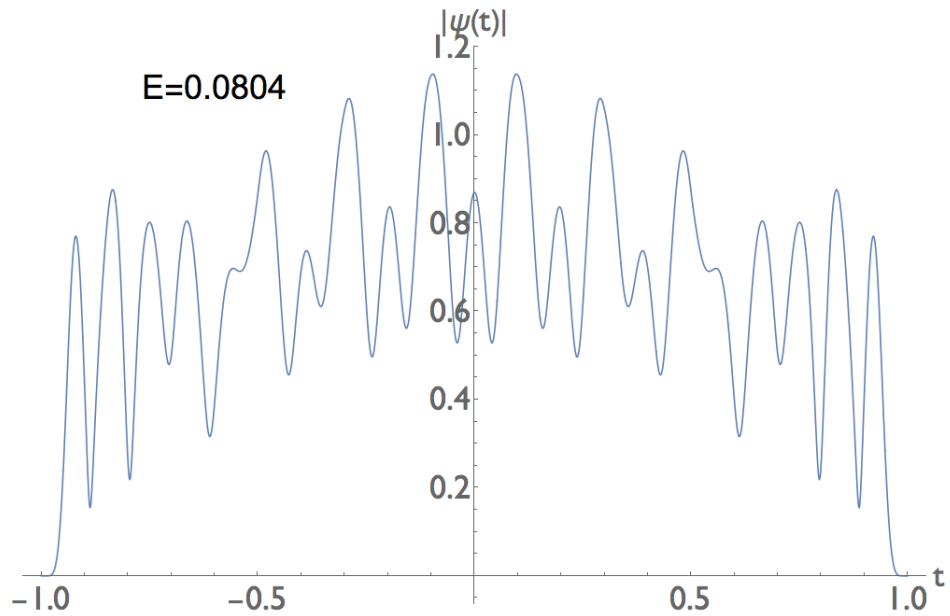


Figure 4.18: Plot of the absolute value of the eigenfunction associated with the discrete real eigenvalue  $E = 0.0804$  for  $\epsilon = -3.8$ .

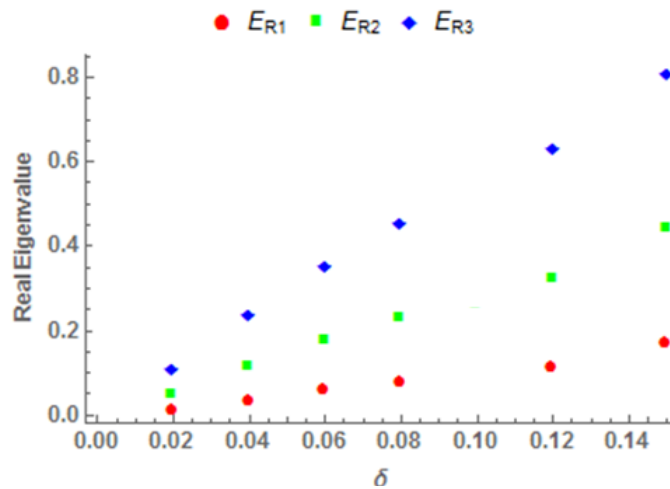


Figure 4.19: First three real eigenvalues of the Hamiltonian  $p^2 + x^2(ix)^\epsilon$  plotted as functions of the parameter  $\delta$ , where  $\epsilon = -4 + \delta$ . The eigenvalues clearly approach 0 as  $\delta \rightarrow 0$  and we see strong evidence that the eigenvalues vanish linearly with  $\delta$ .

# Chapter 5

## Series Solution of $\mathcal{PT}$ -Symmetric Schrödinger Equation

*This chapter contains the materials published in a paper [\[124\]](#), which represents work performed by me under the supervision of my advisor, C. M. Bender.*

## 5.1 Numerical Procedure

The area of research known as  $\mathcal{PT}$ -symmetric quantum theory began with the discovery that the complex  $\mathcal{PT}$ -symmetric Schrödinger equation

$$-\psi''(z) - (iz)^N \psi(z) = E\psi(z) , \quad (5.1)$$

has real spectra if  $N > 2$  [2, 24, 108]. This is called the region of *unbroken*  $\mathcal{PT}$  symmetry. If  $0 < N < 2$  the spectrum is partly real and partly complex; this is called the region of *broken*  $\mathcal{PT}$  symmetry. Since this early work, research on  $\mathcal{PT}$ -symmetric systems has spread to many other areas of physics such as optics [56, 111, 113] and nonlinear wave equations [55, 125] to mention just a few.

If  $N$  is integer, the eigenfunctions are entire functions and the complex plane splits naturally into  $N + 2$  Stokes wedges. (For the numerical technique described in this paper  $N$  need not be an integer, as we will see in section 5.3). Energy quantization is a consequence of demanding that  $\psi(z)$  decay exponentially in a  $\mathcal{PT}$ -symmetric pair of Stokes sector. For special values of  $E$  one can find solutions that decay in two (noncontiguous) wedges. (Note that we are using the notation  $-(iz)^N$  that was used in [2] to represent  $\mathcal{PT}$ -symmetric potentials. Subsequently, the notation  $x^2(ix)^\epsilon$  was used. However, the original notation is more suitable for the series techniques described in this chapter.)

In [126] a technique for finding the eigenvalues of a Schrödinger equation (5.1) was explored that involved expanding the eigenfunctions as formal perturbation series in powers of the energy  $E$ . The technique was moderately effective, although it sometimes required the use of summation techniques to handle divergent series. In this chapter we

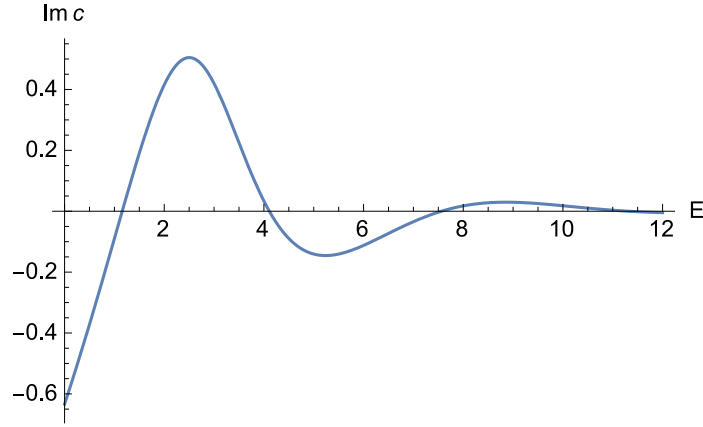


Figure 5.1: The value of  $\text{Im } c$  plotted as a function of  $E$ . The first few energy levels in the  $N = 3$  theory appear as roots of  $\text{Im } c$ .

extend this technique to include series in powers of *both*  $iz$  and  $E$ . Consider the double power series

$$\psi_1 = \sum_{p=0}^{\infty} \sum_{q=0}^{\infty} a_{p,q} (iz)^{(N+2)p+2q} E^q, \quad (5.2)$$

where the  $a_{p,q}$  are constants. Because the parameter  $N$  appears in the power of  $iz$ , if we insert this series into the Schrödinger equation (5.1), we obtain a particularly simple recursion relation for the coefficients  $a_{p,q}$ :

$$[(N+2)p+2q-1][(N+2)p+2q] a_{p,q} = a_{p-1,q} + a_{p,q-1}. \quad (5.3)$$

Viewing  $a_{p,q}$  as a matrix, (5.3) expresses the element  $a_{p,q}$  in terms of the elements that are immediately adjacent. Thus, on fixing the top left element  $a_{0,0}$  one can, in principle, determine all the other elements. For the convenient choice  $a_{0,0} = 1$  all the  $a_{p,q}$  are positive rational number. (This is because the  $\mathcal{PT}$  symmetry of the series representation is enforced this structure). With this choice  $\psi_1(0) = 1$  and  $\psi_1'(0) = 0$ .

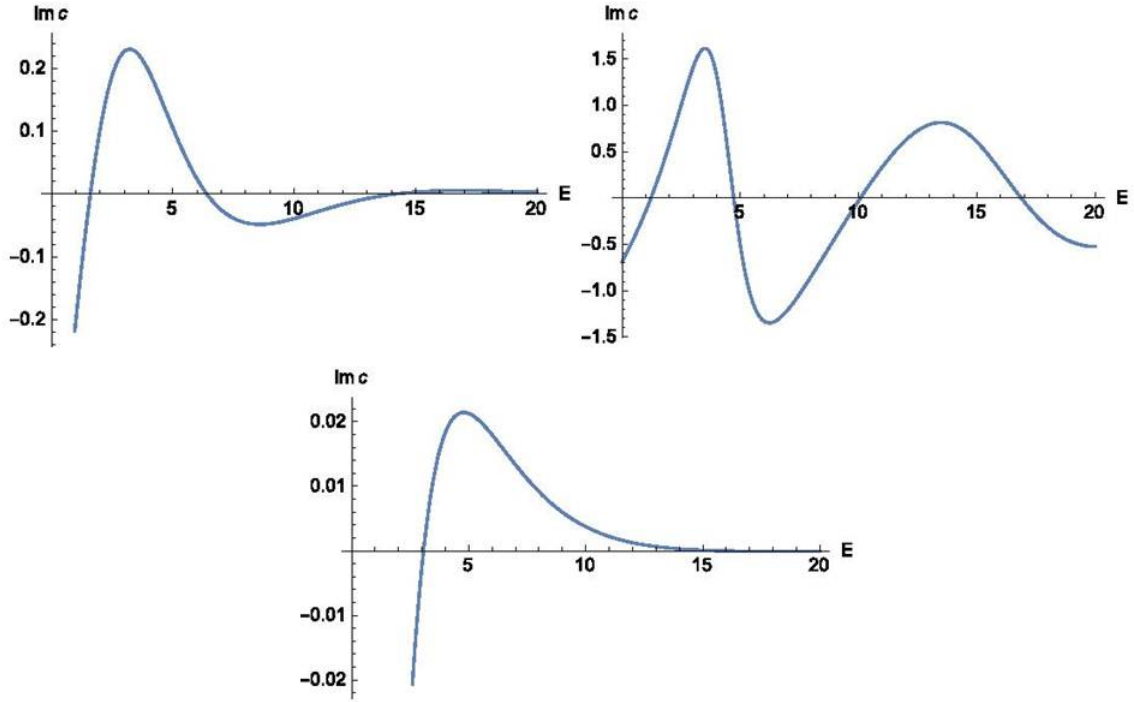


Figure 5.2:  $\text{Im } c$  in the  $N = 7$  theory  $\mathcal{PT}$  symmetric spectra. The upper left plot is for the wedges centered at  $\theta = \pi/6$  and  $\theta = 5\pi/6$ ; the upper right plot has wedges centered at  $\theta = -\pi/18$  and  $\theta = -17\pi/18$ ; the lower plot has wedges centered at  $\theta = -5\pi/18$  and  $\theta = -13\pi/18$ .

A second solution of the Schrödinger equation is

$$\psi_2(z) = \sum_{p=0}^{\infty} \sum_{q=0}^{\infty} b_{p,q} (iz)^{1+(N+2)p+2q} E^q, \quad (5.4)$$

where the coefficients  $b_{p,q}$  satisfy the recursion relation

$$[(N+2)p+2q][(N+2)p+2q+1]b_{p,q} = b_{p-1,q} + b_{p,q-1}. \quad (5.5)$$

It is convenient to take  $b_{0,0} = 1$  so that  $\psi_2(0) = 0$  and  $\psi_2'(0) = i$ .

Now consider a linear combination of the two solution

$$\psi(z) = \psi_1(z) + c\psi_2(z) , \quad (5.6)$$

where  $c$  is a complex constant. By a suitable choice of  $c$  one can ensure that  $\psi(z)$  decays exponentially in any one of the  $N + 2$  Stokes sectors. For example, to obtain decay in the sector centered at (the anti-stokes line)  $\theta = -\frac{1}{2}\pi(N - 2)/(N + 2)$  take

$$c = - \lim_{r \rightarrow \infty} \frac{\psi_1(re^{i\theta})}{\psi_2(re^{i\theta})} \Big|_{\theta = -\frac{1}{2}\pi(N-2)/(N+2)} \quad (5.7)$$

This works for any  $E$  but it only gives a decaying wave function in one of the  $N + 2$  sectors. However, the key point is that *if both  $E$  and  $c$  are real, then the solution will also decay in the  $\mathcal{PT}$  image of the sector*. This is the crucial step in the numerical procedure because it makes explicit use the  $\mathcal{PT}$  symmetry of the potential.

To determine the spectrum associated with a  $\mathcal{PT}$  symmetric pair of sectors it suffices to determine the real energies for which  $c$  is real. This can be implemented graphically by plotting  $\text{Im}(c)$  as a function of  $E$ . The zeros of this plot correspond to the energy levels. In Fig. 5.1  $\text{Im}(c)$  is plotted for  $N = 3$ . Note that as  $E$  increases,  $\text{Im}(c)$  approaches zero in an oscillatory fashion.  $\text{Im}(c)$  has no roots for negative  $E$ . To produce this plot we made two approximations:

- i In the double power series (5.2) and (5.4) we retained all terms with  $p + q \leq 100$ .
- ii In (5.7) a large finite value of  $r$  (in this case  $r = 8$ ) was taken instead of the  $r \rightarrow \infty$  limit.

Table 5.1: Energy levels and  $c$  values in the  $N = 3$  theory.

$n$	$E_n$	$c_n$
0	1.1562670719881132937	0.53871550451988192490
1	4.1092287528096515358	2.32727424075874334001
2	7.5622738549788280413	2.69833514190279036708
3	11.314421820195804397	3.37823419494258452822
4	15.291553750392532	3.90980926012776641
5	19.451529130691	4.41178037226863
6	23.766740435	4.87570168194
7	28.2175249	5.312499663

In matrix language the truncation is *anti-diagonal* in sense that entries below the  $p + q = 100$  line are discarded. By applying a root-finding algorithm to the approximation for  $c(E)$  we can compute the energy levels and associated values of  $\text{Re}(c)$ . These are given in table 5.1.

For large values of  $n$  the values of  $c_n$  is approximately  $-\sqrt{E_n}$ . To investigate the accuracy of the numerical scheme one can vary the  $p + q \leq 100$  truncation and the  $r$  value. The numerical results for the first few energy levels are not affected by taking  $r = 7$  instead of  $r = 8$  at least to 20 significant figures. Similarly, increasing the truncation to  $p + q \leq 150$  does not change the first few energy levels (again to 20 significant figures). However, the higher energy levels are more sensitive to changes in  $r$  and to the truncation. We have quoted  $E_4$  to 17 rather than 20 significant figures as the missing three change when the truncation is improved. For higher  $n$  the accuracy drops further. As the double power series expansions in  $iz$  and  $E$ , we expect that the truncation is less accurate for higher energies. Our energy levels are consistent with the Runge-Kutta based reported in [6].

For higher  $N$  there is more than one pair of (nonadjacent)  $\mathcal{PT}$ -symmetric sector [23]. Indeed, if  $N$  is odd, there are  $\frac{1}{2}(N - 1)$  such pairs. If  $N$  is even, there are  $\frac{1}{2}(N + 2)$  pairs; one

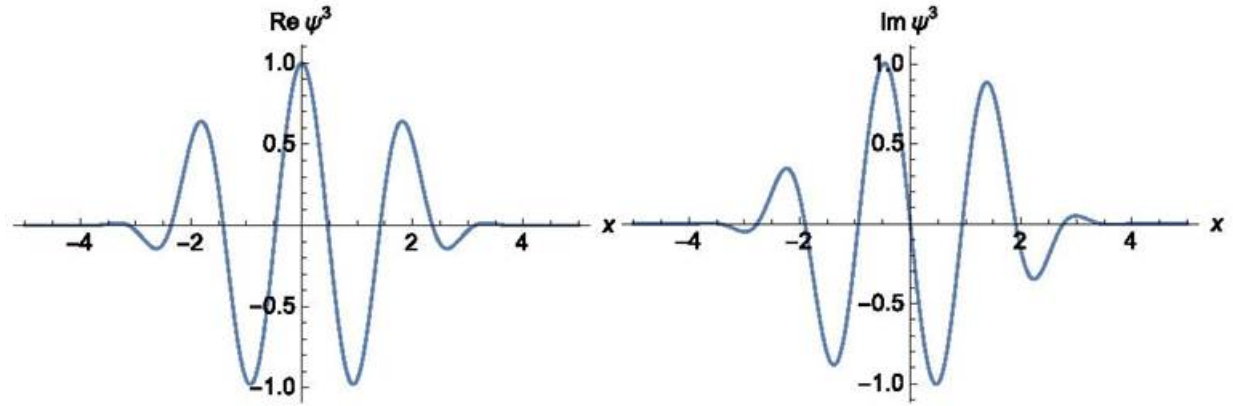


Figure 5.3: Eigenfunction for the third excited state for  $N = 3$  plotted along the real axis.

of these pairs is both  $\mathcal{PT}$  symmetric and  $\mathcal{P}$  symmetric. The graphical method used here is also applicable in this case but the energy eigenstates are of the form  $\psi_1$  (even parity) or  $\psi_2$  (odd parity). In this case one may have to interchange the roles of  $\psi_1$  and  $\psi_2$  in (5.7) to obtain all the eigenvalues. (This is discussed in section 5.3).

To illustrate what happens for large values of  $N$  we examine the case  $N = 7$ . There are three  $\mathcal{PT}$ -symmetric pairs if  $N = 7$ . Each pair gives a distinct real and positive spectrum;  $\text{Im}(c)$  is plotted in Fig. 5.2 as a function of  $E$  for the three pairs.

For higher  $n$  the  $E_n$  have ratios 1.41 : 1 : 3.52 [23]. Although our method is adapted to small  $n$ , such behavior is evident in the third excited state;  $E_3$  has values 23,702, 16.872, 59.026. The ratios of the energies are different;  $E_0$  has values 1.6047, 1.2247, 3.0686.

For the upper spectrum (that is, with wedges centered at  $\theta = \pi/6$  and  $\theta = 5\pi/6$ ) the  $c_n$  values are positive with  $c_n \approx -\sqrt{E_n}$ . The plots were produced via the same  $p + q \leq 100$  truncation but with  $r = 3$  rather than  $r = 8$ . Similar result can be obtained for higher  $N$ . For example, the  $N = 19$  model has 9 distinct spectra (4 giving positive  $c_n$ , 5 with negative  $c_n$ ).

Table 5.2: Energy levels and  $c$  values in the  $N = 3$  theory.

$n$	0	1	2	3
m				
1	0.5900725330i	0.9820718380i	1.2054807539i	1.3796870779i
2	0	0	0	0
3	0.4625068288i	1.6436915011i	3.0249095421i	4.5257687286i
4	0.3898751086	2.3060330480	5.2092431933	8.9202066199

## 5.2 Nodes and expectation values

The truncations considered here can be used to identify the nodes and expectation values of the energy eigenstates. Although our truncation is inaccurate for large enough  $|z|$ , at least for the first few energy levels the nodes are close enough to the origin for them to be determined with high precision. Returning to the  $N = 3$  case, we note that all energy eigenfunctions have an infinite string of zeros on the imaginary axis; for each energy level these lie above the classical turning point at  $iE_n^{1/3}$ . In addition, the  $n$ th excited state has  $n$  nodes below the real axis (the first excited state has a node at  $z = -0.661296226442715413308i$ ). The  $n$  nodes arch above and between the classical turning points at  $E_n^{1/3}e^{-i\pi/6}$  and  $E_n^{1/3}e^{-i5\pi/6}$  [127].

An interesting question considered in [29] is the precise form of the arch for large  $n$ . Unlike the  $N = 2$  harmonic oscillator the nodes do not lie on the classical trajectory joining two turning points. In fact, for  $N = 3$  this trajectory is exactly circular with its center at the turning point on the imaginary axis.

The approximation method introduced here may be used to compute expectation values. If  $\psi(z)$  is an energy eigenstate, then the expectation value of  $z^m$  is ratio of contour

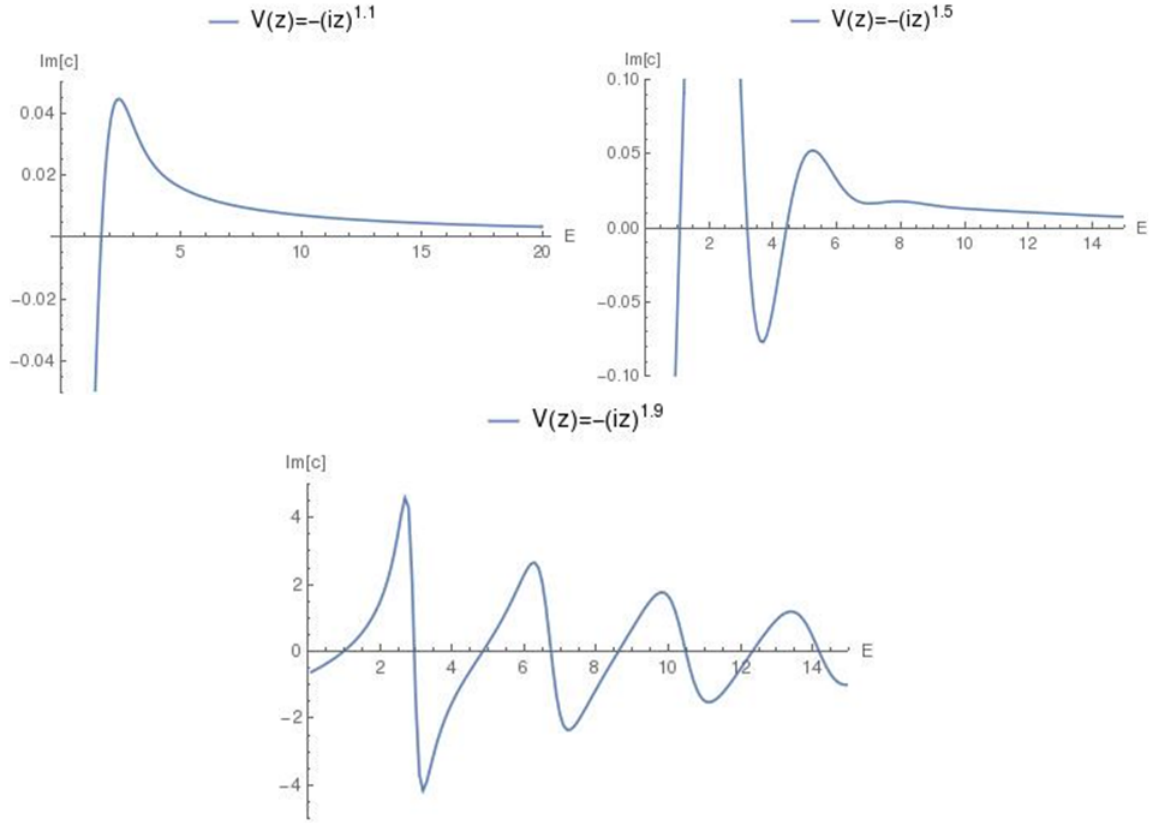


Figure 5.4: Plot of  $\text{Im } c$  for the  $N = 1.1$ ,  $N = 1.5$ , and  $N = 1.9$  theories. All three of these theories are in the  $\mathcal{PT}$  broken region. In the first case there is only one eigenvalue, in the second case there are three real eigenvalues, and in the third case there are many real eigenvalues. In all cases the numerical method used here provides highly accurate results.

integrals<sup>1</sup>:

$$\langle z^m \rangle = \frac{\int_C dz \psi(z) z^m \psi(z)}{\int_C dz \psi(z) \psi(z)} \quad (5.8)$$

where  $C$  is any curve that divides the complex plane in two and starts in one wedge and ends in the  $\mathcal{PT}$ -symmetric wedge. For  $N = 3$  one can simply choose  $C$  to be the real line:

<sup>1</sup>Note that if  $\psi$  is not an energy eigenstate, this formula is not valid. Expectation values must then be computed via modified inner product in terms of a new operator  $\mathcal{C}$  [38]. This inner product is related to the Dirac inner product via a nonunitary similarity transformation [128]

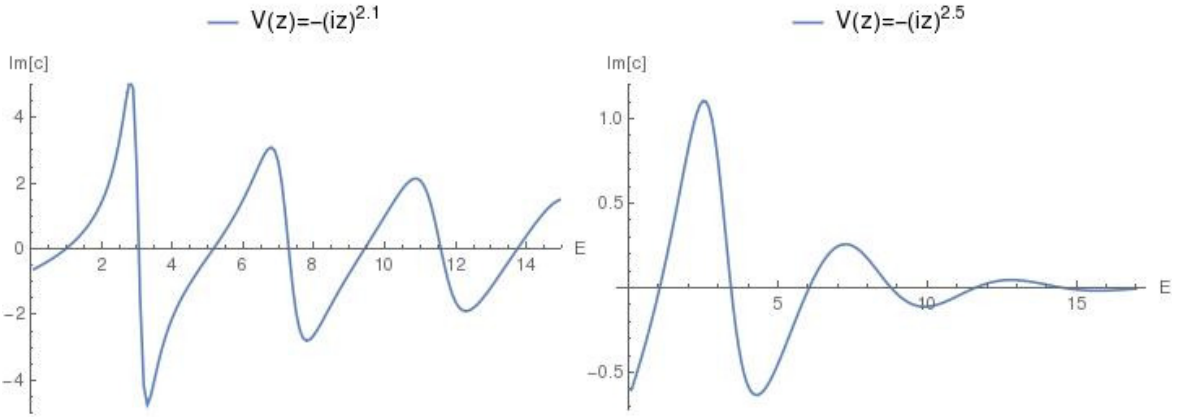


Figure 5.5: Plot of  $\text{Im } c$  for the  $N = 2.1$  and  $N = 2.5$  theories. These theories are in the  $\mathcal{PT}$  unbroken region.

$$\langle z^m \rangle_n = \frac{\int_{-\infty}^{\infty} dz \psi^n(z) z^m \psi^n(z)}{\int_{-\infty}^{\infty} dz \psi^n(z) \psi^n(z)} \quad (5.9)$$

where  $\psi^n$  is the  $n$ th energy eigenstate ( $n = 0, 1, 2, 3, \dots$ ). As the wave functions decay exponentially these integrals over the real line are well approximated by integrals over a finite range  $[-\lambda, \lambda]$  for sufficiently large  $\lambda$ . We have computed expectation values for the first few energy eigenstates in the  $N = 3$  model. We have cut off the integrals at  $\lambda = 5$  and have approximated the  $\psi_1$  and  $\psi_2$  with the truncation ( $p + q \leq 100$ ) describes above. Plots of the wave functions indicate that the cut off  $\lambda = 5$  is a good approximation for the first few eigenstates; a plot of  $\psi^3(x)$  is given in Fig. 5.3 and the expectation values  $\langle z^m \rangle_n$  in the  $N = 3$  are listed in table 5.2.

In our approximation  $\langle z^2 \rangle_n$  is small ( $\langle z^2 \rangle_0 \approx 10^{-11}$ ). This is because  $\langle z^2 \rangle_n$  is exactly zero. To see why this is true, we note that  $I = \int_{-\infty}^{\infty} dx x^2 \psi^2(x) = \frac{1}{3} \int_{-\infty}^{\infty} d(x^3) \psi^2(x)$ . Upon integration by parts, we get  $I = -\frac{2}{3} \int_{-\infty}^{\infty} dx x^3 \psi(x) \psi'(x)$ . Finally, we use the Schrödinger equation (5.1) with  $N = 3$  to replace  $x^3 \psi(x)$  with a linear combination of  $\psi''(x)$  and  $\psi(x)$  and observe that each term is an exact derivative that integrates to zero.

Table 5.3: Eigenvalue in the broken  $\mathcal{PT}$  regime for noninteger value of  $N$ .

N=1.1		N=1.5		N=1.9	
n	Series Soln.	n	Series Soln.	n	Series Soln.
0	1.6836723247	0	1.08692903345877	0	1.0015867791272
1	-	1	3.195783621829	1	2.957492901530
2	-	2	4.42201575335	2	4.85886246929
3	-	3	-	3	6.7482128957
4	-	4	-	4	8.6180610339

### 5.3 Numerical scheme applied to other potentials

The numerical scheme describe in section 5.1 does not require that  $N$  be an integer. Therefore, we can consider noninteger values of  $N$  in both the broken and unbroken  $\mathcal{PT}$ -symmetric regions. We first study three values of  $N$  in the  $\mathcal{PT}$  broken region:  $N = 1.1, 1.5, 1.9$ . As one can see in [2] there is only one real eigenvalue for  $N = 1.1$ , three real eigenvalues for  $N = 1.5$ , and many real eigenvalues for  $N = 1.9$  as indicated by the results in Fig. 5.4 and table 5.3.

Next we examine two values of  $N$  in the  $\mathcal{PT}$  unbroken region:  $N = 2.1$  and  $N = 2.5$ . In this case there are an infinite number of real eigenvalues and no complex eigenvalues. Once again, our numerical procedure gives highly accurate results for these cases. See Fig. 5.5 and table 5.4.

A particularly interesting  $\mathcal{PT}$ -symmetric potential is  $V = -(iz)^4$ . While this may naively appear to be an upside down potential, when we quantize the theory by imposing boundary conditions in a pair of Stokes sectors in the complex plane, we find that the spectrum is entirely real and positive. (An elementary proof of this is given in [129]). Moreover, the spectrum of this potential is different from that of the quartic anharmonic oscillator

Table 5.4: Eigenvalue in the broken  $\mathcal{PT}$  regime for noninteger value of  $N$ .

N=2.1		N=2.5	
n	Series Soln.	n	Series Soln.
0	1.003097514661	0	1.048954090261
1	3.06113230366	1	3.43453593249
2	5.16708540045	2	6.05173796085
3	7.2921244575	3	8.7910138373
4	9.4332388593	4	11.6206954696

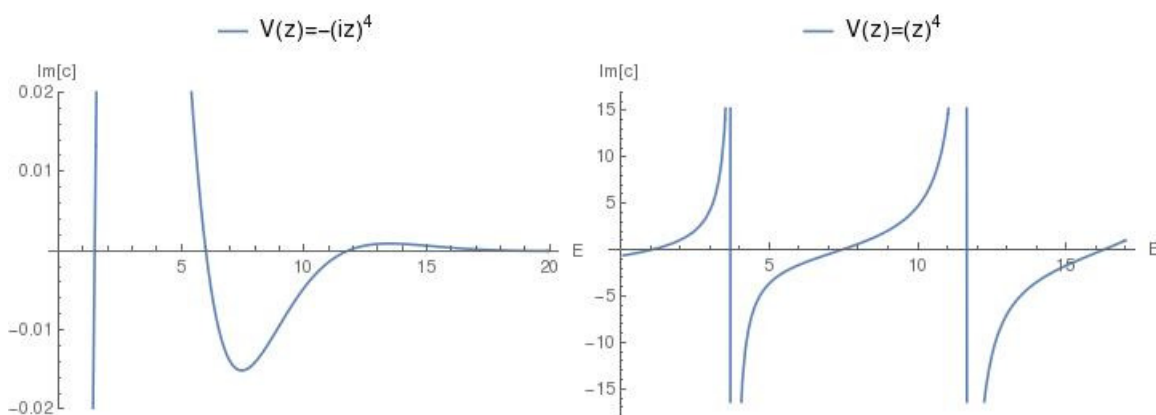


Figure 5.6: Plot of  $\text{Im } c$  for the  $V = -x^4$  and  $V = x^4$ .

( $V = x^4$ ). We can easily apply the numerical techniques described in this chapter to find the eigenvalues of both of these potentials because both potentials are functions of  $iz$  (see Fig. 5.6).

The eigenvalues for the potentials  $V = -x^4$  and  $V = x^4$  and also those of the harmonic oscillator  $V = x^2$  listed below in table 5.5. As we can see in Fig. 5.6, for potentials that are parity symmetric, such as  $x^4$ , the slope of the curve typically alternates between being very steep and not very steep when it crosses the horizontal axis. When the slope is steep it is numerically more difficult for the computer software to determine the precise value of  $E$ . This explains the varying accuracy in the eigenvalues for the  $x^2$  potential, for example. To improve numerical accuracy one can do two things. First, one can compute the curve

Table 5.5: Eigenvalues of the harmonic oscillator  $V = x^2$  ( $N = 2$ ), the  $\mathcal{PT}$ -symmetric quartic oscillator  $V = -x^4$  ( $N = 4$ ), and the conventional anharmonic oscillator  $V = x^4$  obtained by using the numerical methods described before.

$V = x^2$		$V = -x^4$		$V = x^4$	
n	Series Soln.	n	Series Soln.	n	Series Soln.
0	1.00000000000004	0	1.4771508111864	0	1.060363864841
1	2.999999999999993	1	6.0033861147867	1	3.799673009836
2	4.99999999997	2	11.8024336007832	2	7.45569799483
3	6.99999999997	3	18.458818772430	3	11.6447453215
4	9.000000001	4	25.79178997784	4	16.2618260301

using a finer mesh of grid points. Second, one can interchange the roles of  $\psi_1$  and  $\psi_2$  in (5.7) to make the curve less steep.

Finally, we emphasize that our numerical technique is not limited to monomial potentials. It applies equally well to multinomial potentials  $V(z)$  that are  $\mathcal{PT}$  symmetric; this is, potentials that are real functions of  $iz$ . Thus, for the Schrödinger equation (5.1) in which the potential has the form

$$V(z) = c_1(iz)^N + c_2(iz)^M \quad (5.10)$$

we define the two solutions  $\psi_1$  and  $\psi_2$  as triple sums rather than double sums:

$$\psi_1(z) = \sum_{p=0}^{\infty} \sum_{r=0}^{\infty} \sum_{q=0}^{\infty} a_{p,q,r}(iz)^{(N+2)p+(M+2)r+2q} E^q \quad (5.11)$$

and

$$\psi_2(z) = \sum_{p=0}^{\infty} \sum_{r=0}^{\infty} \sum_{q=0}^{\infty} b_{p,q,r}(iz)^{1+(N+2)p+(M+2)r+2q} E^q \quad (5.12)$$

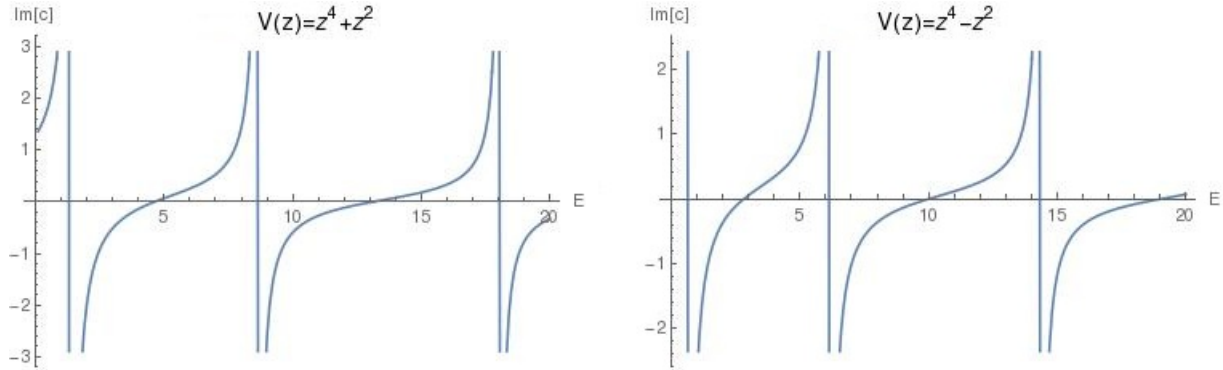


Figure 5.7: Plot of  $\text{Im } c$  for the anharmonic oscillator potential  $V = x^4 \pm x^2$ .

Table 5.6: Eigenvalues of the single-well ( $V = x^4 + x^2$ ) and double-well ( $V = x^4 - x^2$ ) quartic anharmonic oscillators obtained by using the numerical methods described. The numerical accuracy is excellent and is roughly the same for either oscillator.

$V = x^4 + x^2$		$V = x^4 - x^2$	
n	Series Soln.	n	Series Soln.
0	1.39235191352537	0	0.657656758014
1	4.648811867490	1	2.834533175294
2	8.65505000457	2	6.16390133772
3	13.1568037536	3	10.0386458708
4	18.0575574491	4	14.372406513
5	23.2974414415	5	19.085714647

These lead to the two recursion relations

$$[(N+2)p + (M+2)r + 2q] [(N+2)p + (M+2)r + 2q - 1] a_{p,r,q} = -c_1 a_{p-1,r,q} - c_2 a_{p,r-1,q} + a_{p,r,q-1}$$

and

$$[(N+2)p + (M+2)r + 2q + 1] [(N+2)p + (M+2)r + 2q] b_{p,r,q} = -c_1 b_{p-1,r,q} - c_2 b_{p,r-1,q} + b_{p,r,q-1}$$

which are the generalization of (5.3) and (5.5).

Table 5.7: This table shows that this numerical methods fail if the potential is not  $\mathcal{PT}$  symmetric; that is, it is not a real function of the variable  $iz$ .

$V = x^4 + x$		
n	Wrong!	Exact
0	0.991863	0.9305
1	1.53021	3.7819
2	8.42823	7.4351
3	17.4568	11.6283
4	27.8829	16.2478

If we apply these techniques to the massive quartic anharmonic oscillators with either positive or negative mass terms  $V(x) = x^4 \pm x^2$ , we again obtain excellent numerical results for the low-lying eigenvalues (see Fig. 5.7). Indeed, table 5.6 shows the numerical scheme works equally well for the single-well and the double-well anharmonic oscillator.

However, if the potential is *not* a real function of the variable  $iz$ , then the numerical methods described here do not work. To illustrate this we consider the potential  $V(x) = x^4 + x$ . Table 5.7 shows that the eigenvalue calculate fails.

In conclusion, we have demonstrated an extremely powerful and highly accurate technique for computing the eigenvalues (and eigenfunction) of a  $\mathcal{PT}$ -symmetric potential. We have established the accuracy of the method by studying a large number of examples. Our technique is important because it addresses the difficult problem of solving complex non-Hermitian eigenvalue problems. Most conventional techniques for solving real Hermitian eigenvalue problem fail to work for complex eigenvalue problems because complex eigenvalue problems must be solved subject to boundary conditions imposed in Stokes sectors in the complex plane. Of course, our technique also works very well for real eigenvalue problem, so long as the real potential is  $\mathcal{PT}$  symmetric.

# References

- [1] C. M. Bender and S. A. Orszag, *Advanced mathematical methods for scientists and engineers I: Asymptotic methods and perturbation theory*. Springer Science & Business Media, 2013.
- [2] C. M. Bender and S. Boettcher, "Real spectra in non-hermitian hamiltonians having p t symmetry," *Physical Review Letters*, vol. 80, no. 24, p. 5243, 1998.
- [3] F. J. Dyson, "Thermodynamic behavior of an ideal ferromagnet," *Physical Review*, vol. 102, no. 5, p. 1230, 1956.
- [4] J. L. Cardy and R. Sugar, "Reggeon field theory on a lattice," *Physical Review D*, vol. 12, no. 8, p. 2514, 1975.
- [5] R. C. Brower, M. A. Furman, and M. Moshe, "Critical exponents for the reggeon quantum spin model," *Physics Letters B*, vol. 76, no. 2, pp. 213–219, 1978.
- [6] C. M. Bender, "Making sense of non-hermitian hamiltonians," *Reports on Progress in Physics*, vol. 70, no. 6, p. 947, 2007.
- [7] B. C. Harms, S. T. Jones, and C.-I. Tan, "New structure in the energy spectrum of reggeon quantum mechanics with quartic couplings," *Physics Letters B*, vol. 91, no. 2, pp. 291–295, 1980.
- [8] F. Scholtz, H. Geyer, and F. Hahne, "Quasi-hermitian operators in quantum mechanics and the variational principle," *Annals of Physics*, vol. 213, no. 1, pp. 74–101, 1992.
- [9] T. Hollowood, "Solitons in affine toda field theories," *Nuclear Physics B*, vol. 384, no. 3, pp. 523–540, 1992.
- [10] V. Buslaev and V. Grecchi, "Equivalence of unstable anharmonic oscillators and double wells," *Journal of Physics A: Mathematical and General*, vol. 26, no. 20, p. 5541, 1993.
- [11] N. Hatano and D. R. Nelson, "Localization transitions in non-hermitian quantum mechanics," *Physical Review Letters*, vol. 77, no. 3, p. 570, 1996.

- [12] C. M. Bender, D. C. Brody, and H. F. Jones, "Complex extension of quantum mechanics," *Physical Review Letters*, vol. **89**, no. 27, p. 270401, 2002.
- [13] S. Bittner, B. Dietz, U. Günther, H. L. Harney, M. Miski-Oglu, A. Richter, and F. Schäfer, "P t symmetry and spontaneous symmetry breaking in a microwave billiard," *Physical review letters*, vol. **108**, no. 2, p. 024101, 2012.
- [14] C. M. Bender, B. K. Berntson, D. Parker, and E. Samuel, "Observation of pt phase transition in a simple mechanical system," *American Journal of Physics*, vol. **81**, no. 3, pp. 173–179, 2013.
- [15] G. Barton, *Introduction to Advanced Field Theory*. Wiley, 1963.
- [16] T. Y. Kawai, T., *Algebraic Analysis of Singular Perturbation Theory*. American Mathematical Society, 2005.
- [17] J. Heading, *An introduction to phase-integral methods*. Courier Corporation, 2013.
- [18] R. E. Meyer, "A simple explanation of the stokes phenomenon," *SIAM review*, vol. **31**, no. 3, pp. 435–445, 1989.
- [19] G. G. Stokes *Trans. Camb. Phil. Soc.*, vol. **10**, pp. 106–128, 1857.
- [20] T. D. Tai, "On the simpleness of zeros of stokes multipliers," *Journal of Differential Equations*, vol. **223**, no. 2, pp. 351–366, 2006.
- [21] Y. Sibuya, *global Theory of a Second Order Linear Differential Equation with a Polynomial Coefficients citation link*. North-Holland, Amsterdam, 1975.
- [22] G. Wentzel, "Eine verallgemeinerung der quantenbedingungen für die zwecke der wellenmechanik," *Zeitschrift für Physik*, vol. **38**, no. 6-7, pp. 518–529, 1926.
- [23] S. Schmidt and S. P. Klevansky, "Generation of families of spectra in pt-symmetric quantum mechanics and scalar bosonic field theory," *Phil. Trans. R. Soc. A*, vol. **371**, no. 1989, p. 20120049, 2013.
- [24] P. Dorey, C. Dunning, and R. Tateo, "Spectral equivalences, bethe ansatz equations, and reality properties in -symmetric quantum mechanics," *Journal of Physics A: Mathematical and General*, vol. **34**, no. 28, p. 5679, 2001.
- [25] P. Dorey, C. Dunning, and R. Tateo, "A reality proof in pt-symmetric quantum mechanics," *Czechoslovak journal of physics*, vol. **54**, no. 1, pp. 35–41, 2004.
- [26] A. Mostafazadeh, "Pseudo-hermiticity versus pt symmetry: the necessary condition for the reality of the spectrum of a non-hermitian hamiltonian," *Journal of Mathematical Physics*, vol. **43**, no. 1, pp. 205–214, 2002.

- [27] Z. Ahmed, "C-, PT- and CPT-invariance of pseudo-hermitian hamiltonians," *Journal of Physics A: Mathematical and General*, vol. **36**, no. 37, p. 9711, 2003.
- [28] M. Znojil, "Three-hilbert-space formulation of quantum mechanics," *Symmetry, Integrability and Geometry. Methods and Applications*, vol. **5**, 2009.
- [29] C. M. Bender, S. Boettcher, and V. M. Savage, "Conjecture on the interlacing of zeros in complex sturm-liouville problems," *Journal of Mathematical Physics*, vol. **41**, no. 9, pp. 6381–6387, 2000.
- [30] C. M. Bender and Q. Wang, "Comment on a recent paper by mezincescu," *Journal of Physics A: Mathematical and General*, vol. **34**, no. 15, p. 3325, 2001.
- [31] S. Weigert, "Completeness and orthonormality in PT-symmetric quantum systems," *Physical Review A*, vol. **68**, no. 6, p. 062111, 2003.
- [32] P. A. M. Dirac, "Bakerian lecture. the physical interpretation of quantum mechanics," *Proceedings of the Royal Society of London. Series A, Mathematical and Physical Sciences*, pp. 1–40, 1942.
- [33] C. M. Bender, P. N. Meisinger, and Q. Wang, "Calculation of the hidden symmetry operator in PT-symmetric quantum mechanics," *Journal of Physics A: Mathematical and General*, vol. **36**, no. 7, p. 1973, 2003.
- [34] C. M. Bender and H. F. Jones, "Semiclassical calculation of the C operator in pt-symmetric quantum mechanics," *Physics Letters A*, vol. **328**, no. 2-3, pp. 102–109, 2004.
- [35] C. M. Bender and G. V. Dunne, "Exact solutions to operator differential equations," *Physical Review D*, vol. **40**, no. 8, p. 2739, 1989.
- [36] C. M. Bender and G. V. Dunne, "Integration of operator differential equations," *Physical Review D*, vol. **40**, no. 10, p. 3504, 1989.
- [37] C. M. Bender, G. V. Dunne, P. N. Meisinger, and M. Simsek, "Quantum complex hénnon–heiles potentials," *Physics Letters A*, vol. **281**, no. 5-6, pp. 311–316, 2001.
- [38] C. M. Bender, J. Brod, A. Refig, and M. E. Reuter, "The operator in PT-symmetric quantum theories," *Journal of Physics A: Mathematical and General*, vol. **37**, no. 43, p. 10139, 2004.
- [39] C. M. Bender, D. C. Brody, and H. F. Jones, "Extension of PT-symmetric quantum mechanics to quantum field theory with cubic interaction," *Physical Review D*, vol. **70**, no. 2, p. 025001, 2004.

- [40] C. M. Bender, D. C. Brody, and H. F. Jones, "Scalar quantum field theory with a complex cubic interaction," *Physical review letters*, vol. **93**, no. 25, p. 251601, 2004.
- [41] C. M. Bender and B. Tan, "Calculation of the hidden symmetry operator for a PT-symmetric square well," *Journal of Physics A: Mathematical and General*, vol. **39**, no. 8, p. 1945, 2006.
- [42] A. Mostafazadeh, "PT-symmetric cubic anharmonic oscillator as a physical model," *Journal of Physics A: Mathematical and General*, vol. **38**, no. 29, p. 6557, 2005.
- [43] R. Newton, *Scattering of Wave and Particles*. McGraw Hill, 1967.
- [44] D. Wintgen and H. Friedrich, "Classical and quantum-mechanical transition between regularity and irregularity in a hamiltonian system," *Physical Review A*, vol. **35**, no. 3, p. 1464, 1987.
- [45] T. Kato, *erturbation theory of linear operators*. Springer, 1966.
- [46] M. Berry, "Pancharatnam, virtuoso of the poincaré sphere: an appreciation," *Current Science*, vol. **67**, no. 4, pp. 220–223, 1994.
- [47] S. Pancharatnam *Proc. Ind. Acad. Sci.*, vol. **XLII**, p. 86, 1955.
- [48] M. V. Berry and D. H. J. O'dell, "Diffraction by volume gratings with imaginary potentials," *Journal of Physics A: Mathematical and General*, vol. **31**, no. 8, p. 2093, 1998.
- [49] J. Doppler, A. A. Mailybaev, J. Böhm, U. Kuhl, A. Girschik, F. Libisch, T. J. Milburn, P. Rabl, N. Moiseyev, and S. Rotter, "Dynamically encircling an exceptional point for asymmetric mode switching," *Nature*, vol. **537**, no. 7618, pp. 76–79, 2016.
- [50] H. Xu, D. Mason, L. Jiang, and J. G. E. Harris, "Topological energy transfer in an optomechanical system with exceptional points," *Nature*, vol. **537**, no. 7618, pp. 80–83, 2016.
- [51] H. Eleuch and I. Rotter, "Exceptional points in open and pt symmetric systems," *arXiv preprint arXiv:1311.6320*, 2013.
- [52] T. Kottos, "Optical physics: Broken symmetry makes light work," *Nature Physics*, vol. **6**, no. 3, pp. 166–167, 2010.
- [53] K. G. Makris, R. El-Ganainy, D. N. Christodoulides, and Z. H. Musslimani, "Beam dynamics in PT-symmetric optical lattices," *Physical Review Letters*, vol. **100**, no. 10, p. 103904, 2008.

- [54] R. El-Ganainy, K. G. Makris, D. N. Christodoulides, and Z. H. Musslimani, "Theory of coupled optical PT-symmetric structures," *Optics letters*, vol. **32**, no. 17, pp. 2632–2634, 2007.
- [55] Z. H. Musslimani, K. G. Makris, R. El-Ganainy, and D. N. Christodoulides, "Optical solitons in PT-periodic potentials," *Physical Review Letters*, vol. **100**, no. 3, p. 030402, 2008.
- [56] A. Guo, G. J. Salamo, D. Duchesne, R. Morandotti, M. Volatier-Ravat, V. Aimez, G. A. Siviloglou, and D. N. Christodoulides, "Observation of p t-symmetry breaking in complex optical potentials," *Physical Review Letters*, vol. **103**, no. 9, p. 093902, 2009.
- [57] C. Dembowski, H.-D. Gräf, H. L. Harney, A. Heine, W. D. Heiss, H. Rehfeld, and A. Richter, "Experimental observation of the topological structure of exceptional points," *Physical review letters*, vol. **86**, no. 5, p. 787, 2001.
- [58] B. Peng, Ş. K. Özdemir, F. Lei, F. Monifi, M. Gianfreda, G. L. Long, S. Fan, F. Nori, C. M. Bender, and L. Yang, "Parity-time-symmetric whispering-gallery microcavities," *Nature Physics*, vol. **10**, no. 5, pp. 394–398, 2014.
- [59] J. Lee, S.-B. and Yang, S. Moon, S.-Y. Lee, J.-B. Shim, S. W. Kim, J.-H. Lee, and j. v. n. p. y. p. An, K., "Observation of an exceptional point in a chaotic optical microcavity,"
- [60] J. Wiersig, S. W. Kim, and M. Hentschel, "Asymmetric scattering and nonorthogonal mode patterns in optical microspirals," *Physical Review A*, vol. **78**, no. 5, p. 053809, 2008.
- [61] N. G. A. J. Lipkin, H. J. and Meshkov, "Validity of many-body approximation methods for a solvable model:(i). exact solutions and perturbation theory," *Nuclear Physics*, vol. **62**, no. 2, pp. 188–198, 1965.
- [62] N. Meshkov, A. J. Glick, and H. J. Lipkin, "Validity of many-body approximation methods for a solvable model:(ii). linearization procedures," *Nuclear Physics*, vol. **62**, no. 2, pp. 199–210, 1965.
- [63] A. J. Glick, H. J. Lipkin, and N. Meshkov, "Validity of many-body approximation methods for a solvable model:(iii). diagram summations," *Nuclear Physics*, vol. **62**, no. 2, pp. 211–224, 1965.
- [64] W. D. Heiss, F. G. Scholtz, and H. B. Geyer, "The large n behaviour of the lipkin model and exceptional points," *Journal of Physics A: Mathematical and General*, vol. **38**, no. 9, p. 1843, 2005.

- [65] F. Leyvraz and W. D. Heiss, "Large-n scaling behavior of the lipkin-meshkov-glick model," *Physical review letters*, vol. **95**, no. 5, p. 050402, 2005.
- [66] C. M. Bender, M. Gianfreda, N. Hassanpour, and H. F. Jones, "Comment on on the lagrangian and hamiltonian description of the damped linear harmonic oscillator[j. math. phys. 48, 032701 (2007)]," *Journal of Mathematical Physics*, vol. **57**, no. 8, p. 084101, 2016.
- [67] P. S. Bauer, "Dissipative dynamical systems. i.," *Proceedings of the National Academy of Sciences*, vol. **17**, no. 5, p. 311314, 1931.
- [68] D. R. Davis, "The inverse problem of the calculus of variations in higher space," *Transactions of the American Mathematical Society*, vol. **30**, no. 4, p. 710736, 1928.
- [69] M. Morse, "A generalization of the sturm separation and comparison theorems inn-space," *Mathematische Annalen*, vol. **103**, no. 1, pp. 52–69, 1930.
- [70] H. Bateman, "On dissipative systems and related variational principles," *Physical Review*, vol. **38**, no. 4, p. 815, 1931.
- [71] V. K. Chandrasekar, M. Senthivelan, and M. Lakshmanan, "On the lagrangian and hamiltonian description of the damped linear harmonic oscillator," *Journal of mathematical physics*, vol. **48**, no. 3, p. 032701, 2007.
- [72] H. Goldstein, *Classical Mechanics*. Pearson, 1950.
- [73] F. Riewe, "Nonconservative lagrangian and hamiltonian mechanics," *Physical Review E*, vol. **53**, no. 2, p. 1890, 1996.
- [74] J. R. Ray, "Lagrangians and systems they describehow not to treat dissipation in quantum mechanics," *American Journal of Physics*, vol. **47**, no. 7, pp. 626–629, 1979.
- [75] H. Dekker, "Classical and quantum mechanics of the damped harmonic oscillator," *Physics Reports*, vol. **80**, no. 1, pp. 1–110, 1981.
- [76] C.-I. Um, K.-H. Yeon, and T. F. George, "The quantum damped harmonic oscillator," *Physics Reports*, vol. **362**, no. 2, pp. 63–192, 2002.
- [77] G. Dito and F. J. Turrubiates, "The damped harmonic oscillator in deformation quantization," *Physics Letters A*, vol. **352**, no. 4, pp. 309–316, 2006.
- [78] J. R. Choi, "The effects of nonextensivity on quantum dissipation," *Scientific reports*, vol. **4**, 2014.
- [79] M. Blasone, P. Jizba, and G. Vitiello, "Dissipation and quantization," *Physics Letters A*, vol. **287**, no. 3, pp. 205–210, 2001.

- [80] R. Egger, H. Grabert, and U. Weiss, "Crossover from coherent to incoherent dynamics in damped quantum systems," *Physical Review E*, vol. **55**, no. 4, p. R3809, 1997.
- [81] E. G. Harris, "Quantum tunneling in dissipative systems," *Physical Review A*, vol. **48**, no. 2, p. 995, 1993.
- [82] V. K. Chandrasekar, M. Senthilvelan, and M. Lakshmanan, "A nonlinear oscillator with unusual dynamical properties,"
- [83] V. K. Chandrasekar, M. Senthilvelan, and M. Lakshmanan, "On the complete integrability and linearization of nonlinear ordinary differential equations. ii. third-order equations," in *Proceedings of the Royal Society of London A: Mathematical, Physical and Engineering Sciences*, vol. **462**, pp. 1831–1852, The Royal Society, 2006.
- [84] L. G. S. Duarte, S. E. S. Duarte, and L. Da Mota, "A method to tackle first-order ordinary differential equations with liouvillian functions in the solution," *Journal of Physics A: Mathematical and General*, vol. **35**, no. 17, p. 3899, 2002.
- [85] J. D. Jackson, *Electrodynamics*. Wiley Online Library.
- [86] B.-G. Englert, "Quantization of the radiation-damped harmonic oscillator," *Annals of Physics*, vol. **129**, no. 1, pp. 1–21, 1980.
- [87] C. M. Bender and M. Gianfreda, "symmetric interpretation of the electromagnetic self-force," *Journal of Physics A: Mathematical and Theoretical*, vol. **48**, no. 34, p. 34FT01, 2015.
- [88] E. W. Weissein, ""strum-liouville equation,"," *Math World-A Wolfram Web Ressorce*, vol. <http://mathworld.wolfram.com/Sturm-LiouvilleEquation.html>.
- [89] M. Abramowitz and I. A. Stegun, *Handbook of mathematical functions: with formulas, graphs, and mathematical tables*, vol. **55**. Courier Corporation, 1964.
- [90] M. S. Swanson, "Transition elements for a non-hermitian quadratic hamiltonian," *Journal of Mathematical Physics*, vol. **45**, no. 2, pp. 585–601, 2004.
- [91] A. Mostafazadeh, "Exact pt-symmetry is equivalent to hermiticity," *Journal of Physics A: Mathematical and General*, vol. 36, no. 25, p. 7081, 2003.
- [92] C. M. Bender, A. Felski, N. Hassanpour, S. Klevansky, and A. Beygi, "Analytic structure of eigenvalues of coupled quantum systems," *Physica Scripta*, vol. 92, no. 1, p. 015201, 2016.
- [93] C. M. Bender and T. T. Wu, "Analytic structure of energy levels in a field-theory model," *Physical Review Letters*, vol. **21**, no. 6, p. 406, 1968.

- [94] C. M. Bender and T. T. Wu, "Anharmonic oscillator," *Physical Review*, vol. 184, no. 5, p. 1231, 1969.
- [95] W. D. Heiss, "The physics of exceptional points," *Journal of Physics A: Mathematical and Theoretical*, vol. 45, no. 44, p. 444016, 2012.
- [96] C. M. Bender and H. F. Jones, "Interactions of hermitian and non-hermitian hamiltonians," *Journal of Physics A: Mathematical and Theoretical*, vol. 41, no. 24, p. 244006, 2008.
- [97] I. L. Aleiner, B. L. Altshuler, and Y. G. Rubo, "Radiative coupling and weak lasing of exciton-polariton condensates," *Physical Review B*, vol. 85, no. 12, p. 121301, 2012.
- [98] C. M. Bender, M. Gianfreda, Ş. K. Özdemir, B. Peng, and L. Yang, "Twofold transition in pt-symmetric coupled oscillators," *Physical Review A*, vol. 88, no. 6, p. 062111, 2013.
- [99] C. M. Bender, M. Gianfreda, and S. P. Klevansky, "Systems of coupled pt-symmetric oscillators," *Physical Review A*, vol. 90, no. 2, p. 022114, 2014.
- [100] I. V. Barashenkov and M. Gianfreda, "An exactly solvable-symmetric dimer from a hamiltonian system of nonlinear oscillators with gain and loss," *Journal of Physics A: Mathematical and Theoretical*, vol. 47, no. 28, p. 282001, 2014.
- [101] A. Beygi, S. P. Klevansky, and C. M. Bender, "Coupled oscillator systems having partial pt symmetry," *Physical Review A*, vol. 91, no. 6, p. 062101, 2015.
- [102] C. M. Bender and A. Turbiner, "Analytic continuation of eigenvalue problems," *Physics Letters A*, vol. 173, no. 6, pp. 442–446, 1993.
- [103] C. M. Bender and S. P. Klevansky, "Families of particles with different masses in pt-symmetric quantum field theory," *Physical review letters*, vol. 105, no. 3, p. 031601, 2010.
- [104] C. M. Bender, N. Hassanpour, D. W. Hook, S. Klevansky, C. Sünderhauf, and Z. Wen, "Behavior of eigenvalues in a region of broken pt symmetry," *Physical Review A*, vol. 95, no. 5, p. 052113, 2017.
- [105] C. M. Bender, K. A. Milton, M. Moshe, S. S. Pinsky, and L. M. Simmons Jr, "Logarithmic approximations to polynomial lagrangians," *Physical review letters*, vol. 58, no. 25, p. 2615, 1987.
- [106] C. M. Bender, K. A. Milton, M. Moshe, S. S. Pinsky, and L. M. Simmons Jr, "Novel perturbative scheme in quantum field theory," *Physical Review D*, vol. 37, no. 6, p. 1472, 1988.

- [107] C. M. Bender, K. A. Milton, S. S. Pinsky, and L. M. Simmons Jr, "A new perturbative approach to nonlinear problems," *Journal of Mathematical Physics*, vol. **30**, no. 7, pp. 1447–1455, 1989.
- [108] C. M. Bender, S. Boettcher, and P. N. Meisinger, "Pt-symmetric quantum mechanics," *Journal of Mathematical Physics*, vol. **40**, no. 5, pp. 2201–2229, 1999.
- [109] P. Dorey, C. Dunning, and R. Tateo, "The ode/im correspondence," *Journal of Physics A: Mathematical and Theoretical*, vol. **40**, no. 32, p. R205, 2007.
- [110] J. Rubinstein, P. Sternberg, and Q. Ma, "Bifurcation diagram and pattern formation of phase slip centers in superconducting wires driven with electric currents," *Physical review letters*, vol. **99**, no. 16, p. 167003, 2007.
- [111] C. E. Rüter, K. G. Makris, R. El-Ganainy, D. N. Christodoulides, M. Segev, and D. Kip, "Observation of parity–time symmetry in optics," *Nature physics*, vol. **6**, no. 3, p. 192, 2010.
- [112] K. F. Zhao, M. Schaden, and Z. Wu, "Enhanced magnetic resonance signal of spin-polarized rb atoms near surfaces of coated cells," *Physical Review A*, vol. **81**, no. 4, p. 042903, 2010.
- [113] Z. Lin, H. Ramezani, T. Eichelkraut, T. Kottos, H. Cao, and D. N. Christodoulides, "Unidirectional invisibility induced by p t-symmetric periodic structures," *Physical Review Letters*, vol. **106**, no. 21, p. 213901, 2011.
- [114] L. Feng, M. Ayache, J. Huang, Y.-L. Xu, M.-H. Lu, Y.-F. Chen, Y. Fainman, and A. Scherer, "Nonreciprocal light propagation in a silicon photonic circuit," *Science*, vol. **333**, no. 6043, pp. 729–733, 2011.
- [115] J. Schindler, A. Li, M. C. Zheng, F. M. Ellis, and T. Kottos, "Experimental study of active lrc circuits with pt symmetries," *Physical Review A*, vol. **84**, no. 4, p. 040101, 2011.
- [116] N. M. Chtchelkatchev, A. A. Golubov, T. I. Baturina, and V. M. Vinokur, "Stimulation of the fluctuation superconductivity by p t symmetry," *Physical review letters*, vol. **109**, no. 15, p. 150405, 2012.
- [117] C. Zheng, L. Hao, and G. L. Long, "Observation of a fast evolution in a parity-time-symmetric system," *Phil. Trans. R. Soc. A*, vol. **371**, no. 1989, p. 20120053, 2013.
- [118] I. W. Herbst and B. Simon, "Dilation analyticity in constant electric field," *Communications in Mathematical Physics*, vol. **80**, no. 2, pp. 181–216, 1981.

- [119] “The appearance of a singularity in the eigenspectrum when the power of  $x$  in the potential is 1 is reminiscent of the singularity of the riemann  $\zeta$  function  $\zeta(z)$  at  $z = 1.$ ,”
- [120] I. W. Herbst, “Dilation analyticity in constant electric field,” *Communications in Mathematical Physics*, vol. **64**, no. 3, pp. 279–298, 1979.
- [121] G. Lévai, P. Siegl, and M. Znojil, “Scattering in the-symmetric coulomb potential,” *Journal of Physics A: Mathematical and Theoretical*, vol. **42**, no. 29, p. 295201, 2009.
- [122] M. Znojil, “Pt-symmetric quantum toboggans,” *Physics Letters A*, vol. **342**, no. 1-2, pp. 36–47, 2005.
- [123] “<http://reference.wolfram.com/language/ref/eigensystem.html>,”
- [124] C. M. Bender, C. Ford, N. Hassanpour, and B. Xia, “Series solutions of  $\mathcal{PT}$ -symmetric schrödinger equations,” *Journal of Physics Communications*, vol. 2, no. 2, p. 025012, 2018.
- [125] C.-Q. Dai, X.-G. Wang, G.-Q. Zhou, *et al.*, “Stable light-bullet solutions in the harmonic and parity-time-symmetric potentials,” *Physical Review A*, vol. **89**, no. 1, p. 013834, 2014.
- [126] C. M. Bender and H. F. Jones, “Calculation of low-lying energy levels in quantum mechanics,” *Journal of Physics A: Mathematical and Theoretical*, vol. **47**, no. 39, p. 395303, 2014.
- [127] C. M. Bender, F. Cooper, P. N. Meisinger, and V. M. Savage, “Variational ansatz for pt-symmetric quantum mechanics,” *Physics Letters A*, vol. **259**, no. 3-4, pp. 224–231, 1999.
- [128] A. Mostafazadeh, “Pseudo-hermiticity and generalized pt-and cpt-symmetries,” *Journal of Mathematical Physics*, vol. **44**, no. 3, pp. 974–989, 2003.
- [129] C. M. Bender, D. C. Brody, J.-H. Chen, H. F. Jones, K. A. Milton, and M. C. Ogilvie, “Equivalence of a complex p t-symmetric quartic hamiltonian and a hermitian quartic hamiltonian with an anomaly,” *Physical Review D*, vol. **74**, no. 2, p. 025016, 2006.